INFORMATION TO USERS

This reproduction was made from a copy of a document sent to us for microfilming. While the most advanced technology has been used to photograph and reproduce this document, the quality of the reproduction is heavily dependent upon the quality of the material submitted.

The following explanation of techniques is provided to help clarify markings or notations which may appear on this reproduction.

1. The sign or "target" for pages apparently lacking from the document photographed is "Missing Page(s)". If it was possible to obtain the missing page(s) or section, they are spliced into the film along with adjacent pages. This may have necessitated cutting through an image and duplicating adjacent pages to assure complete continuity.

2. When an image on the film is obliterated with a round black mark, it is an indication of either blurred copy because of movement during exposure, duplicate copy, or copyrighted materials that should not have been filmed. For blurred pages, a good image of the page can be found in the adjacent frame. If copyrighted materials were deleted, a target note will appear listing the pages in the adjacent frame.

3. When a map, drawing or chart, etc., is part of the material being photographed, a definite method of "sectioning" the material has been followed. It is customary to begin filming at the upper left hand corner of a large sheet and to continue from left to right in equal sections with small overlaps. If necessary, sectioning is continued again -beginning below the first row and continuing on until complete.

4. For illustrations that cannot be satisfactorily reproduced by xerographic means, photographic prints can be purchased at additional cost and inserted into your xerographic copy. These prints are available upon request from the Dissertations Customer Services Department.

5. Some pages in any document may have indistinct print. In all cases the best available copy has been filmed.

University Microfilms International
300 N. Zeeb Road
Ann Arbor, MI 48106

Holstein, Gay Robbins

EARLY POSTNATAL DEVELOPMENT OF RETINOGENICULATE TERMINATION PATTERNS IN MONKEYS

City University of New York

PH.D. 1983

PLEASE NOTE:

In all cases this material has been filmed in the best possible way from the available copy. Problems encountered with this document have been identified here with a check mark __✓__.

1. Glossy photographs or pages __✓__
2. Colored illustrations, paper or print _____
3. Photographs with dark background __✓__
4. Illustrations are poor copy _____
5. Pages with black marks, not original copy _____
6. Print shows through as there is text on both sides of page _____
7. Indistinct, broken or small print on several pages __✓__
8. Print exceeds margin requirements _____
9. Tightly bound copy with print lost in spine _____
10. Computer printout pages with indistinct print _____
11. Page(s) _____ lacking when material received, and not available from school or author.
12. Page(s) _____ seem to be missing in numbering only as text follows.
13. Two pages numbered _____. Text follows.
14. Curling and wrinkled pages _____
15. Other _____

EARLY POSTNATAL DEVELOPMENT OF RETINOGENICULATE TERMINATION PATTERNS IN MONKEYS

by

Gay Robbins Holstein

A dissertation submitted to the Graduate Faculty in Psychology in partial fulfillment of the requirements for the degree of Doctor of Philosophy, The City University of New York

1983

This manuscript has been read and accepted for the Graduate Faculty in Psychology in satisfaction of the dissertation requirement for the degree of Doctor of Philosophy.

2/24/83
Date

Chairman of Examining Committee

February 24, 1983
Date

Herbert D. Saltzstein
Executive Officer

Dr. Pedro Pasik

Dr. Thomas Frumkes

Dr. Richard Bodnar

Supervisory Committee

The City University of New York

ABSTRACT

EARLY POSTNATAL DEVELOPMENT OF RETINOGENICULATE TERMINATION PATTERNS IN MONKEYS

by

Gay Robbins Holstein

Advisor: Professor Pedro Pasik

The purpose of the present investigation was to provide normative data on the morphologic basis for behaviorally- and physiologically-defined critical periods in the development of the primate visual system. The retinogeniculate pathway comprises the first stage of information processing in the cerebrum, and was selected for study because it presumably represents a less complex system than higher visual centers. In addition, the separate optic projections to magnocellular and parvocellular LGNd laminae constitute the first stage of processing in which the functional distinction between transient and sustained pathways is expressed morphologically. While qualitative ultrastructural observations are of some value for the identification of morphologic features of neural development, the subjectivity of these results limits their generality. To characterize more accurately the ontogenetic sequence, a quantitative stereological analysis was performed.

Profiles of retinal boutons and their synapses in magnocellular lamina 1 (L1) and parvocellular lamina 6 (L6) of the dorsal lateral geniculate nucleus (LGNd) were measured in randomized electron micrographs of newborn, 1-, 2-, 4-, 8- and 17-week old monkeys (M. mulatta). Using a computer-assisted stereological procedure, the frequency distributions of spherical bouton and flat circular synaptic and nonsynaptic contact disk diameters were reconstructed from areal measurements of retinal profiles and length measurements of contacts identified

in at least 1200 μm^2 of net neuropil from each age-lamina condition, representing 1600-3700 μm^2 of actual tissue. These distributions were used to calculate the weighted mean bouton diameter, bouton density, weighted mean synaptic area, synaptic density, weighted mean nonsynaptic contact area, and nonsynaptic contact density. The density values were then adjusted for the growth of laminae to yield estimates of total numbers of boutons and synapses.

Retinal boutons within a lamina tend to increase in size during maturation and mean bouton diameter is significantly larger in L1 than L6 of the newborn, 2-, 4- and 8-week-old monkeys. Bouton density and number decrease during development in both regions, and are consistently higher in L6 than L1.

In the magnocellular LGNd, the estimated number of synapses decreases during early postnatal development; immature elements decline almost monotonically, while the mature population shows no consistent trend. At every age, more immature than mature synapses are present. Retinal (R) to principal cell dendrite (P) synapses follow a similar pattern, while retinal to interneuron dendrite (I) synapses change little in number. The major period of R to P synapse elimination in magnocellular layers occurs in the older ages. The cumulative area of synaptic contact decreases over the first few postnatal weeks, then increases and stabilizes by eight weeks. However, the number of nonsynaptic retinal to P contacts appears constant across development.

In the parvocellular layers, the estimated number of synapses also decreases during maturation. Although, in general, immature synapses are more numerous than mature ones, the greatest loss occurs in the mature population. This progression is due primarily to changes in number of retinal to P synapses, since retinal to I synapses remain relatively constant. The major period of synapse elimination in parvocellular laminae occurs during the first eight weeks. While the cumulative synapse area decreases monotonically over this period, the number

of nonsynaptic contacts dramatically increases.

The present results indicate that substantial bouton disappearance and synapse elimination occur during early postnatal maturation. In addition, the magnocellular pathway, specialized for brightness and movement detection, matures at a different rate from the parvocellular projection, specialized for high acuity and color vision. These morphologic alterations may be at least partially due to early postnatal visual experience. The onset and duration of critical periods in the development of behavioral and physiological responses may reflect the temporal course of changes in neural organization. The observed decreases in bouton and synapse number exemplify a pruning process in which unutilized or unsuccessful connections are eliminated during normal development.

ACKNOWLEDGEMENTS

The research described in this monograph was conducted in the Laboratory of Experimental Neurology, Department of Neurology of the Mount Sinai School of Medicine, under the supervision of Drs. Tauba and Pedro Pasik. I wish to express my gratitude to Drs. Pasik for the research opportunities made available to me, and for the education I have received in their laboratory. I thank the members of my dissertation committee: Drs. Efrain Azmitia, Richard Bodnar, Thomas Frumkes, Dean Hillman and Pedro Pasik for their time and helpful comments on several drafts of this manuscript. I am deeply grateful to Mr. Alexander Pasik for the design and implementation of the computer system used for the quantitative analysis, and to Drs. Ford Calhoun, Judith Goldberg, Charles Peskin, David Ross, Harry Smith and John Thornton for consultations on various aspects of the data analysis and evaluation. I am grateful to Drs. József Hámori and Jorge Pecci Saavedra for their advise, encouragement and teaching while visitors to the laboratory. I am deeply indebted to Mr. Victor Rodriguez for his careful and excellent work fulfilling the seemingly endless photographic requirements of the study, and I am equally beholden to Ms. Minerva Feliciano for processing words with the greatest of speed, finesse, and friendship. I thank Ms. Marilyn Ilvento for assistance with electron microscopy, photography, and headaches from a variety of sources. I am grateful to the T.C. Flying Statistics Squadron (Arleen Antilla, Dawn Larkin and Roger Muzi) for a red-alert, night-raid ANCOVAR, and to my colleagues in schooling, Glenn Bauer, Jean Fisher, Dennis France, Andrew Glover, Michael Gottlieb and Steven Solomon for encouragement and comraderie. I thank the Poor Richard's Neighborhood Marching Band and Bugle Corps: Bambi Begun, Billy Eisenberg, Linda Eisenberg, Kuni Hattori, Bob Hinden, Laurie Lum, Nedmund Peirce, Barry Pohorence, and leading the cakewalk in the finest of style, Miss Dominique Michelle Strandquest, for friendships of a most extraordinary nature.

I am most deeply indebted and grateful to the Holstein and Potegal-Rosenberg families for tolerating prolonged absences and neglect with understanding. And for Michael Potegal, whose encouragement, advice, support, friendship and love, I save my most excellent thanks.

This research was aided by NEI Grants EY-01867, EY-01926 and EY-07014.

DEDICATION

This monograph is dedicated to my parents,

Rosa Lee Cosby Holstein and Elwood Holstein,

with gratitude, admiration and love.

TABLE OF CONTENTS

LIST OF TABLES

LIST OF FIGURES

LIST OF FIGURES (continued)

Chapter I

INTRODUCTION

The early postnatal period of the primate visual system is characterized by a high degree of functional plasticity, as demonstrated by visual deprivation studies (Hubel, Wiesel and LeVay, 1977) and by the (^{14}C) deoxyglucose method (DeRosiers, Sakurada, Jehle, Shinohara, Kennedy and Sokoloff, 1978).

Behavioral studies in humans and monkeys indicate that substantial sensory and perceptual development occurs during this period. The optical and oculomotor properties of the eye are immature at birth, and acuity and stereopsis require approximately one year to mature. The processing of visual information also requires a period of normal visual experience after birth in order to fully develop. Restrictions or alterations in the visual environment of neonatal humans and monkeys result in permanent sensory and perceptual deficits. Similarly, physiological research has demonstrated that a protracted postnatal period is required for functional maturation in the visual system. In general, the specific characteristics of the transient (Y) and sustained (X) subsystems develop at different rates, although both require approximately equal periods to achieve the adult level of refinement in spatial resolution (see Stone, Dreher and Leventhal, 1979).

The behavioral and physiologic changes must have a morphologic substratum represented by transformation in the synaptic organization at different levels of the system. Although light microscopic studies of the retina, lateral geniculate nucleus pars dorsalis (LGNd) and striate cortex have contributed much to the disclosure of these changes, ultrastructural investigations ultimately provide the necessary information for the understanding of rearrangements in neuronal connectivity. The LGNd of the monkey offers a unique opportunity to study differential features in the development of the physiologically-defined X and Y

subsystems, since the neurons of these two subdivisions are almost completely segragated in the parvocellular and magnocellular components of this structure. The first neuronal linkage which occurs in the LGNd is made by the boutons of arriving retinal ganglion cell axons. As the next chapter will show, there is relatively little information concerning the early postnatal maturation of the primate LGNd, and the retinal afferent innervation of that structure. For example, ontogenetic data on the differential projections to magnocellular and parvocellular laminae is lacking. Many synapses made by retinal afferents to the LGNd are not mature at birth, some remain immature for several months, and a differential time course of development is manifest in retinal to principal cell and retinal to interneuron synaptology.

The goal of the present investigation is to identify critical changes in the postnatal development of retinogeniculate articulations with particular emphasis on differential features of the magnocellular and parvocellular laminae of the LGNd. Although qualitative observations are of value in recognizing some of these changes, the dynamic characteristics of maturation can only be evaluated with quantitative techniques. The latter type of analysis is carried out with a stereologic approach and comprises the major body of the results. The findings are expected to contribute toward understanding the complex neuronal interactions present in the maturing visual system. Since the establishment of normal retinogeniculate termination patterns is critical for all subsequent visual information processing, this research may be relevant to all studies of visual system development: behavioral, functional and morphological.

In the following chapter, the behavioral literature on postnatal maturation of visual sensory, perceptual and learning capacities in humans and monkeys is surveyed, as well as deprivation studies relevant to the identification of a critical period in the development of normal visual behavior. Physiological studies which

characterize retinal and LGNd neuron response properties in cat and monkey. correlated with the neuronal morphology and LGNd cytoarchitectonics are reviewed for the adult and developing nervous system. Because they are most directly relevant, anatomical investigations are reported in greater detail. Light microscopic studies in cat, monkey and humans which concern the connectivity, neurocytology, cytoarchitectonics and deprivation effects on the retinogeniculate projection are presented for adult and developmental subjects. Finally, ultrastructural investigations of mature and immature cat and monkey LGNd synaptology are reported and discussed in relation to the present study.

Chapter II

BACKGROUND LITERATURE

A. Behavioral Studies

Neonatal primates are visually alert and responsive, with pupillary and palpebral reflexes already present (Pratt, 1954). Although the optic media are clear (Reinis and Goldman, 1980), anomalies in accommodation (Sivak and Bobier, 1978; Braddick, Atkinson, French and Howland, 1979) and refraction (Duke-Elder, 1963) suggest that the optical properties of the eye are not fully developed at birth. Accommodative abnormalities persist for one month in the monkey (Howland, Boothe and Kiorpes, 1982) and four months in the human (Braddick et al, 1979). Astigmatism is prevalent in humans younger than one year; the 45-60% incidence in infants does not decline to the adult level of 8% for two to three years (Howland, Atkinson, Braddick and French, 1978; Mohindra, Held, Gwiazda and Brill, 1978). In addition, poor fixation, primarily due to unusually large saccadic eye movements, has been observed in four- and five-year-old children (Kowler and Martins, 1982).

Similarly, the perceptual abilities of young primates are immature at birth. Visual acuity in human infants has been assessed using optokinetic nystagmus (Gorman, Cogan and Gellis, 1957), the preferential looking paradigm (Fantz, Ordy and Udelf, 1962), and visual evoked potentials (Harter and Suitt, 1970). In general, the reported acuity values are at least 20/400 (using Snellen notation) in newborns, with gradual improvement to 20/100 in four- to six-month-old infants and to the adult level by two years (Fantz, 1961; Dobson and Teller, 1978; Atkinson, Braddick and French, 1979; Mayer and Dobson, 1980). Contrast sensitivity increases slowly, with a concomitant peak shift toward higher frequencies. The low spatial frequency fall-off which is characteristic of the adult contrast sensitivity function appears in infants only after two postnatal months (Atkinson, Braddick and

Braddick, 1974; Banks and Salapatek, 1976, 1978).

In the monkey (N. nemestrina), the minimum resolvable stripe width (threshold detection) steadily decreases from 14' of arc at one week to 3.7' of arc in animals older than six weeks. This represents a two octave improvement in acuity, accomplished in approximately six weeks in the monkey and six months in the human (Teller, Regal, Videen and Pulos, 1978; Teller and Boothe, 1979). The adult macaque acuity level of 0.7' of arc (Weiskrantz and Cowey, 1963; Miller, Pasik and Pasik, 1980) is attained within approximately six months (Teller et al., 1978). Contrast sensitivity increases with age, although different portions of the contrast sensitivity function follow disparate rates of development. By 20 weeks, sensitivity to low spatial frequencies approximates that of the adult (DeValois, Morgan and Snodderly, 1974; Harding and Yates, 1976; Miller et al., 1980), while the greatest increase in the high frequency end of the function occurs during the twenty-first through the twenty-eighth weeks (Teller and Boothe, 1979; Boothe, Williams, Kiorpes and Teller, 1980).

Depth perception is demonstrable in newborn humans (Gibson and Walk, 1960) and in three-day-old rhesus monkeys (Rosenblum and Cross, 1963) as a preference for the optically shallow area of a visual cliff, and form discrimination has been shown by the preferential looking technique in humans as young as ten hours (Fantz, 1961). In the eight-week-old infant, size constancy, shape constancy, and orientation discrimination have been demonstrated using an operant conditioning paradigm, although higher level processing of this information (e.g. discrimination of pictorial cues) is not evident (Bower, 1964, 1966). Binocular vision may develop exclusively during the postnatal period, since stereopsis is not detectable by evoked potentials (Amigo, Fiorentini, Pirchio and Spinelli, 1978; Petrig, Julesz, Kropfl, Baumgartner and Anliker, 1981) or by random dot stereograms (Fox, Aslin, Shea and Dumais, 1980) in human infants for

two to three months. Color vision also requires protracted development; although the two-month-old human infant can discriminate red, blue, yellow and green from gray, and has spectral sensitivities similar to the adult, color percepton does not fully mature for several additional months (Staples, 1932; Dobson, 1976). Studies on the development of visual illusions indicate that some (e.g. the Usnadze illusion) increase in power with age, while others, including many of the classic illusions (e.g. the Poggendorff illusion) have a diminishing effect with maturation (Dember and Warm, 1979).

The visual learning capacities of rhesus monkeys also develop postnatally (Zimmerman, 1958). The ability to solve brightness discrimination problems is first demonstrable in eight- to eleven-day-old infants, while that of form and pattern discriminations requires 15-25 days and reversal learning 40 days to become manifest. The emergence of these skills depends on normal maturation, but not on specific learning experience. In general, postnatal age appears to dictate the level of complexity of the soluble problems, although learning set formation is still immature in one-year-old monkeys.

The existence of a critical period in the development of human visual perception is suggested by clinical data demonstrating recovery of visual function after cataract removal in adult patients with long-term blindness, although cataracts in infants cause irreversible loss of sight (von Senden, 1960). In a related study (Hess, France and Tulunay-Keesey, 1981), spatial and temporal contrast sensitivity functions have been obtained from six individuals (7-22 years old) with monocular pattern deprivation resulting from congenital cataracts manifest during the first year after birth. In two individuals with severe monocular amblyopia, no spatial vision was demonstrable with stationary or temporally-modulated sine wave gratings at or above thresholds, and temporal perception was limited to flicker detection, and was affected most severely at

higher temporal frequencies. In patients with milder amblyopia, the loss of spatial sensitivity is greater at middle and high frequencies, and a shift in peak sensitivity toward lower spatial frequencies is apparent. Temporal perception in these individuals is not frequency-dependent; a constant proportional loss is observable at all temporal frequencies. In general, therefore, this early pattern deprivation is more deleterious to spatial than to temporal abilities. These deficits seem permanent, since replicative tests one year later yield similar results. Irreversible deprivation amblyopia can result from other retinal image occlusions, such as corneal opacities, ptosis and traumatic cataracts present in the neonate (von Noorden and Maumanee, 1968). In one individual, onset at two years old produced a persistent acuity level of 20/800. In addition, the critical period for the development of binocularity appears to last several years: strabismus in children is maximally deleterious during the first two and one-half years (Hohmann and Creutzfeldt, 1975), although some deficits may result from onset as late as six years old (Banks, Aslin and Letson, 1975).

Deprivation studies in monkeys also indicate the existence of a sensitive period for the development of normal visual behavior, although the duration of that period is unclear. In rhesus monkeys with monocular lid suture or artificial esotropia during the first four (Von Noorden and Dowling, 1970; von Noorden, Dowling and Ferguson, 1970) or eight (von Noorden, 1973) postnatal weeks, severe amblyopia is observed with reverse-suture testing of the deprived eye, and no subsequent recovery occurs although the electroretinogram is normal and no ophthalmic abnormalities are detectable. One animal, with monocular lid suture at four weeks, was unable to resolve a 240' of arc Landolt ring. However, when visual deprivation is initiated at or after three months, functional recovery to normal acuity levels rapidly follows eye re-opening. In a related study (Hendrickson, Boles and McLean, 1977), two animals (M. nemestrina) with

unilateral lid fusion at three weeks received focal lesions in the undeprived eye, creating a "critical segment" in the deprived eye, and were reverse-sutured at nine months for subsequent testing on grating acuity, visual behavior and visual fields. When the focal lesion is sustained at three months old, overall visual behavior is competent, but acuity is 20/1,250. With the focal lesion placed at nine months of age, poor initial visual performance and acuity of 20/400 results, but substantial recovery occurs and acuity improves rapidly to 20/80. Evidently, the creation of a critical segment after the critical period allows significant recovery of visual performance and acuity, although the same lesion sustained during the critical period causes irreversible damage. In a recent study (Harwerth, Crawford, Smith and Boltz, 1981), deprived and non-deprived eyes were compared in three rhesus monkeys with monocular lid suture for two postnatal weeks, followed by nine and one-half months of normal experience. Severe deficits in contrast sensitivity are observed in the deprived eye, with the high spatial frequency cut-off six octaves lower than in the non-deprived eye. The acuity level of 20/2,000 is as poor as in animals with 19-23 months of continuous monocular deprivation. In addition, spectral sensitivity is reduced, and the absolute threshold for light detection is elevated by three to four log units.

A causal relationship betwen visual deprivation and myopia is uncertain. In one study, both monocular and binocular lid fusion in 10 neonatal monkeys reportedly caused axial myopia, attributable to a deprivation-induced elongation of the eye globe (Wiesel and Raviola, 1977). The severity of myopia increases with duration of eye closure, and the impairment is irreversible. However, a similar study using 13 rhesus monkeys (von Noorden and Crawford, 1978) found no consistent relationship between neonatal lid suture and the degree of myopia.

Taken together, the studies cited above indicate that the sensory and perceptual capacities of human and monkey visual system require a period of

normal postnatal experience in order to mature fully. The optics, eye movements, acuity, contrast sensitivity, binocularity, perceptual and visual learning abilities of primate infants all exhibit immature characteristics. The deprivation research clearly suggests that behavioral deficits result from restricted visual experience in early life. These aspects of behavioral development, under both normal and abnormal conditions, must have morphologic correlates. For example, it is possible that differential rates of maturation are operative in different functional pathways of the visual system. To explore this possibility, it is appropriate to investigate the postnatal morphologic development of the retinogeniculate pathway, in which the discrete projections to magnocellular and parvocellular laminae reflect a functional subdivision.

B. Physiological Studies

Differences in the receptive field characteristics, response latencies, and conduction velocities have been used to classify retinal and LGNd neurons into three functional types: X, Y, and W (see Stone et al., 1979). Following stimulation by sinusoidally-modulated grating patterns, X-system cells in the retina and LGNd of the cat (Enroth-Cugell and Robson, 1966; Cleland, Dubin and Levick, 1971; Stone and Fukuda, 1974) and monkey (Dreher, et al., 1976; Sherman et al., 1976; Marrocco, 1976; DeMonasterio, 1978) produce sustained responses which summate linearly across small receptive fields. The X-cell axons conduct slowly, have long latencies to antidromic and orthodromic activation, and are relatively unresponsive to fast-moving stimuli. In contrast, Y-system cells generate transient responses with nonlinear summation over large receptive fields, and support fast-conducting axons with short latencies. W cells are the slowest-conducting, and apparently do not comprise a significant projection to LGNd (Stone et al., 1979).

Morphologic correlates of these functional classes have been described in

the cat (Wilson, Rowe and Stone, 1976); LeVay and Ferster, 1977; Ferster and LeVay, 1978; Friedlander, Lin and Sherman, 1979) and monkey (Sherman et al., 1976; Dreher et al., 1976). X cells, characterized by medium-sized somata, medium caliber axons and small dendritic fields, are prevalent in the central retina and project to the A laminae of the cat and the parvocellular layers of the monkey LGNd. Y cells have large somata, thick axons and extensive dendritic fields; they are predominant in peripheral retina and project to the A laminae of the cat and the magnocellular layers of the monkey. W retinal ganglion cells have medium-small somata in the cat, but are infrequently observed in the monkey retina.

The response properties, morphology, and localization of these cells suggest that the two functional classes present in the retinogeniculate projection process different types of visual information (Stone et al., 1979). The X pathway appears to mediate a variety of high resolution discriminatory abilities, including color vision, while the Y pathway seems to be specialized for brightness and movement detection.

Developmental studies of physiologically characterized visual neurons in the cat LGNd indicate that all X-cell attributes except spatial resolution reach maturity before those of Y cells (Norman, Pettigrew and Daniels, 1977; Daniels, Pettigrew and Norman, 1978; Ikeda and Tremain, 1978). Spatial resolution of X cells improves rapidly over the first postnatal month (Blakemore and Vital-Durand, 1979) but stabilizes at the adult level only after six months (Mangel, Wilson and Sherman, 1980). In comparison, most Y-cell characteristics require a prolonged developmental period (Wilson, Tessin and Sherman, 1982): nonlinearity reaches adult proportions by eight weeks, latency and receptive field size by 12 weeks. However, the spatial resolution of Y cells, like X cells, requires approximately six months to fully mature.

It is clear that the physiological characteristics of the X and Y pathways mature at different rates. In general, the sustained system, specialized for high acuity and color vision, matures before the transient pathway mediating brightness and movement detection. However, both systems require approximately equal periods to develop spatial resolution maximally. Since the sustained X pathway projects exclusively to the parvocellular LGNd layers in monkey, and the transient Y pathway to magnocellular laminae, the exact nature of the developmental pattern in each subsystem can be investigated, and compared, morphologically.

C. Anatomical Studies

1. Light microscopy.

In cat, monkey, and humans, retinal afferents continue the course of the optic tract into the LGNd, and spread fanwise into fiber layers delineating the cellular laminae of the nucleus (Polyak, 1957). These axons are myelinated and usually coarse. The preterminal arborizations of the optic nerve fibers appear as dense brushes enclosing a nest of postsynaptic principal cell and interneuron somata and dendrites (Tello, 1904; Ramón y Cajal, 1911; Polyak, 1957; Szentágothai, 1963). The retinal terminals form a dense plexus, primarily oriented perpendicularly to the laminar plane, with short basket or claw-shaped branches. The postsynaptic elements often nestle in the crenulations of the presynaptic terminals, establishing axodendritic synapses usually with the distal portions of dendrites or their appendages (Szentágothai, 1963). There is divergence of single or neighboring optic nerve fiber input to several postsynaptic cells and convergence of several retinal axons onto one postsynaptic element (Glees, 1941; Glees and Clark, 1941; Polyak, 1957; Szentágothai, 1963). With Golgi (Polyak, 1957) and horseradish peroxidase (HRP) (Mason and Robson, 1977; Robson and Mason, 1977; Robson, Mason and Guillery, 1978) techniques, several types of

terminal arborizations can be distinguished, based on the number and distribution of terminal branches, the size and shape of the telodendron and the orientation of the terminals relative to the plane of the laminae.

The characteristic pattern of LGNd lamination in primates includes six cell layers, numbered ventro-dorsally, which form a concentric array around a ventral hilum(Figure 1). Although the conventional description of these six laminae differentiated two ventral magnocellular layers from four dorsal parvocellular laminae, a recent autoradiographic study comparing seven species of primates (Kaas, Huerta, Weber and Harting, 1978) suggests a more parsimonious segregation into two dorsal parvocellular layers which may subdivide into four "leaflets", two middle magnocellular layers, and two highly variable ventral layers. A distinctive feature of the monkey LGNd is the monocular projection of the contralateral and ipsilateral retinae to different cellular laminae (Minkowski, 1920). In nonhuman primates, no overlap of the retinal terminal distributions from the two eyes has been observed within a lamina and no significant termination sites have been demonstrated in the interlaminar zones using axonal degeneration (Campos-Ortega and Glees, 1967a, b; Laemle and Noback, 1970; Tigges and Tigges, 1970; Hendrickson, Wilson and Toyne, 1970), transneuronal degeneration (Minkowski, 1920; Matthews, Cowan and Powell, 1960; Doty, Glickstein and Calvan, 1966) and autoradiographic tracer (Hendrickson et al., 1970; Tigges and O'Steen, 1974; Kaas, Lin and Casagrande, 1976; Kaas, Harting and Huerta, 1977; Hubel, Wiesel and LeVay, 1977) techniques. Using conventional nomenclature, axons from the ipsilateral retina terminate in laminae 2, 3 and 5, while those from the contralateral retina innervate laminae 1, 4 and 6 (Minkowski, 1913; Brouwer and Zeeman, 1926; Walls, 1953). In addition, sets of cells in successive laminae are arranged in columns (Minkowski, 1913; Talbot and Marshall, 1941; Garey and Powell, 1967; Guillery, 1967) innervated by the same point in the visual field and

Figure 1

Light micrographs of the monkey LGNd. The laminae are numbered 1-6 ventrodorsally, conforming to conventional nomenclature. Left: LGNd of a two-week-old monkey; the two parallel lines provide an example of location and orientation of a tissue block obtained for electron microscopy. Cresyl violet stain, X30. Right: Montage of a 1 μm thick survey section through a tissue block from a 17-week-old monkey. The trapezoids in L1 and L6 indicate the location and relative size of mesas trimmed for thin sectioning. Toluidine blue stain, X110. Note also the nick at the upper right corner which aided in the identification of lamina 6.

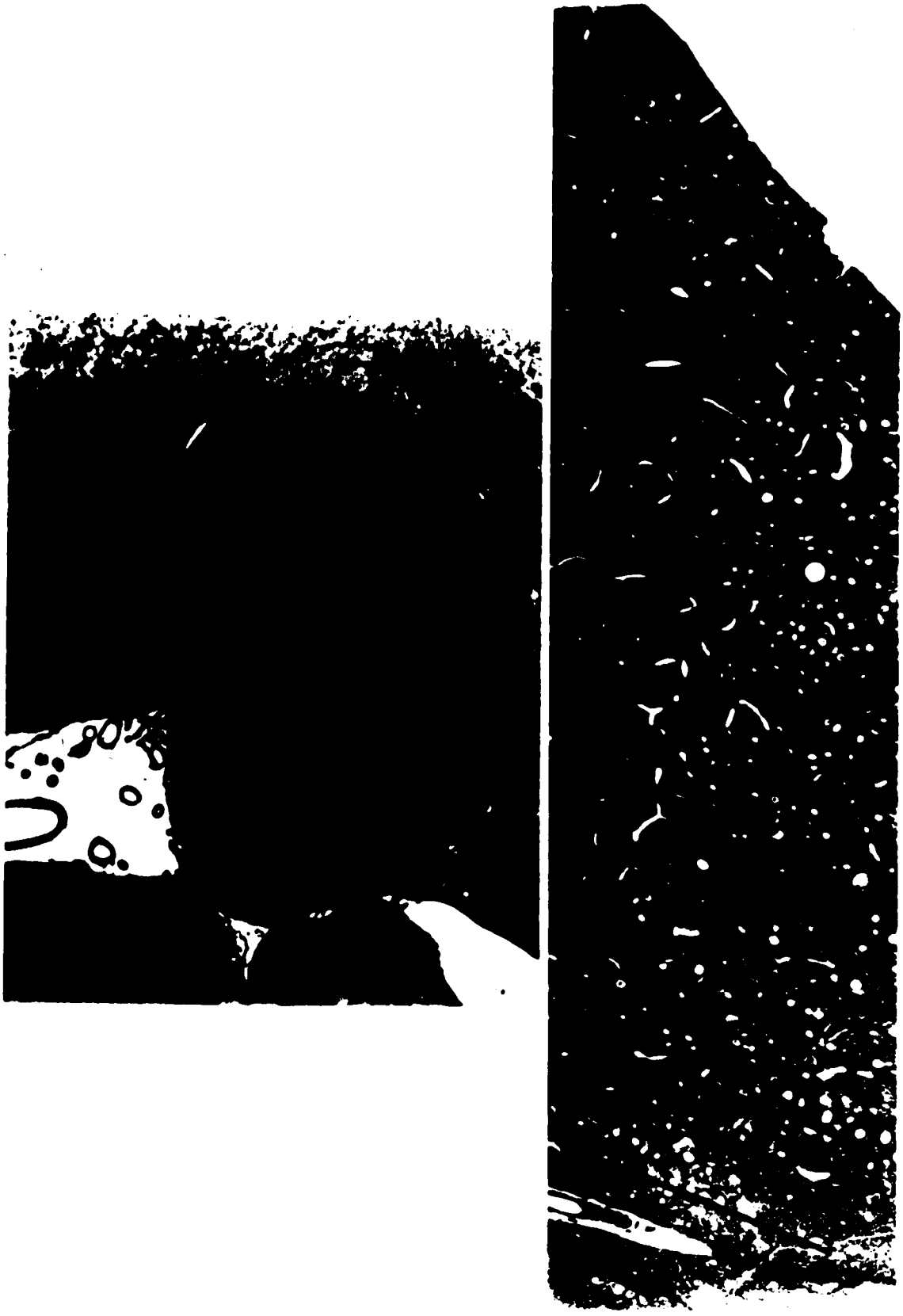

projecting to the same cortical region. In general, these "lines of projection" (Bishop, Kozak, Levick and Vakkur, 1962) are oriented perpendicularly to the plane of the laminae (Walls, 1953; Polyak, 1957; Hubel and Wiesel, 1961; Bishop et al., 1962).

In the human LGNd, seven laminae were originally distinguished (Minkowski, 1913) and were numbered dorso-ventrally. This description has subsequently been revised to conform to the nomenclature applied in monkey. Six cell layers are now distinguished (Hickey, 1977b); two ventral magnocellular laminae and four dorsal parvocellular layers which may further subdivide into six leaflets.

Golgi-impregnation studies in cat (O'Leary, 1940; Guillery, 1966) and monkey (Taboada, 1927-28; Polyak, 1957; Ball', Portugalov and Shkol'nik-Yarros, 1965; Campos-Ortega, Glees and Neuhoff, 1968; Wong-Riley, 1972; Pasik, Pasik, Hámori and Szentágothai, 1973; Saini and Garey, 1981; Wilson and Hendrickson, 1981) indicate the existence of at least two major classes of LGNd neurons; long axon projection or principal cells and short axon Golgi type II interneurons, with several subtypes identified within each class. Although questioned by one investigator (LeVay, 1971), axonal processes of the interneurons have also been observed in the LGNd of cat and monkey (Guillery, 1966; Szentágothai, Hámori and Tömböl, 1966; Famiglietti and Peters, 1972; Pasik et al., 1973; Hámori, Pasik and Pasik, 1978). Apart from the larger size of neurons in the magnocellular laminae, no substantive differences in cell morphology have been observed in Golgi-impregnated neurons of parvocellular and magnocellular regions. There is a gradual increase in the average size of cells from dorsal to ventral through the parvocellular layers (Headon, Sloper, Hiorns and Powell, 1981a).

In general, the cellular composition of the laminae in humans is similar to that of monkey (de Courten and Garey, 1982), although the presence of many intermediate types obscures classification in the magnocellular region (Hickey and

Guillery, 1981). Dendrites of neurons in the parvocellular layers are oriented along the lines of projection and rarely cross laminar borders, while in the magnocellular region dendrites are observed running parallel as well as perpendicular to the laminar plane, often traversing to an adjacent layer (Hickey and Guillery, 1981).

The prenatal development of monkey LGNd has been investigated with autoradiographic techniques. These studies indicate that LGNd neurons destined for magnocellular laminae, followed by those for parvocellular laminae, migrate from their origin at the surface of the third ventricle to the lateral area of the diencephalon in an outside-to-inside pattern (Rakic, 1976a). As the neurons reach their destinations, the nucleus rotates about its sagittal and transverse axes, while shifting ventrally, such that laterally-placed neurons form the ventral lamaine, and the more dorsal neurons are displaced caudally (Rakic, 1976a; 1977b). There is a minimum time lag of three to six days between the proliferation of retinal ganglion cells and LGNd cells (Rakic, 1976a). Although the LGNd contains a full set of neurons, and synaptogenesis has begun by embryonic day (E) 61, the axons from the two retinae are still intermixed at E64 (Rakic, 1976b; Hendrickson and Rakic, 1977). This initial overlap in projection from the two retinae is also observed in rat (Lund, Remington and Lund, 1976) and cat (Richards and Kalil, 1974). During subsequent development, the segregation of monocular inputs coincides with the maturation of lamination. Thus, lamination begins at E91; there is differentiation of magnocellular from parvocellular layers, and the retinal fibers begin to segregate. At E110, the six laminae are somewhat identifiable, and the monocular inputs are present as irregular patches. By E130, the laminae appear completely formed, and retinal axon segregation is complete. Viable projections from both eyes are essential for the formation of normal lamination patterns, although not for segregation into magnocellular and parvocellular

regions (Rakic, 1981). In addition, the total number of optic nerve fibers from each eye has been estimated from areal density measurements using electron micrographs of fetal and early postnatal rhesus monkeys (Rakic and Riley, 1982). From E47 through E95 proliferation from 0.7 $x10^6$ to 2.85 $x10^6$ is observed; then a sharp reduction occurs between E95 and E110, coincident with the period of retinal axon segregation and articulation of the six LGNd cell layers. Following a more gradual and prolonged elimination process, the adult value to 1.2-1.3 $x10^6$ optic nerve fibers is attained after two postnatal months.

Golgi impregnations of developing LGNd neurons (Garey and Saini, 1981) indicate the presence of several transient immature characteristics, including a profusion of filopodia and growth cones in prenatal material and "hair-like processes" in late fetal and newborn monkeys. A sharp increase in the number of dendritic spines is observed during the first few postnatal weeks, before the number falls to the adult level by one month. There is also some suggestion that Golgi-impregnated neurons in the magnocellular layers appear mature before those in the parvocellular laminae. However, measurements of cross-sectional somata and nuclear area during postnatal development (Gottlieb et al., 1980) indicate that maximum cell size in monkeys occurs between one and four weeks in the parvocellular region, but after eight weeks in magnocellular layers. Adult dimensions are achieved between four and eight weeks in parvocellular, and after eight weeks in magnocellular LGNd. Mean cell size, as well as variability, is greater in magnocellular layers, and in both laminar types the adult dimension is approximately 25% above the mean cell size present at birth. The major changes in the size of the cell nucleus occur between four and eight weeks in parvocellular, and after 16 weeks in magnocellular layers. In both mean cell and mean nuclear size measurements, the four parvocellular laminae develop at equal rates. In addition, no significant differences are observed in the average sizes of

parvocellular neurons in "young" (ranging in age from 80-440 days) and adult monkeys, although neurons in L2 of young animals are substantially smaller than in the adult (Headon et al., 1981a), suggesting later magnocellular maturation. The total volume of the LGNd laminae doubles during postnatal development; most parvocellular growth occurs between the second and fourth weeks, while magnocellular dimensions increase steadily after four weeks (Gottlieb et al., 1981).

In humans, the pattern of LGNd lamination becomes apparent during the sixth fetal month (Rakic, 1977a). At birth, the average cross-sectional area of neurons is 60% of the adult standard; neurons in parvocellular laminae grow rapidly over the subsequent six postnatal months and reach adult size by one year, while cells in the magnocellular region continue to grow rapidly for a full year and attain adult dimensions after two years (Hickey, 1977a, b). The cellular composition and retinal termination patterns in the human infant are similar to monkey (Skhol'nik-Yarros, 1962). In addition, Golgi-impregnated LGNd neurons from human neonates, like monkeys, sport growth cones, filopodia, dendritic spines and hair-like processes which flourish during the first four postnatal months, before receding to attain mature form by nine months (de Courten and Garey, 1982)

In cat, retinal afferents arrive in LGNd at E37, prior to the onset of lamination (Anker, 1977). There is caudal displacment of the anterior pole of the nucleus and 180^{o} rotation of the major LGNd axis around the sagittal plane which begins prenatally and is completed in the 20th postnatal week (Elegeti, Elegeti and Fleischhauer, 1976; Kalil, 1978). In addition, the volume of the nucleus increases to 66% of the adult standard during the first postnatal month, although achievement of mature dimensions requires a prolonged postnatal period (Kalil, 1978). The size of neuronal somata in all regions of the nucleus increases

precipitously during the second to fourth postnatal weeks, primarily due to a decrease in the proportion of small cells and a rise in the percentage of large (300-400 μm^2) neurons (Garey, Fisken and Powell, 1973; Kalil, 1978; Hickey, 1980). The larger cells continue to increase in size and number over the subsequent four weeks (Hickey, 1980), and mean cell area stabilizes at the adult level by the eighth postnatal week (Kalil, 1978).

Monocular deprivation in young monkeys clearly results in morphologic alterations in the LGNd. In infant monkeys with monocular lid closure for 1-102 days, cells of deprived eye-recipient layers of LGNd are small and pale in comparison to those of the nondeprived laminae (Headon and Powell, 1973; von Noorden, 1973), and the effect is greatest (20-30% size difference) when deprivation begins at birth. This shrinkage is more marked in magnocellular than parvocellular layers, and least noticeable in the monocular segment (von Noorden, 1973; von Noorden and Middleditch, 1975). When a LGNd "critical segment" is produced by retinal lesion with opposite eye closure, the deprived cells within the segment are approximately equal in size to open-eye neurons, while deprived neurons outside the segment are 35% smaller than normal (Hendrickson, Lund and Kalina, 1975; von Noorden, Crawford and Middleditch, 1976). However, the final cell size may be related to the age of onset and the duration of deprivation. With lid closure initiated during the early postnatal period, the size difference between deprived and nondeprived cells is directly proportional to duration of deprivation, while after two months, regardless of duration, closure is ineffectual in producing LGNd neuron shrinkage (von Noorden and Crawford, 1978a, b). The maximum effect in parvocellular layers occurs after four weeks of closure, whereas shrinkage in the magnocellular region is more protracted. However, a recent study comparing 11 monocularly deprived rhesus monkeys with normal controls (Headon, Sloper, Hiorns and Powell, 1981b) indicates that lid closure between

three months and one year causes a 20% reduction in the size of cells in deprived parvocellular layers and a 14% decrease in non-deprived cells. A slight change is found in cell size of deprived magnocellular laminae and no change in magnocellular non-deprived cells. Apparently, late monocular deprivation effects are manifest throughout the LGNd.

2. Electron microscopy.

The optic nerve terminals in LGNd of cat and monkey form distinctly large profiles which contain large round vesicles and pale mitochondira (Colonnier and Guillery, 1964; Szentágothai et al., 1966; Peters and Palay, 1966). Secondary degeneration is apparent in these terminals following optic nerve transection (Szentágothai et al., 1966). A second type of axonal profile (the RSD of Guillery and Colonnier, 1970) is smaller and darker, with dense packing of round vesicles. Although these constitute approximately 50% of all terminals observed, their origin(s) is uncertain. Because they are more common in the general neuropil, where degeneration of small profiles is most frequently observed following occipital cortex lesions, they may represent, at least in part, corticogeniculate axons (Szentágothai et al, 1966; Jones and Powell, 1969; Pasik et al., 1973). Golgi type II interneurons have also been identified in the LGNd of monkey, surviving after complete occipital cortex removal. Dendritic processes of these remaining cells contain accumulations of synaptic vesicles (Pasik et al., 1973) and correspond to the F profiles of Guillery (1971) and the "presynaptic dendrites" described in the ventrobasal thalamus (Ralston and Herman, 1969) and LGNd (Famiglietti, 1970) of the cat.

The most characteristic synaptic relationship observed in the LGNd is a triadic arrangement in which a retinal afferent contacts the dendritic profile of a principal cell and an interneuron presynaptic dendrite, which in turn synapses on the same principal neuron (see Szentágothai, 1973). Triadic synapses are present

in glomerular as well as interstitial regions of the cat (Famiglietti and Peters, 1972) and monkey (Hámori, Pasik, Pasik and Szentágothai, 1974) LGNd. In the interstitial regions, the principal cell profile is usually represented by the soma or proximal dendrite, and the interneuron profile may be a presynaptic soma (Pasik et al., 1973; Hámori et al., 1974). In addition, serial and reciprocal synaptic arrangements involving interneuron presynaptic dendrites have been demonstrated using serial electron micrograph reconstructions (Pasik, Pasik and Hámori, 1977). The interstitial neuropil is also characterized by the presence of many small RSD profiles and by the absence of large dendritic elements (Guillery, 1969). Although several early studies comparing magnocellular and parvocellular laminae in monkeys (Campos-Ortega et al., 1968; Wong-Riley, 1972) failed to find marked differences in synaptic organization, more recent quantitative estimates in the mature macaque indicate that 15.6% of the neurons in magnocellular layers are interneurons, in comparison with 4.4% in the parvocellular region (Hámori, Pasik and Pasik, in press). In addition, presynaptic dendritic profiles are more numerous (Wilson and Hendrickson, 1981), and a higher proportion of retinal to presynaptic dendrite synapses (Winfield, 1980) and a lower percentage of retinal to principal cell dendrite synapses are present in the magnocellular layers, as compared to the parvocellular laminae.

In the cat (Cragg, 1975), most LGNd synaptogenesis occurs during the first postnatal month, although the ratio of symmetric to asymmetric synapses does not attain adult proportions until 60-70 postnatal days (Winfield, Headon and Powell, 1976). Quantitative studies of newborn, 1-, 2-, 4- and 8-week-old monkeys demonstrate the integrity of the dendritic and axonal arborizations of interneurons at birth, although the dendrodendritic synaptic element of the triadic arrangement does not begin to appear for two weeks. Over the first eight weeks, the number of presynaptic dendritic contacts increases, while the number of

contacts made by axonal elements of the interneurons simultaneously decreases (Hámori et al., 1975; Pasik et al., 1975). A preliminary quantitative analysis of synapses made by retinal afferent in the LGNd (Pasik et al., 1978) indicates that approximately 60% of the cumulative length of retinal to principal cell synapses present in the newborn is immature, as defined by the presence of membrane specializations without an accumulation of vesicles against the presynaptic thickening. The total length of immature synaptic profiles decreases over the first four weeks, with no change in the mature population. As the retinal terminals grow over subsequent weeks, the total extent of mature contact doubles, the cumulative length of retinal synapses on interneurons steadily increases, and immature synapses are no longer observed. Apparently, the immature contacts between retinal afferents and principal neurons present at birth fail to mature.

The paucity of information concerning postnatal morphologic development in the primate visual system is evident from the preceding literature review. Although retinal and LGNd neurogenesis, and retinogeniculate fiber ingrowth, occur primarily during the prenatal period, radical changes in ultrastructural organization are expressed during postnatal development. The aim of the present study was to provide normative ultrastructural data on the ontogeny of the retinogeniculate termination pattern, in order to extend current knowledge of the time course and magnitude of maturational changes in the visual nervous system. The discrete retinal projections to magnocellular and parvocellular LGNd laminae were examined independently, in an effort toward identifying differences in the developmental course of the transient and sustained functional pathways.

Electron microscopic data were used in the stereological reconstruction of retinal boutons and synapses in LGNd magnocellular lamina 1 and parvocellular lamina 6 of newborn, 1-, 2-, 4-, 8- and 17-week-old monkeys. For both layers in

all subjects, the following were determined at the ultrastructural level: (1) the size, density and absolute number of retinal boutons, (2) the size, density, number and maturational stage of retinal to principal cell, and retinal to interneuron synapses, (3) the size, density and number of retinal to principal cell nonsynaptic contacts, (4) the total area of synaptic contact, (5) the total area of nonsynaptic contact, and (6) the average number of synapses per retinal bouton. Qualitative observations were limited to descriptions of characteristic morphologic features of development present in the laminar neuropil at each postnatal age.

The quantitative analysis of development, based on the application of stereologic principles to electron microscopy, was thought to provide a more sensitive and informative index of maturation than qualitative observations allow. As a result, changes in ultrastructural organization were expected to emerge during the 17-week period surveyed, perhaps with different time courses in magnocellular and parvocellular laminae.

Chapter III

METHOD

A. Subjects and General Histologic Technique

The subjects were newborn, 1-, 2-, 4-, 8- and 17-week-old monkeys (M. mulatta), delivered to the laboratory at the precise age and perfused on arrival. The selection of the subjects' ages provided more resolution in the early developmental stages, in which maturational changes were expected to occur more rapidly. The age, gestation period, weight and sex of each animal are presented in Table 1. Although the study included one animal of each age for quantitative analysis, three additional subjects (newborn, one and 16 weeks old) were used for supplementary qualitative observations. The newborn and one-week-old monkeys used for quantification resulted from timed pregnancies and were delivered by Caesarean section on the 168th day of gestation. They were received by the laboratory on the same day or after one week for immediate sacrifice. Under deep barbiturate narcosis (50 mg/kg sodium pentobarbital, administered intraperitoneally), the axillary arteries and abdominal aorta were ligated; a catheter was inserted in the aorta above the ligature and toward the heart, secured and connected to the perfusion bottle. Heparin (300 units/kg) and a 3% solution of sodium nitrite (0.2 ml/kg) were pressure-injected before the fixative mixture (1% formaldehyde, obtained from paraformaldehyde and 1% purified glutaraldehyde in 0.12M phosphate buffer at pH 7.2-7.4 with 0.002% calcium chloride). The total volume of fixative was 1600 ml/kg; 80% of this was passed in the first 30 minutes and the remainder during the subsequent 60 minutes. Fluid was drained through the severed inferior vena cava. The monkey head was stored overnight in the same fixative at 4^0C. The following morning, one cerebral hemisphere was cut in 1 mm coronal slices through the LGNd using a stereotaxic instrument with a razor blade guided by an electrode carrier. Blocks

TABLE 1

POSTNATAL AGE, GESTATION PERIOD, WEIGHT and SEX OF SUBJECTS

Monkey Number	Age (in weeks)	Gestation Period (in days)	Weight (in grams)	Sex
1008	0	180	600	M
1020*	0	168	475	F
1009*	1	163	550	F
1018*	1	168	450	M
1013*	2	171	500	M
1010*	4	168	400	M
1007*	8	?	?	M
1006	16	?	?	M
873*	17	?	1000	F

*Used for quantitative analysis.

were dissected from the slices and collected in the same fixative. Each block, 2 mm x 0.8 mm x 0.5 mm, contained all six laminae and was shaped to aid orientation (Figure 1, right). After 1-2 hours, the blocks were washed 3 times in phosphate buffer, postfixed for 3 hours at 4^0C in a 2% osmium tetroxide solution in 0.12 M phosphate buffer containing 7% glucose and 0.002% calcium chloride. Specimens were dehydrated and flat-embedded in Epon-Araldite so that the coronal surface of the block face was available for sectioning.

B. Microtomy

Survey sections of the full block face, 1 µm thick, were cut with glass knives, mounted on microscope slides, stained with 1% toluidine blue with 1% sodium borate in distilled water, and examined with a light microscope to identify the laminae and assess the quality of the material (Figure 1, right). Well-perfused tissue was indicated by non-swollen nuclei, minimal extracellular space, and the absence of a gap between cytoplasm and unit membrane. From each animal, three blocks of well-fixed tissue containing adequate representation of all six laminae, without holes or embedding imperfections, were selected for ultramicrotomy. Because the original location of individual blocks within an LGNd was not known, it was considered essential to obtain L6 and L1 sections from the same blocks to minimize problems in data interpretation arising from topographical variations.

The surface of each selected block was trimmed to a "mesa": a three-dimensional trapezoid, approximately 50 µm high, cut from a preselected area of the block. The advantage of mesa trimming was that much of the underlying material remained intact for future use. In general, mesas of L6 material were obtained first. On average, 250 silver-gray sections (approximately 70 nm thick) of each mesa were cut with a diamond knife and mounted onto 10-14 copper 300-mesh grids. These sections were stained with 5% aqueous uranyl acetate and 0.15% lead acetate, and examined with an Hitachi 12A electron microscope.

The thin sections from most of the material were acceptable: free of knife marks, compression, holes, and stain deposits. Lead carbonate precipitate from the lead acetate staining was ubiquitous in the thin sections from two blocks, which were then re-cut (using the same mesa) and stained, and were then found acceptable. After obtaining the electron micrographs from the L6 material of a particular block, the mesa was leveled and the entire microtomy procedure was repeated for L1.

Electron-dense deposits were visible in the thin sections from both laminae of one animal (#873). Because this artifact was apparent in unstained tissue from a number of different blocks, each sectioned at several levels through the thickness of the specimen, the deposits were attributed to osmium tetroxide treatment. Although unsightly, this precipitate did not alter the configuration or integrity of the neuropil.

C. Electron Microscopy

Two types of electron micrographs were used in this study: prints for profile and contact analysis, and prints for neuropil quantification, i.e. determination of the percentage of neuropil within each lamina. Measurements from both sets were taken directly on the micrographs using an electronic graphics calculator (Numonics Corp., North Wales, Pa.) with 0.25 mm resolution. This instrument converts graphic measurements to either linear or areal digital data after the subject is traced with the associated pointer arm.

For profile and contact analysis, 12 micrographs of optimally fixed neuropil were taken from the thin sections of each mesa at a nominal magnification of 10,000X. The fields were chosen at a magnification and illumination too low to permit identification of individual profiles, but sufficient to judge the quality of fixation and tissue condition, lack of precipitates, and relative absence of cell

bodies, myelin, and blood vessels. To obtain a broad sample of the material, maxima of one micrograph/section and three sections/grid were established for the photography regimen. To ensure randomness, all grids were examined for suitable sections and all such sections were scanned for neuropil fields systematically in alternating sweeps from the upper left corner. From the set of 12 negatives derived from each block, the 8-9 with the highest proportion of well-fixed, accurately focussed neuropil were selected for printing and analysis. Since three blocks were similarly processed, this yielded an initial sample of 24-25 electron micrographs from each monkey-lamina. During the subsequent data analysis, sample variability of two monkey-laminae (#1010-L1 and #873-L6) was found unacceptably high (see below). In an attempt to decrease the variability, four additional micrographs from each of the three blocks were included in the analysis of these two cases, giving a total sample of 36-37 prints.

Two identical prints were made from each selected negative at the final precise magnification of 25,000X (see below). The sets allowed the profile identification and labeling to be conducted independently by two observers, each working with a separate series. A 204 mm x 153 mm rectangular outline, which at the chosen magnification corresponds to 50 μm^2 of tissue, was drawn on each print using a plexiglass template positioned consistently by alignment of the lower right corners of the template and print. Only these 50 μm^2 tissue area samples were included in the analysis and quantification. In addition, the prints from each lamina were randomized across ages, and assigned a code number. The complete micrograph code, with deciphering information on monkey, age, and lamina of origin, was stored on computer disk.

For neuropil quantification, i.e. to determine the proportion of neuropil in L1 and L6 of each animal, a separate group of random electron micrographs was obtained without regard for the presence or absence of cell bodies, myelin, or

blood vessels. The sample included 10 prints from each mesa, granting 30 prints for each monkey-lamina condition. To explore the full depth of each mesa, grids were selected from the beginning, middle and end of the cutting series. Again, maxima of one micrograph section and three sections/grid were established, and grids were scanned systematically to ensure randomness. Sections without holes, knife marks, or compression, and which fully covered a grid window were centered in the microscope and photographed at a nominal magnification of 6,000X. Using the calibration measurements (see below), all of these negatives were further enlarged in the printing process to precisely 18,000X. A 191 mm x 170 mm rectangular outline, corresponding to 100 μm^2 of tissue, was drawn on each print using a cardboard template positioned without bias, and only these 100 μm^2 tissue samples were included in the neuropil quantification.

Electron microscope calibration -- Because the total magnification of the profiles is critical to the stereological calculations, and because the nominal settings of the microscope are usually inaccurate, the actual magnification of a carbon diffraction grating replica of known periodicity (E.F. Fullam, Inc; 2160 lines/mm) was determined for the 6,000X and 10,000X nominal magnification settings used in the study. Since the actual magnification fluctuates over time and depends, in part, on the construction of individual grid specimen holders, the calibrations were repeated for each holder at regular intervals throughout the study (see Appendix 1). Using corresponding adjustments in the photographic enlargement of the negatives, exact and consistent final magnifications of 18,000x and 25,000X were obtained for all neuropil quantification prints and all profile analysis prints, respectively.

D. Electron Micrographs

In all phases of the analysis, the qualitative evaluation and quantification were completed and recorded before the randomized prints were decoded.

1. Profile and Contact Analyses

Each of the profile analysis prints was examined for features characteristic of ultrastructural development, such as growth cones, and signs of degeneration. In the latter case, an attempt was made to identify the profile involved as glial, axonal, or dendritic in nature. For the quantitative procedure, two observers, working independently with identical sets of micrographs, labeled all profiles of retinal origin recognized within the 50 μm^2 of tissue outlined on each print. Occasionally, preterminal and terminal regions of a retinal axon were visible in one profile; the preterminal area was excluded from measurement, which was restricted to bouton quantification. In addition, elements contacted by the labeled profiles were identified as belonging to principal or projective cell dendrites (P), or to interneuron dendrites (I). Following completion of the profile analysis by the initial observers, the two sets of micrographs were compared. The labeling differences, which amounted to less than 10%, were noted, and the prints submitted to a third investigator for resolution of the profile identification discrepancies. The retinal profiles recognized on each print were numbered, measured with the graphics calculator, recorded in data books and stored on computer disk.

All contacts made by the labeled retinal profiles were reviewed by one or two investigators, and were classified as synaptic or nonsynaptic in relation to the identified postcontact element. The synapses were further characterized as mature or immature on the basis of the presence or absence, respectively, of at least two synaptic vesicles adherent to the presynaptic membrane. The lengths of all synaptic and nonsynaptic contacts were measured with the graphics calculator, serially interfaced for direct data entry to an Apple II Plus microcomputer used for data storage and analysis.

2. Neuropil Quantification

The neuropil quantification prints were used to determine the proportion of neuropil present in L1 and L6 of each monkey. The area occupied by blood vessels, myelinated axons, and somata of neurons and glia was subtracted from the 100 μm^2 sample area delineated on each micrograph (see above). The remainder values were added across all prints for a condition, and that sum was expressed as a proportion of the total sample area. This ratio served as a correction factor for the bouton and contact densities derived from the profile and contact analysis prints, thus permitting the results to be expressed in terms of laminar, rather than neuropil volumes.

E. Quantitative Analysis

All quantitative procedures were performed with the assistance of the Apple microcomputer using Pascal programs written specifically for this project.

1. Sample Variability

A measure of sample variability was obtained from the net neuropil of the profile analysis prints. For each monkey-lamina, micrographs were grouped at random into four sets. The total retinal profile area and the total net neuropil sample area were determined for each set by summation across the values previously measured with the graphics calculator and stored on computer disk. The sample area was transformed from net to gross neuropil using the conversion factor obtained by the neuropil quantification procedure (see above). The area fractions (total retinal profile area/total sample area) of the four sets were computed, the mean and standard deviation of the four area fractions were calculated for each monkey-lamina. Standard deviations less than 30% of the mean were deemed acceptable (Anker and Cragg, 1974), a priori. Larger values were obtained in #1010 - L1 and #873 - L6, for which additional micrographs were added to the samples (see Tables 2 and 3). The tables also reveal that, in general,

Table 2. Variability of Neuropil Samples - Lamina 1

#1020 (Newborn)			#1018 (1 week old)			#1013 (2 weeks old)		
a	A	a/A	a	A	a/A	a	A	a/A
21.813	484.165	0.045	13.688	497.644	0.028	16.252	476.470	0.034
26.397	487.726	0.054	24.773	497.545	0.050	28.774	481.722	0.060
24.030	487.726	0.049	16.830	497.678	0.033	30.437	477.562	0.064
16.867	480.719	0.035	15.822	497.561	0.032	37.952	531.995	0.071
Mean		0.046	Mean		0.036	Mean		0.057
SD		0.007	SD		0.010	SD		0.014
SD as % of Mean		15.28%	SD as % of Mean		27.24%	SD as % of Mean		24.44%

#1010 (4 weeks old)			#1007 (8 weeks old)			#873 (17 weeks old)		
a	A	a/A	a	A	a/A	a	A	a/A
32.263	811.852	0.040	32.090	686.933	0.047	24.253	582.683	0.042
21.767	793.734	0.027	43.226	665.841	0.065	17.374	566.322	0.031
42.511	812.018	0.052	40.832	677.579	0.060	33.716	582.643	0.058
27.968	811.687	0.034	34.315	683.104	0.050	31.167	571.835	0.055
Mean		0.038	Mean		0.056	Mean		0.046
SD		0.009	SD		0.007	SD		0.011
SD as % of Mean		23.68%	SD as % of Mean		13.24%	SD as % of Mean		23.40%

Notes: a = total retinal bouton area (μm^2)
A = total gross neuropil sample area (μm^2)
a/A = area fraction
Notice that a larger sample was necessary for #1010.

Table 3. Variability of Neuropil Samples - Lamina 6

#1020 (Newborn)			#1018 (1 week old)			#1013 (2 weeks old)		
a	A	a/A	a	A	a/A	a	A	a/A
19.637	394.320	0.050	25.443	464.476	0.055	13.567	561.220	0.024
19.418	395.360	0.049	18.994	435.881	0.044	21.370	553.088	0.039
18.713	391.410	0.048	27.676	465.408	0.059	14.379	563.694	0.026
20.926	395.360	0.053	23.936	460.267	0.052	15.811	563.771	0.028
Mean		0.050	Mean		0.052	Mean		0.029
SD		0.002	SD		0.006	SD		0.006
SD as % of Mean		4.34%	SD as % of Mean		11.02%	SD as % of Mean		19.54%

#1010 (4 weeks old)			#1007 (8 weeks old)			#873 (17 weeks old)		
a	A	a/A	a	A	a/A	a	A	a/A
10.235	466.370	0.022	13.110	645.937	0.020	30.538	907.841	0.034
12.209	480.802	0.025	10.931	606.221	0.018	31.870	885.599	0.036
11.250	478.956	0.023	15.956	603.696	0.026	38.212	1005.864	0.038
9.593	471.254	0.020	11.576	637.879	0.018	29.361	877.585	0.033
Mean		0.023	Mean		0.021	Mean		0.035
SD		0.002	SD		0.003	SD		0.002
SD as % of Mean		8.18%	SD as % of Mean		16.47%	SD as % of Mean		6.01%

Notes: a = total retinal bouton area (μm^2)
A = total gross neuropil sample area (μm^2)
a/A = area fraction
Notice that a larger sample was necessary for #873.

the variability was considerably lower in the parvocellular laminae.

2. Stereological Procedure

Distributions of profile diameters were derived from the measured areas of profiles for each monkey-lamina. The size distributions of three-dimensional spherical bouton diameters were obtained from the profile diameter distributions using the method of Coupland (1968), as applied by Anker and Cragg (1974) to central nervous system structures. (For a detailed description of the stereological procedures, see Appendix 2). In short, this procedure corrects for the fraction of smaller profile diameters which are actually derived from larger boutons sectioned at a distance from their centers, and provides an estimate of the error introduced by profiles too small to be recognized in the electron micrographs. The weighted mean bouton diameter was obtained directly from the reconstructed distributions.

Bouton density (number of boutons/mm^3 of tissue) was calculated in two ways: using the method of Palkovits (1976), and the procedure of Anker and Cragg (1974). The Palkovits method is much simpler, but assumes that the boutons are all recognizable, uniform in size, and cubic in shape. Anker and Cragg's approach, although elaborate in computation, yields bouton size distributions, an indication of the number of missed profiles, and allows the separate calculation of density for each size range; it is, therefore, considered more accurate. The two alternative procedures were performed for direct comparison using the same data.

In order to compensate for the growth of the nucleus, an estimate of the total number of boutons in the magnocellular and parvocellular layers was calculated from the density values at each developmental stage. This was given by the product of density and total volume of the corresponding divisions of the LGNd (Gottlieb et al., 1981). In the latter study, volume estimates of the LGNd

were derived from camera lucida tracings of the cell laminae (the interlaminar zones were not included) appearing in equally-spaced Nissl stained coronal sections through the nucleus. The area measurements of the outlines were used to calculate the volumes by Simpson's rule (Tuttle and Satterly, 1925). The resulting values were further corrected by a previously determined factor to compensate for shrinkage occurring during the histological procedure.

The same size distribution reconstruction procedure (Coupland, 1968; Anker and Cragg, 1974) was used for the contact analysis to generate distributions of flat circular contact disks and their weighted mean areas for each monkey-lamina. The Anker and Cragg formulae were applied to determine the densities of mature and immature R to P and R to I synapses, and the density of R to P nonsynaptic contacts in L1 and L6 when sufficient data was available. Each of these density values was converted to an estimate of the absolute number of contacts using the laminar volume data (Gottlieb et al., 1981). In addition, the cumulative areas of mature and immature synaptic specializations and nonsynaptic contacts were calculated from the appropriate size distributions for each laminar type, as well as the average number of synapses associated with one bouton (synaptic density/bouton density).

Chapter IV

RESULTS

Qualitative Observations

The profiles of randomly-sectioned retinal boutons (R) are of variable size and shape, and are characterized by the presence of round vesicles, pale mitochondria with wide intercrestal spaces, and membrane specializations for synaptic and nonsynaptic contacts (Figures 2, 3, 4, 5, 7, 8, 9, 10, 11, 13 and 14) (for a review of the basis for identification of these profiles as retinal in origin, see page 20). In contrast, vesicles and membrane embellishments are not found in the preterminal axonal region, which is distinguished by streams of neurofilaments and microtubules with few, if any, other intracellular organelles. Occasionally, these preterminal features can be seen flowing into the core of a retinal bouton. When this occurs, the tubules and filaments occupy a central area of the profile, which is surrounded by vesicles and mitochondria typical of the preterminal fiber (for example, see Figure 14).

The dendritic profiles of principal cells (P) have been characterized at the ultrastructural level on the basis of indirect evidence (Szentágothai et al., 1966; Guillery and Colonnier, 1970; Hámori et al., 1974) and have been identified more recently by direct electron microscopic visualization of retrograde degeneration following total ablation of cerebral cortical areas 17, 18 and 19 (Hámori, Pasik and Pasik, in press). These profiles contain a dense population of various organelles, including large, dark mitochondria; ribosomes appearing freely scattered through the cytoplasmic matrix, or as polyribosomes, or in association with endoplasmic reticulum; and complicated cisternae. Small dendritic spines of these elements have a pale, organelle-free matrix, save for the infrequently observed convoluted membranes of a spine apparatus (Figures 4, 5, 8, 9, 10, 13 and 14).

Profiles of interneuron dendrites (I) are defined by a pale matrix supporting small mitochondria and few other organelles except scattered pleomorphic flattened vesicles (Figures 2, 3, 4, 5, 9, 11 and 14). Since elements of this description survive unaltered after both chronic and acute complete ablation of visual cortex (Pasik et al., 1973; Hámori et al., in press), they are considered to belong to interneurons. Spines do not occur along the dendritic processes of these neurons.

Many of the R to P, and all observed R to I contacts are synaptic, indicated by asymmetrical membrane thickening, widening of the synaptic cleft, and the presence of vesicles in the presynaptic element (Figures 2a, b, and c). Nonsynaptic R to P contacts are also apparent (Colonnier and Guillery, 1964), distinguished by a symmetrical junction with abundant filamentous material under the P membrane, and by a long, intermittent contact chain without associated vesicles (Figure 2d). However, the plaques at the borders of the chain are often synaptic, and usually appear immature in the nine animals examined qualitatively (Figure 2d). Nonsynaptic R to I contacts have not been observed in the LGNd.

The LGNd neuropil in both laminae of newborn and one-week-old monkeys appears to be densely packed with small profiles of irregular contour (Figures 3-6). Complicated cisternae are ubiquitous in axonal and dendritic elements, and multivesicular bodies are common. In general, the myelin sheaths are poorly developed, with few lamellar wrappings. Growth cones are occasionally observed, with small mitochondria in a filamentous cytoplasmic matrix full of convoluted membranous material (Figures 4 and 6). Streaming tubules and filaments are common within axonal and dendritic profiles, and persist even in the older animals. Signs of degeneration are apparent in glia, dendrites, and a few retinal boutons, manifest as hyperfilamentosis, accompanied by swollen mitochondria and vesicles (Figure 4).

Figure 2

Electron micrographs of retinogeniculate contacts. Scale at lower left applies to all quadrants of the figure and represents 0.5 µm. a. Mature retinal (R) to principal cell dendrite (P) synapse (arrow), characterized by asymmetrical membrane thickening, widening of the synaptic cleft and the presence of synaptic vesicles in the retinal profile with at least two vesicles adherent to the presynaptic membrane. The micrograph was obtained from L6 of a two-week-old monkey (#1013). b. Immature R to P synapses (ringed arrows), with less than two synaptic vesicles adherent to the presynaptic membrane, in L1 of a two-week-old monkey (#1013). c. Mature (arrow) and immature (ringed arrow) R to interneuron dendrite (I) synapses in L1 of an eight-week-old monkey (#1007). d. Nonsynaptic R to P contacts (arrowheads) and immature R to P synapse (ringed arrow) in L2 of a four-week-old monkey (#1010). In the nonsynaptic contact region, note the presence of filamentous material in the P profile.

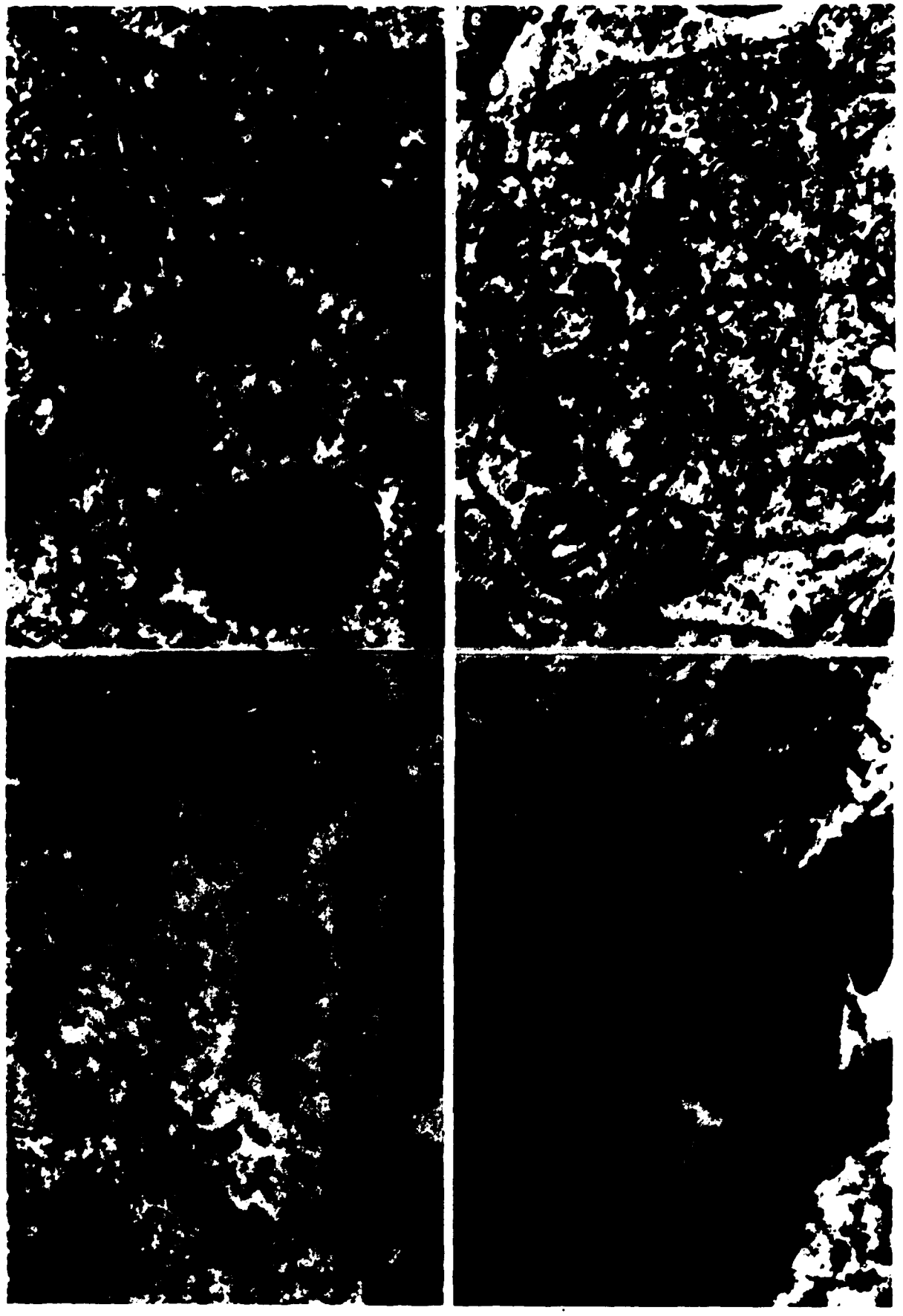

Figure 3

Electron micrograph taken at random from the L1 neuropil of a newborn monkey (#1008). Retinal profiles (R) can be seen making mature (arrows) and immature (ringed arrows) synapses, as well as nonsynaptic contacts (arrowheads), with principal cell dendritic (P) profiles and immature synapses with interneuron dendritic (I) profiles. A myelinated axon (MA) is present in the lower left corner. Note the dense packing of small profiles with irregular contours. X25,000.

Figure 4

Electron micrograph taken at random from the L6 neuropil of a newborn monkey (#1008). Notes as in Figure 3. Several principal cell dendritic spines (s) are observed in postsynaptic relation to R profiles. Hyperfilamentosis (H) is apparent in terminal and preterminal axonal profiles, and multivesicular bodies (mv) are present within several dendritic elements. In addition, a growth cone (GC) is visible within a filamentous cytoplasmic matrix full of convoluted membranous material. The portion of myelinated axon (MA) shown at upper right is a paranodal region, in which the lamellar wrappings terminate. X25,000.

Figure 5

Electron micrograph taken at random from L1 of a one-week-old monkey (#1018). Notes as in Figures 3 and 4. X25,000.

Figure 6

Electron micrograph taken at random from L6 of a one-week-old monkey (#1009). Notes as in Figures 3 and 4. A growth cone (GC) is present with small dark mitochondria, and convoluted cisternae and membranous material. X25,000.


G
M

Figure 7

Electron micrograph taken at random from L1 of a two-week-old monkey (#1013). Notes as in Figure 3. Multivesicular bodies (mv) are present within P elements, and dark degeneration of a presumably retinal bouton is apparent (R*), characterized by a dense cytoplasmic matrix, darkened mitochondria and the presence of lysosomes. X25,000.

Figure 8

Electron micrograph taken at random from L6 of a two-week-old monkey (#1013). Notes as in Figures 3 and 4. The retinal profiles have smoother contours, suggesting maturation of the neuropil. X25,000.

Figure 9

Electron micrograph taken at random from L1 of a four-week-old monkey (#1010). Notes as in Figures 3 and 4. Degeneration, manifest as hyperfilamentosis with swollen mitochondria and vesicles, can be seen in one retinal profile (R*). X25,000.

Figure 10

Electron micrograph taken at random from L6 of a four-week-old monkey (#1010). Notes as in Figures 3 and 4. The profiles appear smoother in contour and less densely packed than in the younger animals. X25,000.

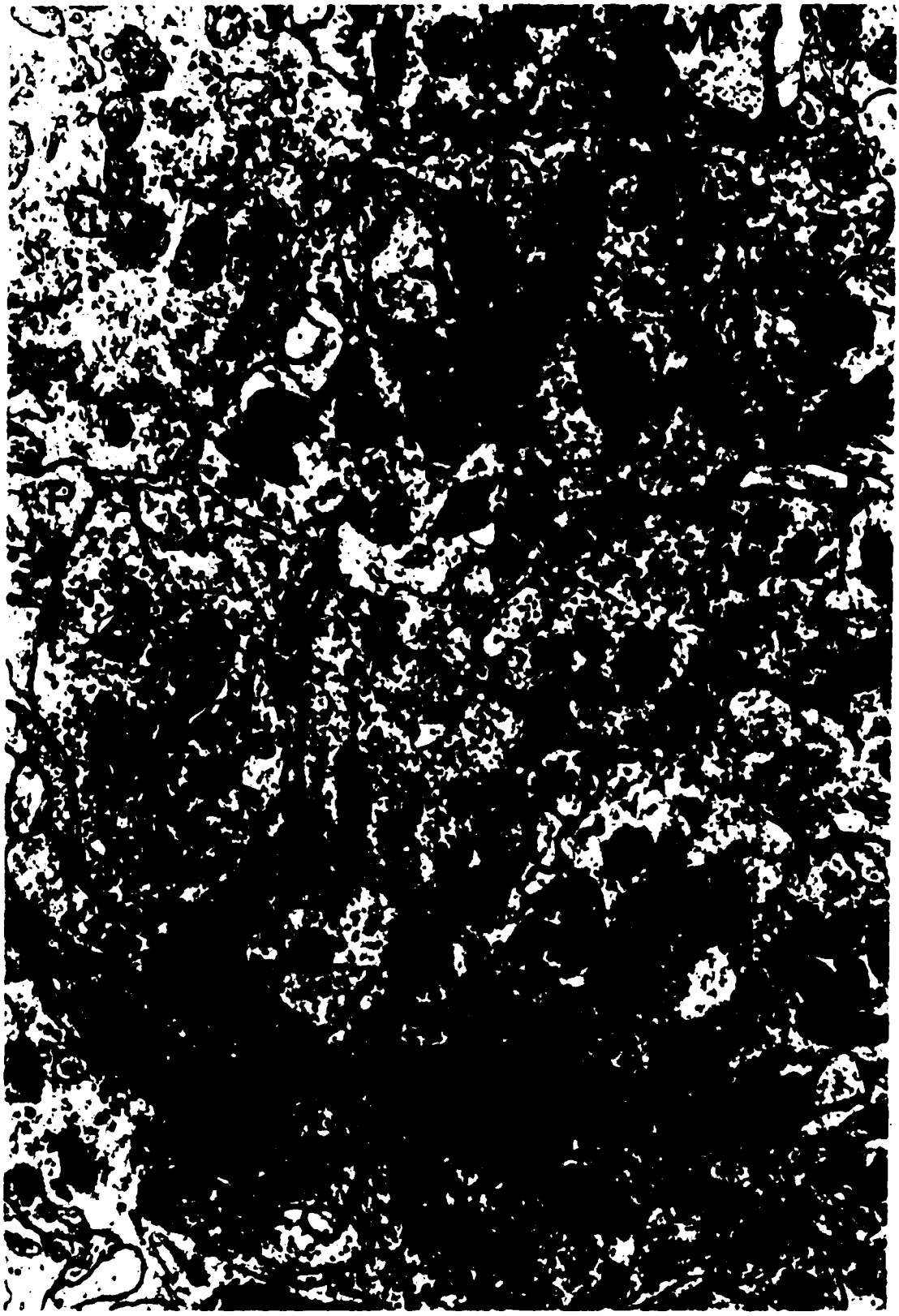

Figure 11

Electron micrograph taken at random from L1 of an eight-week-old monkey (#1007). Notes as in Figures 3 and 4. Large retinal (R), principal cell dendritic (P) and interneuron dendritic (I) profiles are apparent in the neuropil, as well as myelinated axons (MA). X25,000.

Figure 12

Electron micrograph taken at random from L6 of an eight-week-old monkey (#1007). Notes as in Figure 3. Preterminal degeneration (R*) is visible within a myelinated axon probably of retinal origin, suggesting incomplete ultrastructural development. Note the presence of synaptic vesicles within the dark, degenerated cytoplasmic matrix. X25,000.

Figure 13

Electron micrograph taken at random from L1 of a 17-week-old monkey (#873). Notes as in Figures 3 and 4. In general, the neuropil appears fully mature, containing large profiles with smooth contours. X25,000.

Figure 14

Electron micrograph taken at random from L6 of a 17-week-old monkey (#873). Notes as in Figures 3 and 4. Notice the core of preterminal filaments (f) within a retinal profile. By tracing the borders of the core, such regions were excluded from measurement, which was restricted to bouton quantification. X25,000.

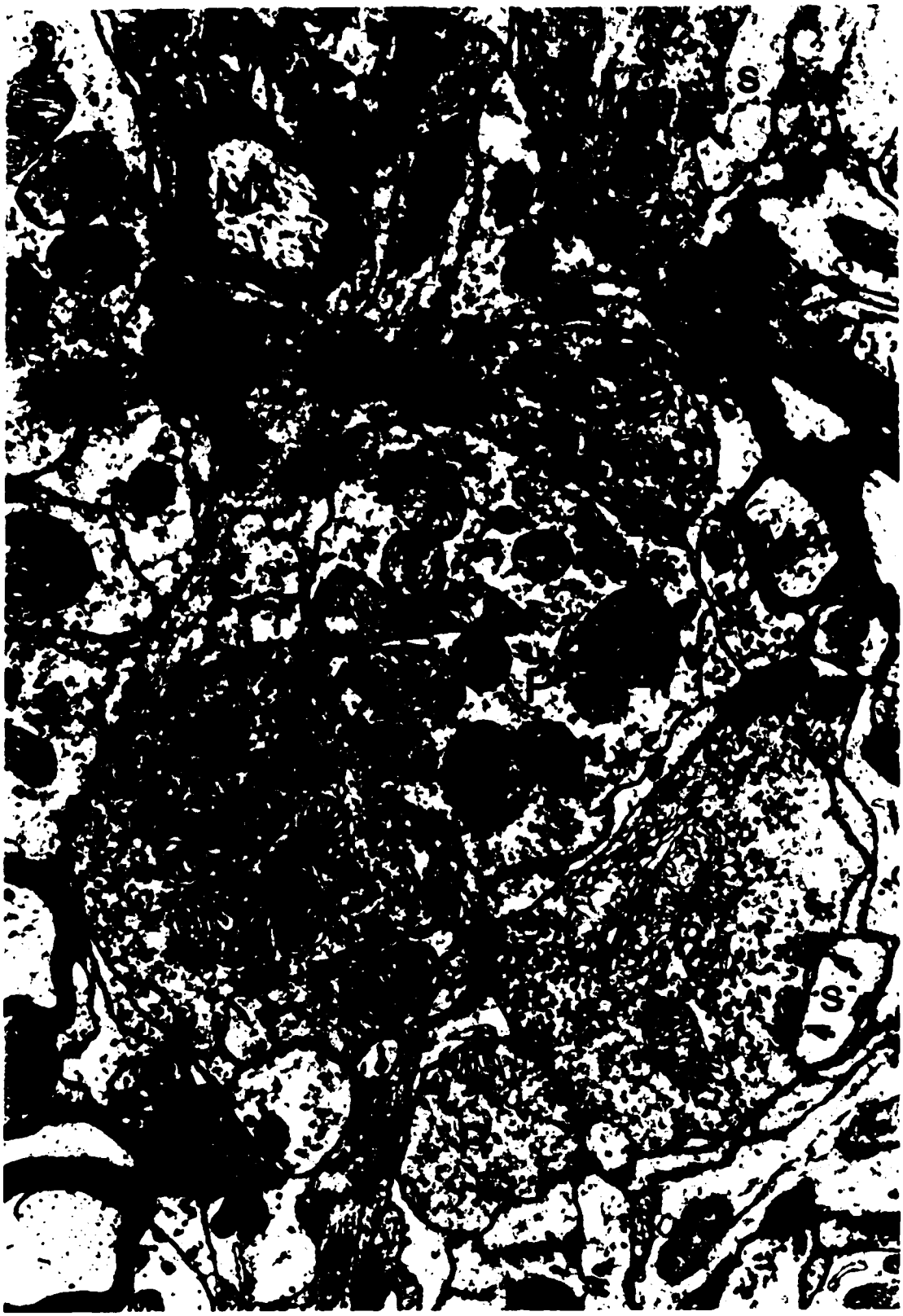
S
S

In the two- and four-week old monkeys, the constituents of the neuropil appear larger and smoother in contour (Figures 7-10). Myelinated axons are more prevalent, the myelin sheaths are thicker, and the terminal boutons are more densely packed with synaptic vesicles. Presynaptic dendritic elements are first apparent in L6 of the two-week-old animal. However, hyperfilamentosis (Figure 9) and dark degeneration, characterized by dark, dense profiles (Figure 7) are still observed in retinal boutons.

Characteristic features of ultrastructural development persist in the eight- and 17-week old animals (Figures 11-14). Although the profiles appear large and rounded as in the adult LGNd, and thick myelinated axons are present (Figures 11, 13 and 14), retinal preterminal degeneration is apparent (Figure 12). At the qualitative level, no salient differences are noticeable between magnocellular and parvocellular neuropil.

Quantitative Analysis

The quantitative analysis of retinal boutons, and synaptic and nonsynaptic contacts made by these terminals, was performed independently on tissue from L1 and L6. The data is presented separately for magnocellular and parvocellular layers, with emphasis on similarities and differences in organization of the two laminar types.

A. Retinal boutons

For the purposes of this analysis, retinal boutons are defined as the three-dimensional elements derived from the stereologic reconstruction of retinal profiles. Retinal profiles are the two-dimensional representations of retinal boutons identified in the electron micrographs. The results reported below arise from the quantitative analysis of data from six animals, each of a different postnatal age.

The size-frequency distributions of retinal profiles and boutons at all ages,

derived from the stereologic method of Coupland (1968; see Appendix 2), are presented for L1 and L6 in Figures 15 and 16, respectively. Eight size categories are selected as the maximum number of intervals which give a full distribution for every condition in all but the smallest diameter class. In each case, the stereological reconstruction of bouton diameters results in a shift of the entire distribution toward the larger diameters with respect to the corresponding profile distribution. The negative values in some of the bouton distributions occurring in the smallest diameter class, provide an estimate of the number of unrecognized elements, represented by profiles too small to be identified as retinal in origin. The absence of negative remainders in some conditions (L6 at eight and 17 weeks, L1 at birth) suggests that profiles with diameters near the upper limit of the lowest interval were recognized and counted in these cases. These histograms demonstrate the usefulness of the Coupland method in providing a more accurate description of the bouton population than that derived solely from areal measurements.

The mean bouton diameter at each age, obtained as a weighted mean from the reconstructed bouton distributions, is shown in Figure 17. Boutons in L1 fluctuate in average size over the first two postnatal weeks, and then stabilize around 1.7 μm in diameter. Those in L6 remain fairly constant in size during the first two weeks, tend toward smaller diameters (1.1 μm) until eight weeks, and subsequently incline toward larger size. The mean diameter is significantly larger in L1, as compared with L6, for the newborn ($t = 2.619$, $p < 0.05$), two-week-old ($t = 6.603$, $p < 0.01$), four-week-old ($t = 5.500$, $p < 0.01$) and eight-week old animals ($t = 5.075$, $p < 0.01$). In general, the major changes in this parameter occur earlier in magnocellular, and later in parvocellular layers.

Retinal bouton densities were calculated using the methods of Anker and Cragg (1974) and of Palkovits (1976) (see Appendix 2). As expected (Mayhew,

Figure 15

The size-frequency distribution of retinal profiles and boutons in L1 for each of the six ages studied, using eight diameter classes. In general, the histograms are symmetrical at each age. In each case, the stereological reconstruction of bouton diameters results in a shift toward the larger diameters of the entire distribution with respect to the corresponding profile distribution. Note that negative values, indicative of unrecognized retinal profiles, are present in all but the newborn case.

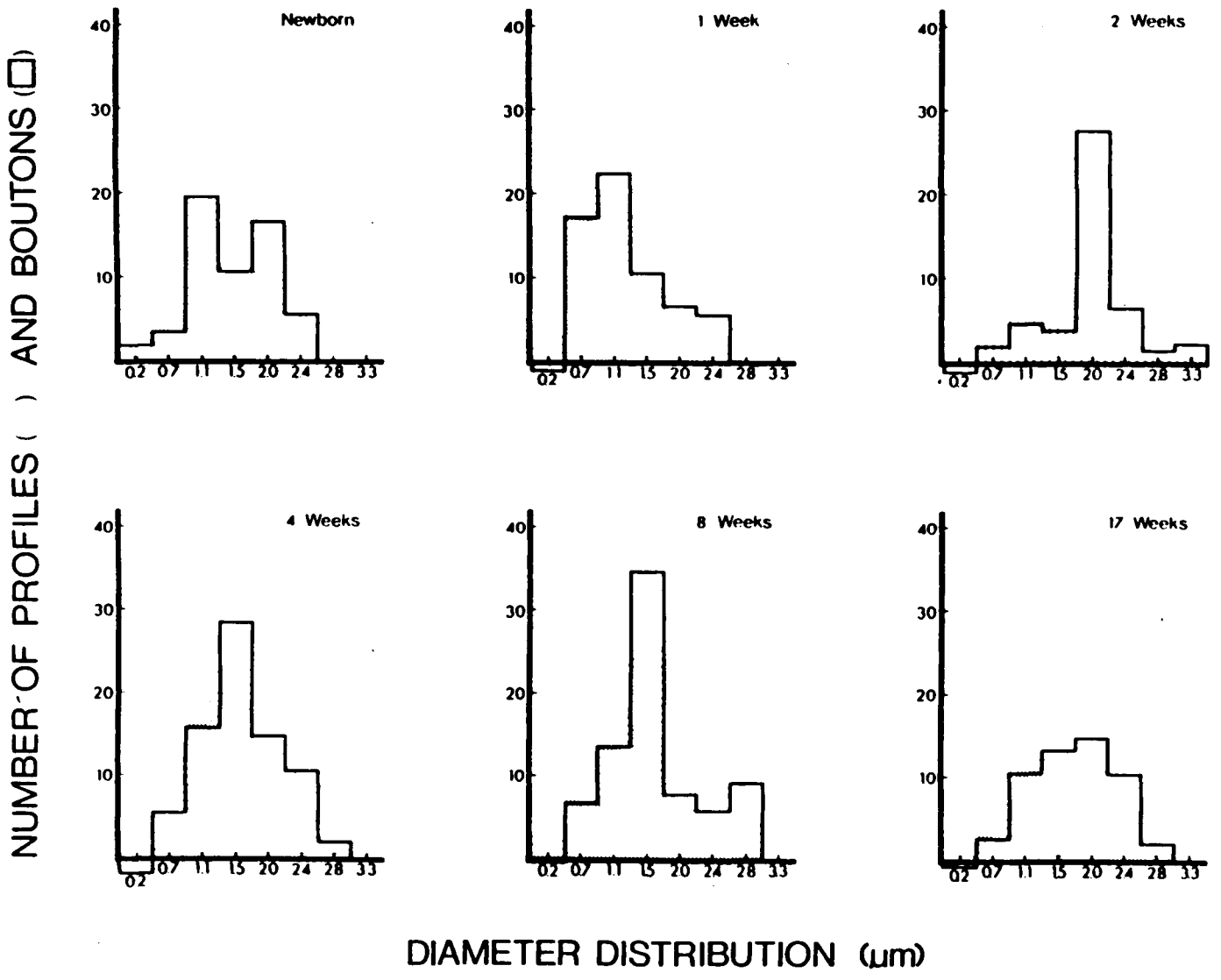
NUMBER OF PROFILES ( ) AND BOUTONS (□)
Newborn
1 Week
2 Weeks
4 Weeks
8 Weeks
17 Weeks
40
30
20
10
0.2 0.7 1.1 1.5 2.0 2.4 2.8 3.3
DIAMETER DISTRIBUTION (µm)

Figure 16

The size-frequency distribution of retinal profiles and boutons in L6 for each of the six ages studied, using eight diameter classes. Notes as in Figure 15, except that negative values are present in all but the eight- and 17-week-old animals.

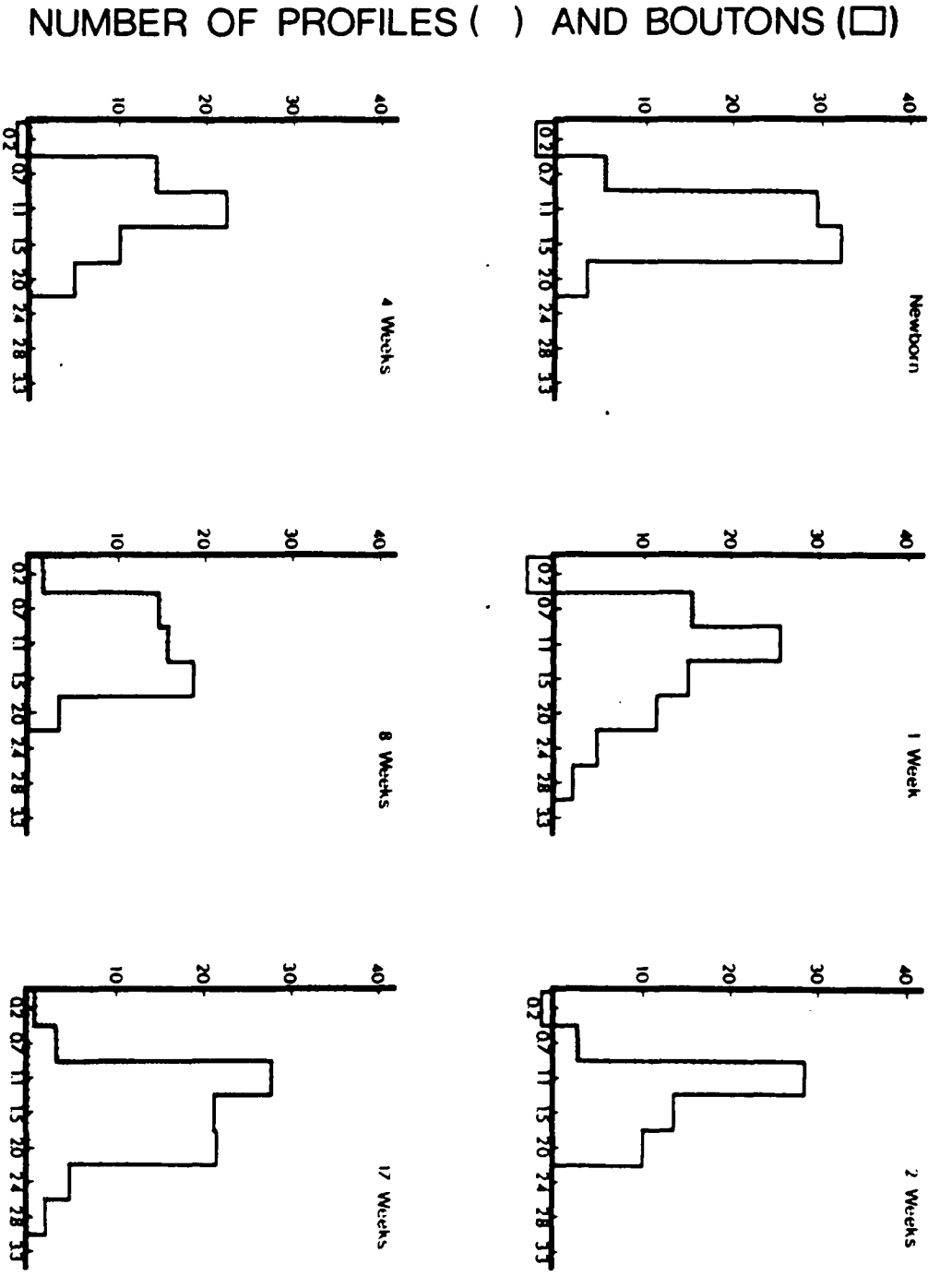
NUMBER OF PROFILES ( ) AND BOUTONS (□)
Newborn
1 Week
2 Weeks
4 Weeks
8 Weeks
17 Weeks
10
20
30
40
0.2
0.7
1.1
1.5
2.0
2.4
2.8
3.3
DIAMETER DISTRIBUTION (µm)

Figure 17

Mean retinal bouton diameter in L1 (solid line) and L6 (dashed line) at each age. Points in the curves are weighted means from the size-frequency distributions. The vertical segments represent the standard errors. Dependent t-tests showed significant differences at the ages marked by single ($p < 0.05$) or double ($p < 0.01$) asterisks.

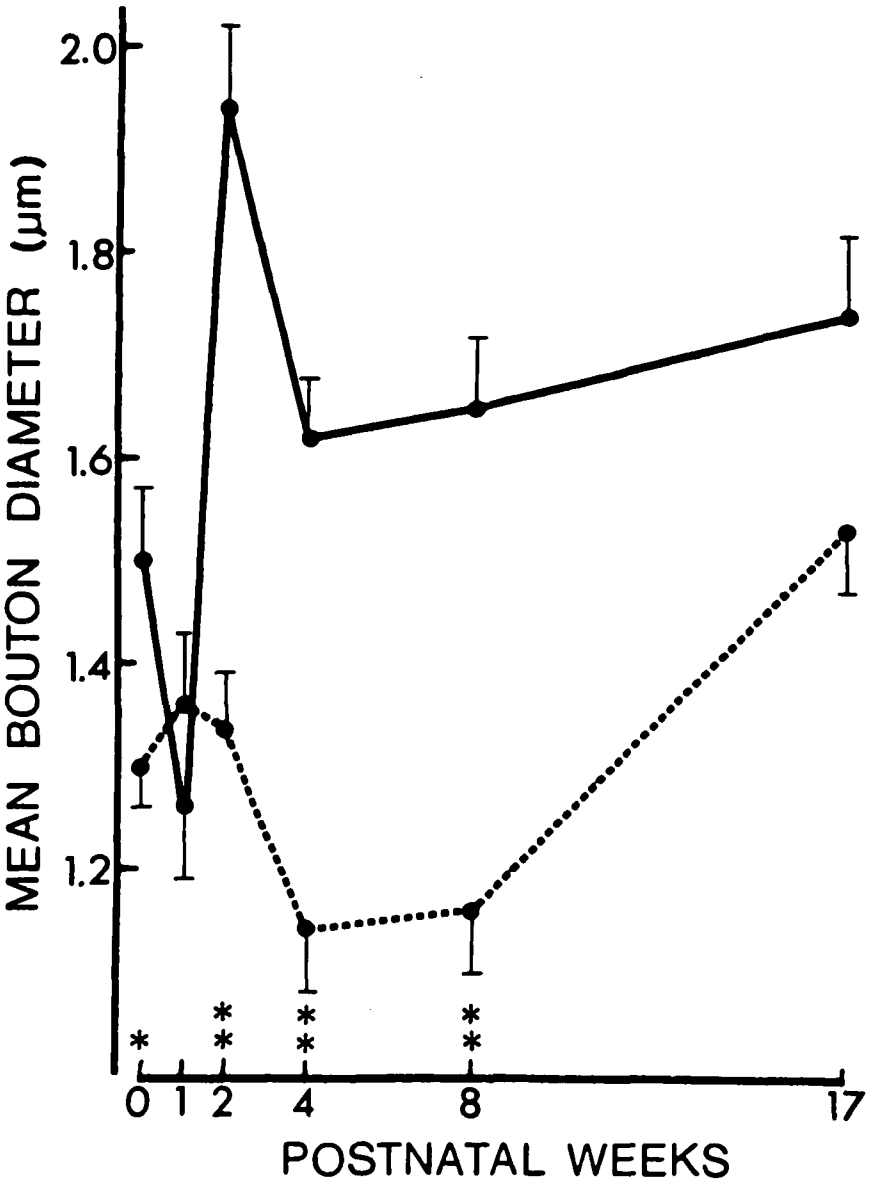
MEAN BOUTON DIAMETER (µm)
2.0
1.8
1.6
1.4
1.2
*
**
**
**
0 1 2 4 8 17
POSTNATAL WEEKS

1979), the functions are similar in form, and the Palkovits procedure yields values which are elevated by, on average, 21.5% in L1 and 24% in L6. Based on the Anker and Cragg approach, peak density of 2.26 $x10^7$ boutons/mm^3 of tissue in L1 occurs at one week (Figure 18, left) and, after a precipitous drop, a secondary peak (1.64 $x10^7/mm^3$) appears at eight weeks before the density returns to a lower level in the oldest animal. A similar two-stage process is apparent in L6 (Figure 18, right), although the primary peak density (2.93 $x10^7/mm^3$) occurs at birth and the secondary peak (2.02 $x10^7/mm^3$) at four weeks. At every age studied, the density of retinal boutons is greater in L6 than in L1 and, based on the differential times of peak proliferation, development in L6 precedes that in L1.

It should also be noted that the most dramatic changes occur in the younger animals. These results are consistent with the expectation that the density of a specific neuropil component decreases during development, due to the disproportionate growth of other constituents of the neuropil, as well as myelinated axons and the capillary network.

To compensate for laminar growth, estimates of total number of boutons in magnocellular and parvocellular LGNd regions were calculated from the density values using the laminar volume data obtained either from the same animals (#1020, #1018) or from monkeys of the same postnatal ages (Gottlieb et al., 1981). In the magnocellular layers (Figure 19, left), bouton number is greatest (19.8 $x10^7$) at one week, least (6.1 $x10^7$) at two weeks, and shows a smaller peak in the eight-week-old monkey. In the parvocellular region (Figure 19, right), the number of boutons also reaches maximum at one week (111.7 $x10^7$) and minimum (60.5 $x10^7$) at two weeks, with a secondary peak at four weeks. In general, the forms of these two functions reliably follow those of bouton density, suggesting that the previously observed decrease in density is due more to a reduction in bouton number than to a relative increase in laminar volume. The only notable

Figure 18

The density of retinal boutons at each age, obtained using the stereological procedures of Palkovits (dashed lines) and Anker and Cragg (solid lines). Although the two stereological approaches yield similar functions across development, the values derived from the Palkovits method are consistently higher. Left: Data from L1. Two peaks, at one and eight weeks, are incorporated within the overall decline in bouton density during maturation. Right: Data from L6. The periods of peak bouton density occur at birth and at four weeks.

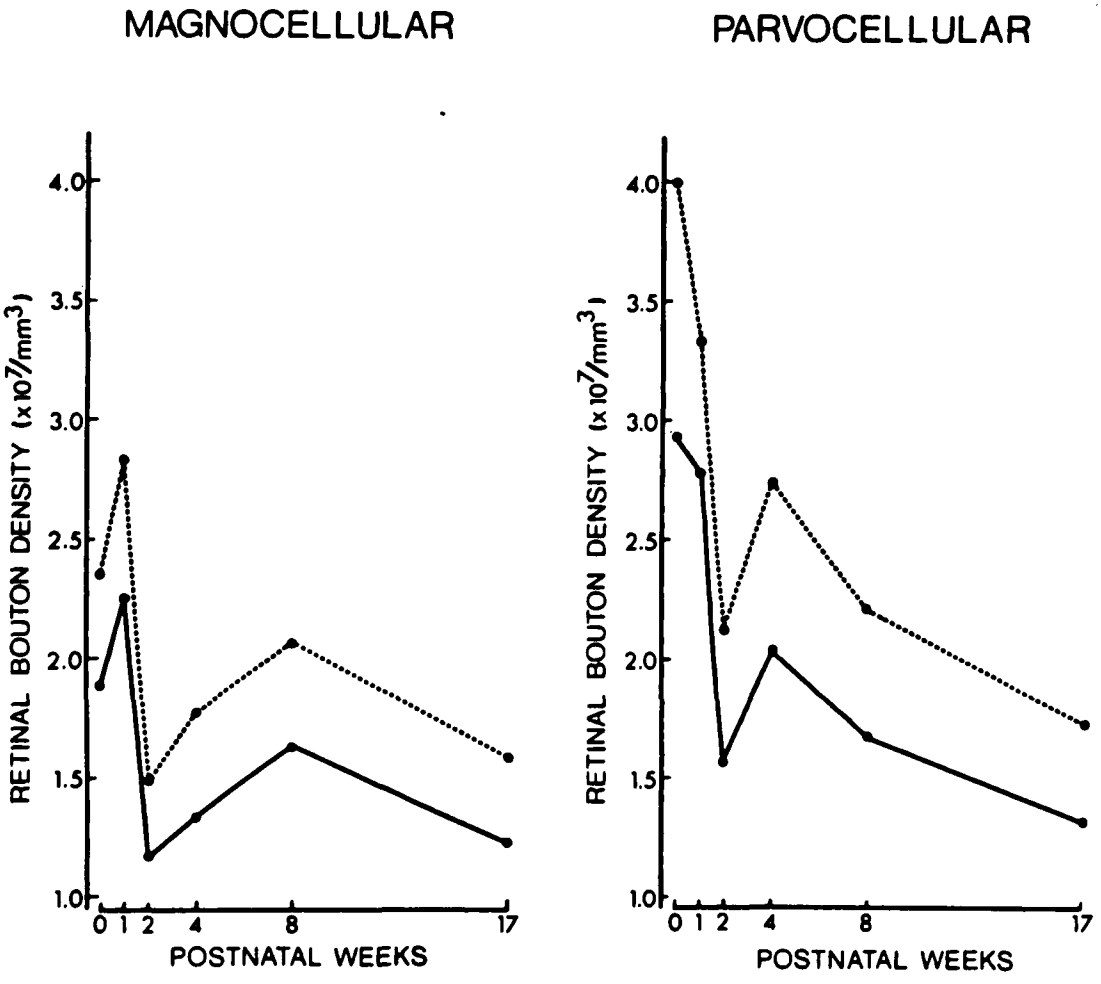
MAGNOCELLULAR
PARVOCELLULAR
RETINAL BOUTON DENSITY (x 10⁷/mm³)
4.0
3.5
3.0
2.5
2.0
1.5
1.0
0 1 2 4 8 17
POSTNATAL WEEKS

Figure 19

The estimated number of retinal boutons at each age. Each point represents the product of bouton density and the corresponding laminar volume. Left: Data from magnocellular laminae. The form of this function reliably follows that of Figure 18 left, and indicates that changes are more marked during the first four postnatal weeks. Right: Data from parvocellular laminae. The form of this function follows Figure 18 right, except for the primary peak shift to the one-week-old monkey. Note the dramatic decrease in bouton number which occurs during the first two postnatal weeks.

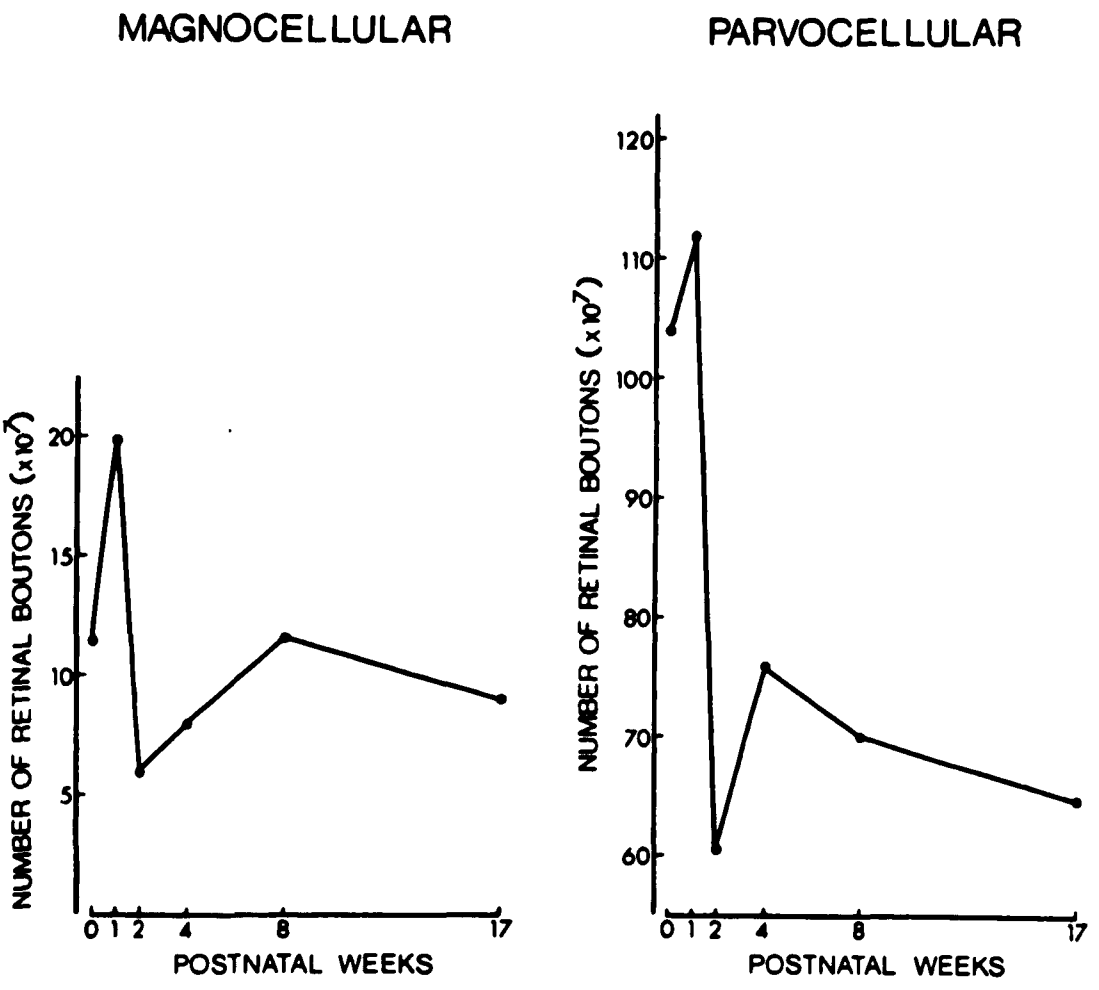
MAGNOCELLULAR
PARVOCELLULAR
NUMBER OF RETINAL BOUTONS (x10⁷)
20
15
10
5
0 1 2 4 8 17
POSTNATAL WEEKS
NUMBER OF RETINAL BOUTONS (x10⁷)
120
110
100
90
80
70
60
0 1 2 4 8 17
POSTNATAL WEEKS

difference is the primary peak shift from L6 bouton density, which is maximal in the newborn, to parvocellular bouton number, which is greatest in the one-week-old monkey. In any case, as with the developmental characteristics described previously, the major changes in total number of boutons occur during the first four postnatal weeks.

Although fluctuations in size and number are apparent throughout the course of retinal bouton development, the most salient aspect of this sequence is the decrease in bouton number observed during the first two postnatal weeks in both laminae. In the magnocellular region, a reciprocal relationship is indicated between average bouton diameter and bouton number. During the first postnatal week, the number of boutons increases substantially, but these boutons are of smaller size; from the first to the second week the number of boutons drops sharply, but those remaining are predominantly large. In the parvocellular layers, however, the changes in bouton number are not size-dependent: the small increase in number from newborn to one week is paralleled by a slight increase in average diameter, and no change in diameter is coincident with the substantial loss of boutons apparent between the first and second postnatal weeks.

B. Retinogeniculate Synaptic and Nonsynaptic Contacts

Estimates of the total number of contacts were obtained by the same stereologic procedure used for the retinal boutons. The density values (see Appendix 3), which do not take into account changes in the volume of the laminae, may be useful for heuristic purposes, but are misleading for data interpretation. Therefore, only the estimates of number of contacts are presented below, together with contact dimensions.

1. Magnocellular Laminae

In the magnocellular region, 52.1 $x10^7$ retinogeniculate synapses are estimated to be present at birth (Figure 20, top left). This value fluctuates over

Figure 20

The estimated number of mature (●——●) and immature (●·····●) synapses made by retinal boutons at each age. Each point represents the product of synaptic density and laminar volume. The number of all synapses in each graph (○——○) was obtained by summation of mature and immature values. Graphs are given separately for total number of synapses (left) and R to P synapses (right). Top: Magnocellular laminae. Note the consistent course of synapse elimination evident in the immature population. Bottom: Parvocellular laminae. Note that the greatest contribution to the observed synapse elimination results from a decrease in number of mature synapses during development.

MAGNOCELLULAR

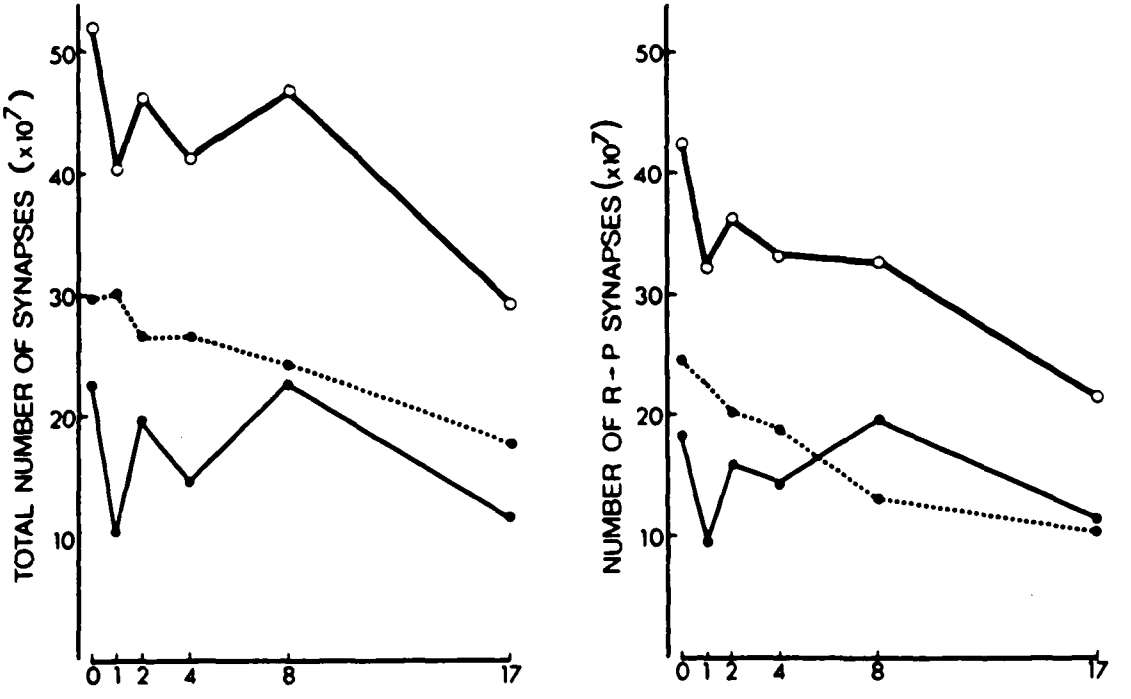

PARVOCELLULAR

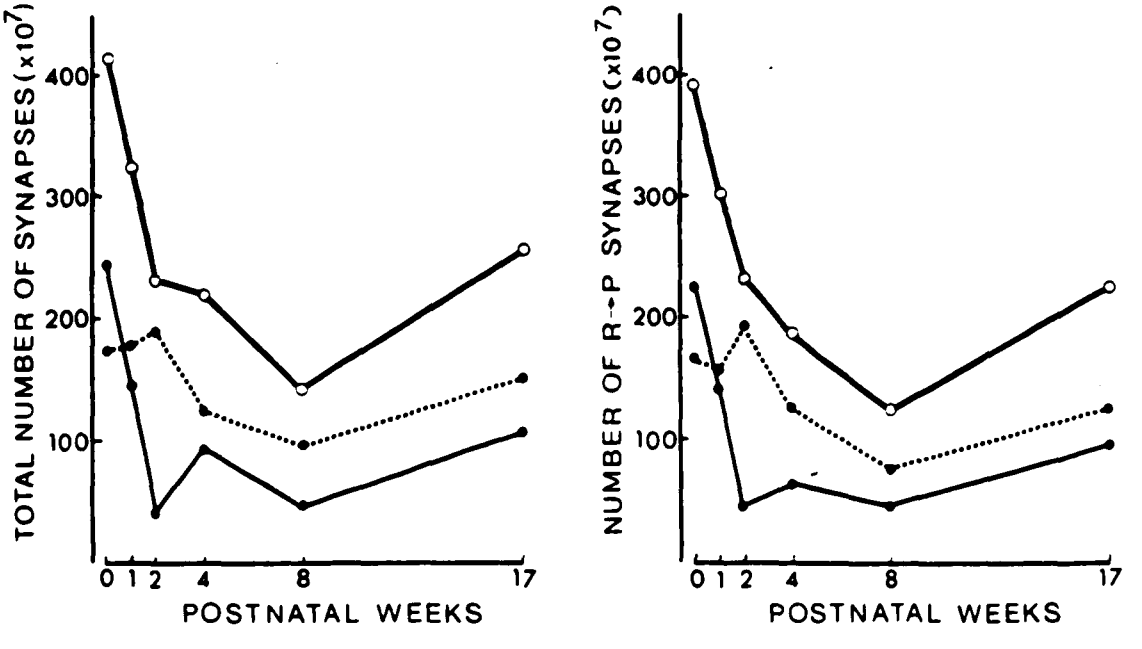

subsequent weeks; a main drop occurs after eight weeks and reaches 29.2 $x10^7$ synapses in the 17-week-old animal. This represents a net reduction of 44% in synapse number. A linear regression analysis reveals a significant correlation between age and total number of synapses ($r = 0.79$, $p < 0.05$). Some insight into the dynamics involved in this maturational sequence results from differentiating the changes of mature and immature synapses. At every age, there are more immature than mature contacts. Immature synapses decline in number almost monotonically, from 29.7 $x10^7$ in the newborn to 17.8 $x10^7$ at 17 weeks ($r = 0.98$, $p < 0.01$). The number of mature synapses varies widely, and no correlation is found with age ($r = 0.31$, NS). However, the value at 17 weeks (11.4 $x10^7$) represents a drop of 50% with respect to the complement present at birth. Taken together, these results demonstrate an ongoing process of synapse elimination which is especially consistent for immature synapses, but also involves the disappearance of mature elements, particularly evident after eight weeks.

In addition to the above analysis, R to P synapses were quantified independently (Figure 20, top right). In general, the change in number of the contacts during development mimics the progression just described for the total number of synapses in the magnocellular layers. R to P synapses decrease from 42.4 $x10^7$ at birth to 21.6 $x10^7$ at 17 weeks; their number is highly correlated with age ($r = 0.89$, $p < 0.01$). Immature synapses diminish monotonically from 24.3 $x10^7$ at birth to 10.2 $x10^7$ at 17 weeks ($r = 0.96$, $p < 0.01$). The number of mature synapses fluctuates over time, although by 17 weeks there is a decrease to 37% of the value at birth. It should be noted that the major period of R to P synapse elimination in magnocellular layers is evident in the older animals studied.

The difference between the total number of retinogeniculate synapses and the number of retinal to principal cell dendrite synapses represents the number of retinal to interneuron dendrite synapses, which were observed too

infrequently to justify an independent stereologic analysis. The total number of such synapses appears somewhat stable, (r = 0.42, NS), and increases from 19% to 24% of the retinogeniculate synaptic population over the 17-week period.

The mean area of the synaptic contact oscillates about the 0.1 μm^2 level during the first eight weeks, with a subsequent increase of almost 100% by the 17th week (Figure 21 top left). The proportion of synaptic disks which were missed because of their small size, represented by the negative remainders in the frequency distributions (Figure 15), is less than 8.5% across the ages examined (Table 4). The mature synapses are always larger than immature forms, which remain relatively stable in size over the period studied.

The total area of synaptic contact at each age is illustrated in Figure 21, top right. The total area of all synapses was obtained as the sum of the corresponding values of mature and immature synapses. These, in turn, were given by the product of mean area and number of synapses. The maximum contact area, 59 mm^2, exists at birth; a 47% reduction to 31 mm^2 occurs over the subsequent two weeks, with a gradual increase thereafter, which asymptotes beyond eight weeks at about 45 mm^2. The data reflects major developmental changes occurring during the early period examined. For the first eight weeks, this developmental pattern is also followed by the mature contacts. Beyond that age, however, mature synapses increase in total area with a corresponding decrease in that of immature synapses.

The number of synapses per bouton (Figure 22) given by the quotient of synapse density and bouton density (see above), attains a maximum of 7 in the magnocellular layers at two weeks, after which a gradual decrease brings the proportion to 3 synapses/bouton in the 17-week-old monkey.

Retinal boutons form nonsynaptic contacts only with principal cell dendritic elements. An estimate of the total number of these nonsynaptic

Table 4

Unrecognized Synaptic Disks

Lamina 1

Postnatal Weeks	Number of Negative Remainders	Total Number of Recognized Disks	Unrecognized Disks as % of Total Synaptic Disks
0	3.39	60.39	5.6%
1	3.26	38.25	8.5%
2	2.77	49.77	5.6%
4	3.25	74.25	4.4%
8	4.86	62.86	7.7%
17	0.99	38.99	2.5%
		Lamina 6	
0	5.14	76.12	6.8%
1	0.63	56.62	1.1%
2	0	49.00	--
4	0	39.00	--
8	0.31	28.30	1.0%
17	3.14	58.13	5.4%

Figure 21

The mean area (left) and total area (right) of synaptic contacts at each age, for mature (●——●), immature (●·····●), and all (○——○) synapses. For the mean area values, each point represents the mean surface area (πr^2) of the synaptic disks reconstructed from the stereologic analysis of the corresponding synaptic profile lengths. For the total area values, each point represents the product of mean area and number of synapses. Standard errors (vertical segments) are only given for the mean of all synapses. Top: Magnocellular laminae. Note that mature synapses are always greater in mean area than immature forms. Bottom: Parvocellular laminae. Note the sharp decrease in total area, primarily due to the decline in the area of mature synapses, over the first eight postnatal weeks.

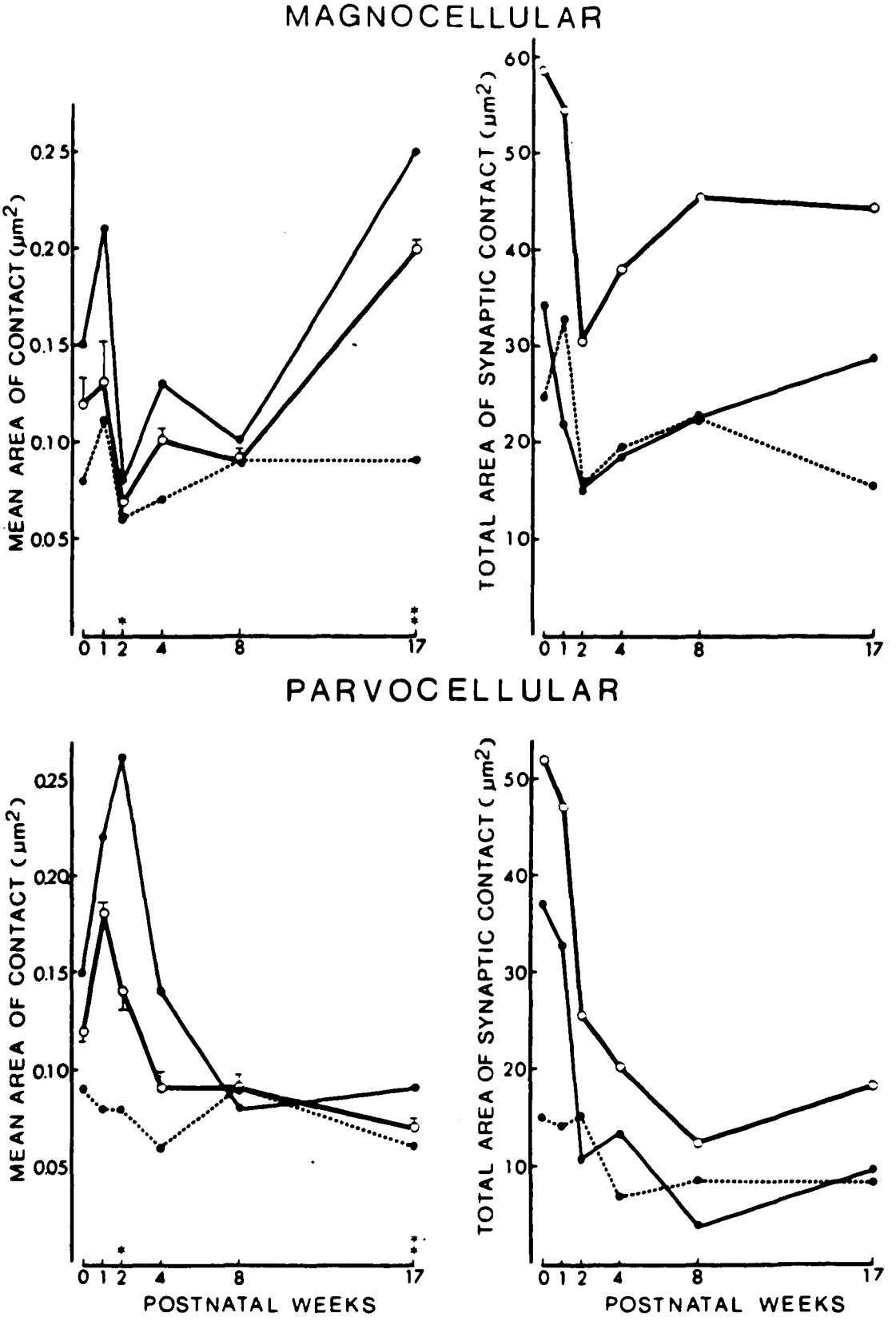
MAGNOCELLULAR
MEAN AREA OF CONTACT (μm²)
0.25
0.20
0.15
0.10
0.05
TOTAL AREA OF SYNAPTIC CONTACT (μm²)
60
50
40
30
20
10
0 1 2 4 8 17
PARVOCELLULAR
MEAN AREA OF CONTACT (μm²)
0.25
0.20
0.15
0.10
0.05
TOTAL AREA OF SYNAPTIC CONTACT (μm²)
50
40
30
20
10
0 1 2 4 8 17
POSTNATAL WEEKS
POSTNATAL WEEKS

Figure 22

The estimated number of synapses per retinal bouton in magnocellular (solid line) and parvocellular (dashed line) LGN laminae. Each point represents the quotient of synaptic density and bouton density for each age-lamina condition.

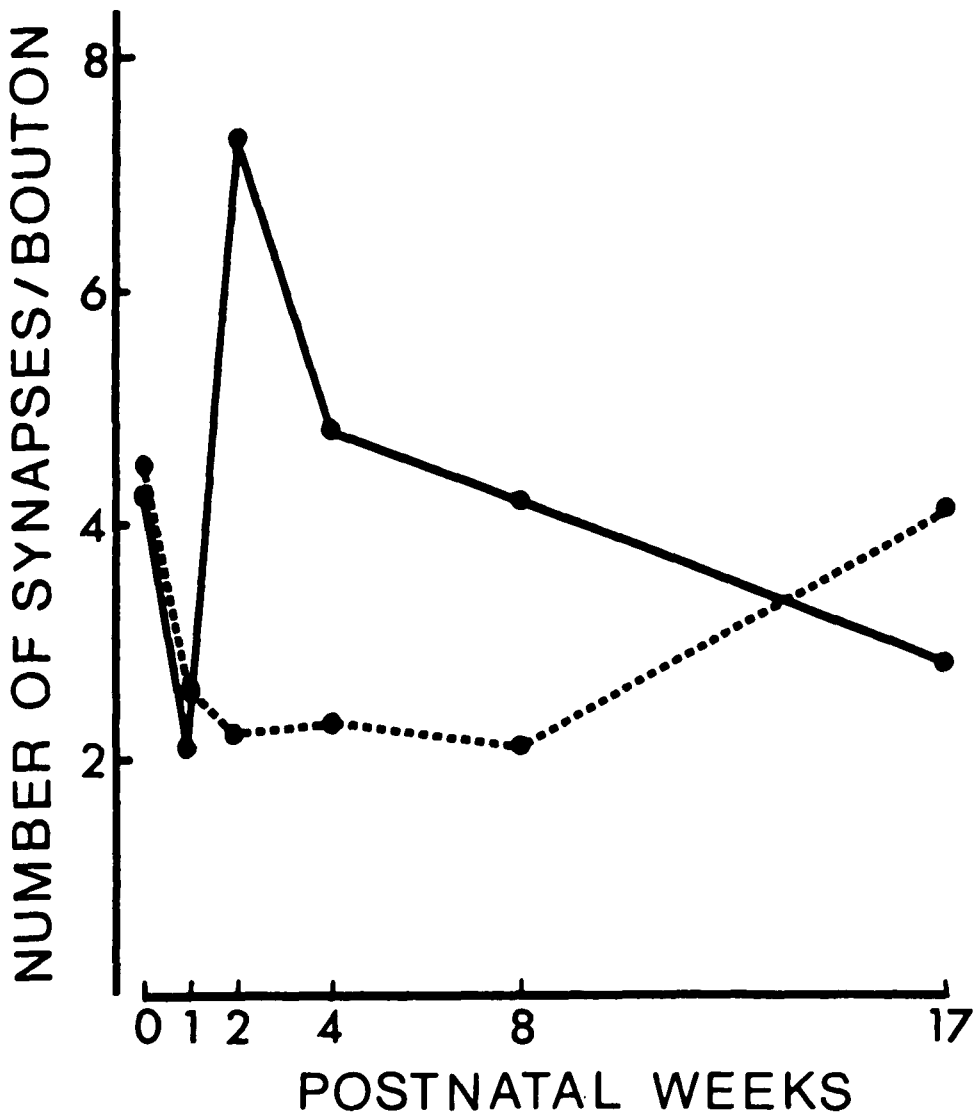
NUMBER OF SYNAPSES/BOUTON
8
6
4
2
0 1 2 4 8 17
POSTNATAL WEEKS

contacts was also obtained for each monkey (Figure 23). In the magnocellular layers, the number remains stable over the period surveyed (r = 0.4, NS), ranging from 11.4 $x10^7$ at birth to 8.7 $x10^7$ at 17 weeks. The mean area of nonsynaptic contact (Figure 24) shows a marked increase over the first four postnatal weeks. The total nonsynaptic contact area also increases from 32 mm^2 at birth to 93 mm^2 at 17 weeks (Figure 25).

2. Parvocellular laminae

In the parvocellular layers, the estimated number of retinogeniculate synapses is 415.5 $x10^7$ at birth (Figure 20, bottom left). This value decreases rapidly over the ensuing two weeks, more slowly until 8 weeks, and then increases, to attain the 17 week old level of 259.3 $x10^7$ synapses. This constitutes a 38% overall reduction in synapse number over the age range studied. The primary source of synapse elimination appears to be the mature synapses, which decline 55% from 241.7 $x10^7$ at birth to 108.3 $x10^7$ at 17 weeks, and follow the same developmental progression as the total. Although, in general, immature synapses are more numerous than mature ones, the net reduction from 173.8 $x10^7$ over the 17 week period is only 13%. Evidently, many of the mature synapses present in the parvocellular layers at birth do not survive. It should be noted that the developmental sequence of these contacts in the parvocellular laminae, in contrast with those of magnocellular layers, show the process of synapse elimination during the first eight weeks.

The number of R to P synapses during development (Figure 20, bottom right) differs only slightly in magnitude and form from the total number of synapses just described. At birth, 392.4 $x10^7$ synapses are estimated to be present and by 17 weeks 226.5 $x10^7$ remain; the number of mature synapses drops 82% from 227.7 $x10^7$ over the first two postnatal weeks, rebounding somewhat to 98.9 $x10^7$ at 17 weeks, while the number of immature synapses changes only 23% from

Figure 23

The estimated number of R to P nonsynaptic contacts in magnocellular (solid line) and parvocellular (dashed line) LGNd laminae. Each point represents the product of nonsynaptic contact density and laminar volume for each age-lamina condition.

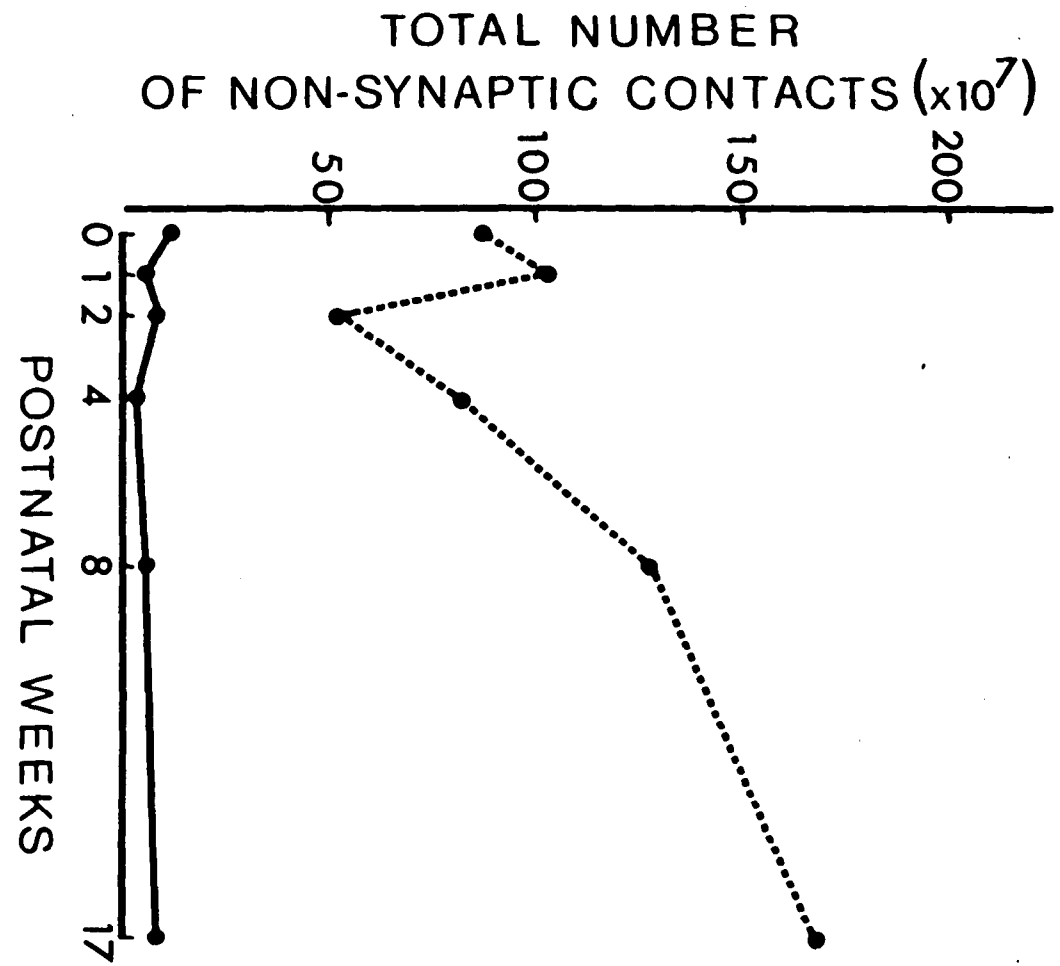
TOTAL NUMBER
OF NON-SYNAPTIC CONTACTS (x10^7)
50
100
150
200
0
1
2
4
8
17
POSTNATAL WEEKS

Figure 24

The mean area of nonsynaptic contact in L1 (solid line) and L6 (dashed line) at each age. Each point represents the mean surface area (πr^2) of the nonsynaptic contact disks reconstructed from the profile length data for each condition.

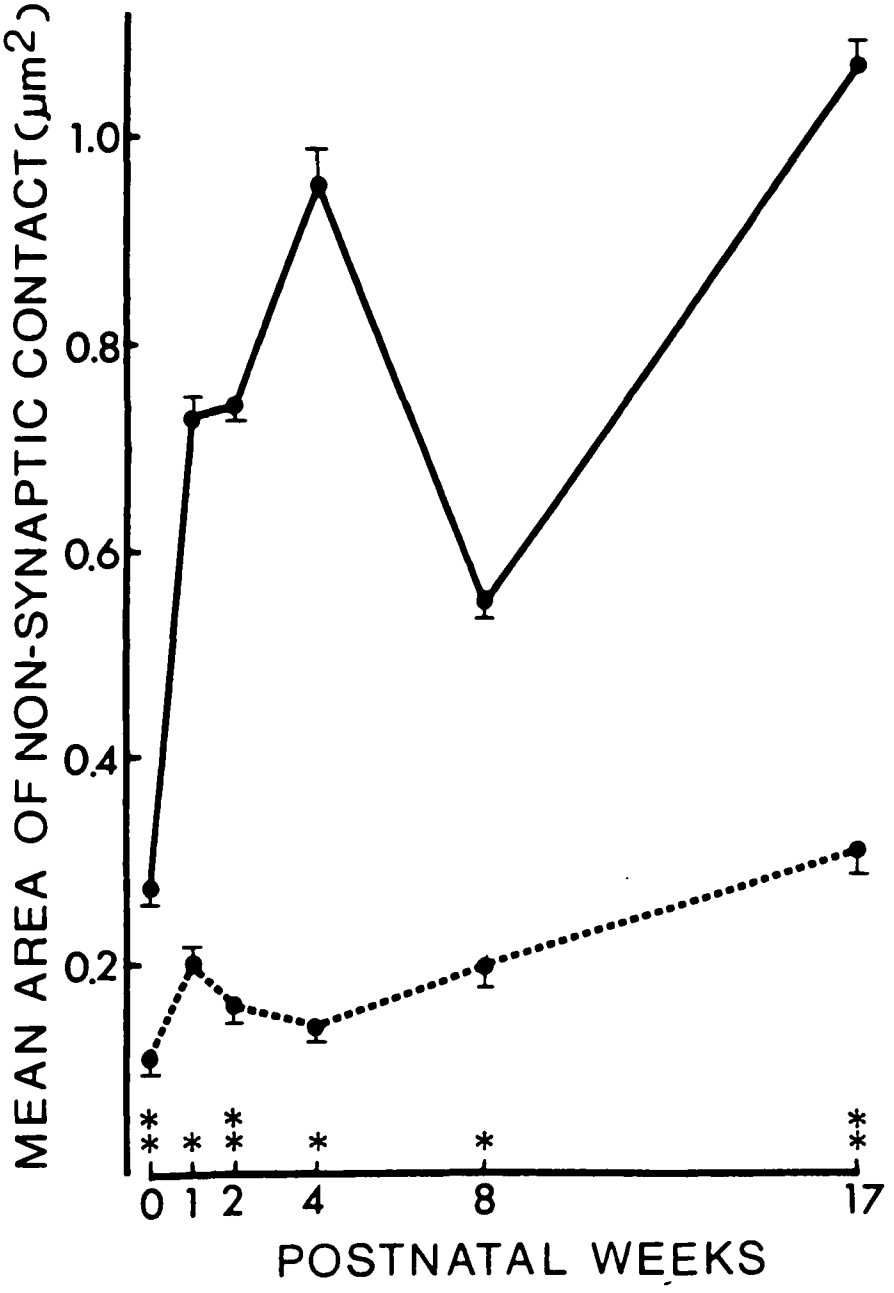
MEAN AREA OF NON-SYNAPTIC CONTACT (μm²)
1.0
0.8
0.6
0.4
0.2
0 1 2 4 8 17
POSTNATAL WEEKS

Figure 25

The total area of nonsynaptic contact in magnocellular (solid line) and parvocellular (dashed line) LGNd laminae. Each point represents the product of mean area and number of contacts. Note the divergence of the area values in the two laminar subdivisions after four weeks.

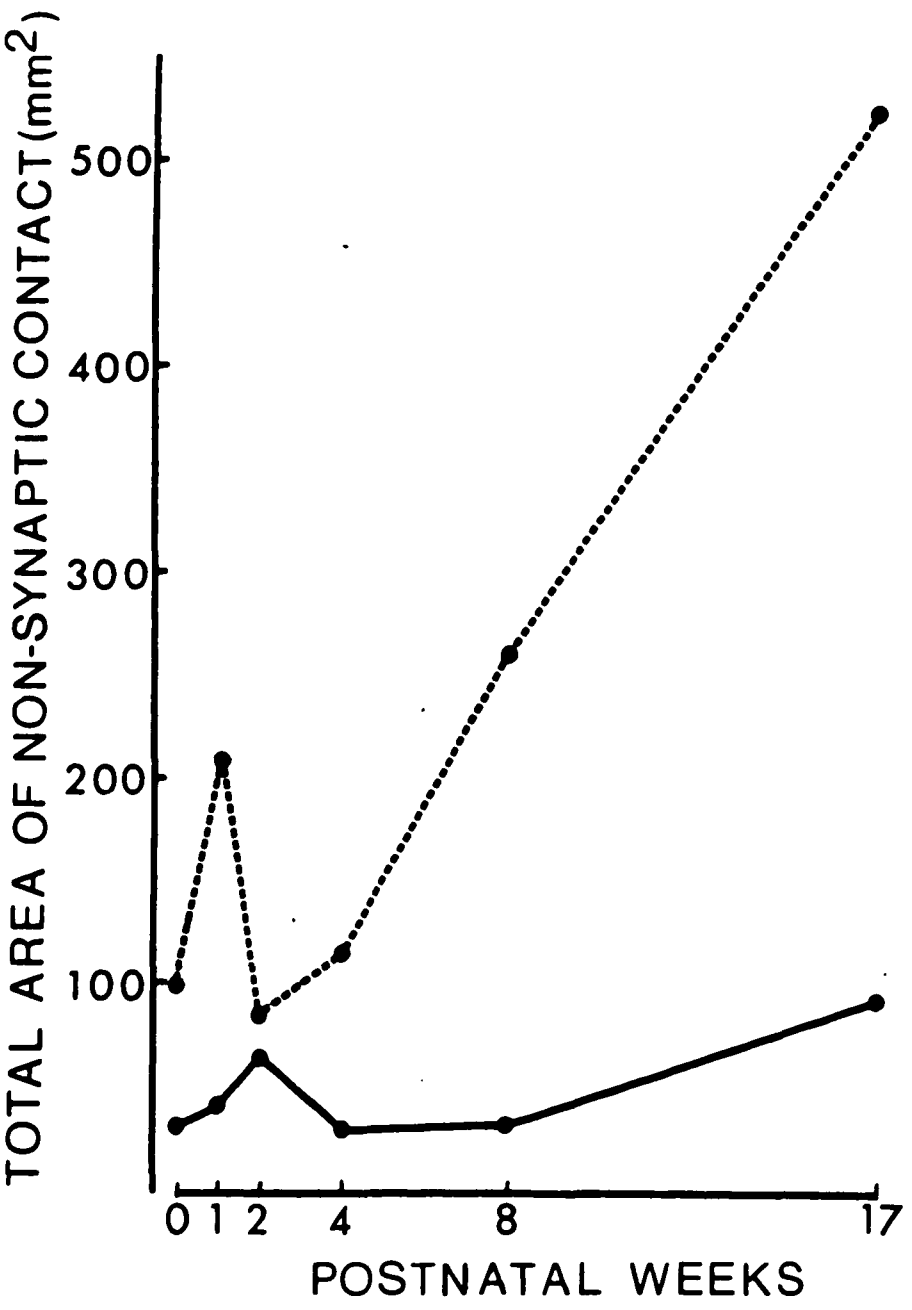
TOTAL AREA OF NON-SYNAPTIC CONTACT (mm²)
500
400
300
200
100
0 1 2 4 8 17
POSTNATAL WEEKS

164.7 $x10^7$ over the 17 week period. Here again, the major period of synapse elimination occurs during the first eight weeks, as opposed to the same process in the magnocellular LGNd which emerges after eight weeks.

An estimate of the number of R to I synapses is provided by the difference between the total number of synapses and total number of R to P synapses. Apparently, 6% of the synapses made by retinal boutons at birth involve I elements and this proportion increases to 13% after four weeks.

The mean area of the synaptic contact in L6 is greatest in the one week old animal (0.18 μm^2) and stabilizes around 0.08 μm^2 by four weeks (Figure 21, bottom left). The proportion of synaptic disks which were unrecognized because of their small size is less than 6.8% across all ages (Table 4). In general, the size of mature synapses follows the same progression as the total, while immature synapses remain fairly stable in mean area across development. A statistical comparison of mean area of contact in magnocellular and parvocellular layers across development reveals that synapses in magnocellular laminae are significantly larger only in the two- ($t = 2.354$, $p < 0.05$) and 17-week-old animal ($t = 4.733$; $p < 0.01$).

The total area of synaptic contact in the parvocellular laminae at each age is presented in Figure 21, bottom right. After a maximum of 519 mm^2 in the newborn, a decrease in contact area occurs over the subsequent four weeks, stabilizing thereafter. The developmental course of the total area of mature synapses parallels that of the whole, whereas the immature contacts only show a decrease between the second and fourth weeks. This pattern, from early maxima through substantial retraction, is reminiscent of the changes observed in both the number of synapses, as well as the average area of synapses in the parvocellular layers. Therefore, these latter two factors contribute to the form and magnitude of the function represented in Figure 21, bottom right. Although synapse

elimination occurs with a different time course in the two laminar types, stabilization occurs only after eight weeks in the magnocellular division.

The number of synapses per retinal bouton (Figure 22) decreases from 4.5 to 2.5 during the first postnatal week, and remains at this low level until eight weeks, when the number begins to climb, nearly reaching the newborn level by 17 weeks. This function represents an interaction between the changes in number of boutons and synapses. Although both decrease during the first week (Figures 19, right and 20, bottom left, respectively), synapse elimination is relatively more pervasive than bouton disappearance. During the period from eight to 17 weeks, bouton number decreases and synapse formation flourishes, resulting in the elevated number of synapses per bouton apparent by 17 weeks.

The total number of nonsynaptic contacts between retinal terminals and P elements increases radically after some transient changes from 54 $x10^7$ at two weeks to 169.4 $x10^7$ at 17 weeks (Figure 23). In general, the increase in number is accompanied by an increase in the average area of such contacts (Figure 24) which occurs after eight weeks, resulting in a dramatic overall increase in total contact area (Figure 25).

Chapter V

DISCUSSION

The results of the present study indicate that structural reorganization occurs in the visual nervous system of normal monkeys after birth. Such changes represent a continuation of the profound prenatal transformations previously noted in this species (Hendrickson and Rakic, 1977). In the retinogeniculate projection, the form and magnitude of these developmental alterations are apparent in both the magnocellular and parvocellular pathways.

Differential Development of Magnocellular and Parvocellular Laminae

Table 4 provides a summary of the major results.

Retinal boutons in the LGNd change in size, density and number during postnatal maturation. However, the most striking finding is a reduction in the number of boutons which occurs primarily during the second postnatal week, and results in over a 50% reduction with respect to the values at birth in both laminar types. This reduction is preceded by some proliferation which is more marked in parvocellular layers. In the magnocellular layers, this period of proliferation is coincident with a decrease in average bouton diameter, and the subsequent elimination of boutons occurs simultaneously with an increase in the mean size. That is, although small boutons proliferate and predominate in L1 during the first postnatal week, more of the larger elements survive in the older animals. In the parvocellular laminae, the reduction in number occurs without a concomitant shift in average diameter. It is possible that a mixed population of boutons is present in the magnocellular neuropil, and that the time course of changes in size and number reflect the differential development of larger and smaller elements. However, the retinal boutons of the parvocellular laminae appear to comprise a single class, with a consensual course of maturation. While the developmental

Table 5

Summary of Results

	Magnocellular	Parvocellular
	Boutons	
Number	67% ↑ from 0-1 50% ↓ from 1-2	8% ↑ from 0-1 >50% ↓ from 1-2
Mean diameter	17% ↓ from 0-1 30% ↑ from 1-2	Stable 0-2
	Synapses	
Number	44% ↓ from 0-17, mostly after 8 Immature ↓ 50% from 0-17 Immature > Mature	66% ↓ from 0-8 Mature ↓ 55% from 0-17 Immature > Mature
Mean contact area	100% ↑ from 8-17 Mature > Immature	32% ↓ from 0-17 Mature > Immature
Cumulative contact area	47% ↓ from 0-2	↓ from 0-4
Synapses/Bouton	↑ from 0-2 ↓ from 2-17	↓ 50% from 0-1 ↑ from 8-17
	Nonsynaptic Contacts	
Number	Stable	100% ↑ from 0-17
Mean area	24% ↑ from 0-4	100% ↑ from 4-17
Cumulative area	190% ↑ from 0-17	430% ↑ from 0-17

pattern is different in the two laminar types, the numerical estimates suggest that neither subdivision achieves stabilization within the 17-week period surveyed in this study.

Other studies comparing the morphologic development of magnocellular and parvocellular laminae in monkeys have yielded equivocal results. Although no major differences, other than size, are apparent in Golgi-impregnated neurons of the two regions in adult monkeys (Headon et al., 1981a), there is some suggestion that immature characteristics present through the first postnatal month are shed earlier in the the magnocellular LGNd than in parvocellular laminae (Garey and Saini, 1981). This interpretation would seem to represent a consistent extension of the prenatal developmental gradient, in which neurons destined for magnocellular layers migrate to the diencephalon before those for the parvocellular region (Rakic, 1976a). However, changes in the size of cell bodies in monkeys (Gottlieb et al., 1980; Headon et al., 1981) and humans (Hickey, 1977a, b), in the size of neuronal nuclei, and in the volume of the LGNd observed in monkeys during development (Gottlieb et al., 1980, 1981) appear to mitigate and stabilize earlier in the parvocellular region. While the results of the present study do not provide strong evidence for earlier maturation of retinal termination patterns in one of the LGNd moieties, it is evident that the time course of developmental changes in the two laminar areas is dissimilar, and that neither pathway is fully mature in the 17-week-old monkey.

Morphologic studies in monkeys have also demonstrated a reduction in optic nerve fiber number, from a peak of 2.85×10^6 at birth, which approaches the adult level after the second postnatal month (Rakic and Riley, 1982). It is possible that part of the decrease in bouton number observed in the present study is due to retinal ganglion cell death, and the consequential disappearance of all boutons associated with their axons. The marked drop in bouton number observed from the

second to the fourth postnatal week, however, cannot solely be attributed to this factor, since there is a 50% decrease in bouton number and less than 10% reduction in optic nerve fiber number observed during that period. It is apparent, therefore, that there is a reduction in the number of boutons per optic nerve fiber which occurs in addition to the pruning of optic nerve fibers. In the Rakic and Riley study (1982), it is not possible to segregate optic axons destined for magnocellular and parvocellular laminae. Therefore, a valid comparison can only be made by summing the number of retinal boutons for the entire LGNd. If the number of optic axons at birth is approximately 1.6 $x10^6$ and decreases to 1.5 $x10^6$ by nine weeks (Rakic and Riley, 1982), and the total number of retinal boutons is about 1,200 $x10^6$ during the first two postnatal weeks, and approximately 800 $x10^6$ at nine weeks, then each optic axon provides about 750 boutons at birth, and only 530 after the second month.

The morphological characteristics of synapses made by retinal boutons in the LGNd also change during ontogeny. The most striking feature which is characteristic of both the magnocellular and parvocellular laminae is the substantial decrease in synapse number, although the time course of reorganization in the two regions is different over the postnatal period.

In the magnocellular layers, synapse elimination is most severe after eight weeks. However, because the mean size of these contacts almost doubles between eight and 17 weeks, the cumulative area of contact remains stable. During the first eight weeks of magnocellular synapse development, the interaction between synapse number and synapse size results in a biphasic pattern of changes in the cumulative area of contact. The total contact area constricts to almost half the neonatal value by the second postnatal week, and then partially expands before reaching an asymptote in the eight-week-old monkey. The early retraction in cumulative area is primarily due to a drop in synapse number during the first

week, and a decrease in average size of synapses during the second week. Similarly, the subsequent expansion in total contact area is attributable primarily to an increase in mean size between two and four weeks, and an increase in synapse number between four and eight weeks. As with the retinal boutons, it appears possible that the synapses in magnocellular LGNd laminae represent a nonhomogeneous population. The fluctuations in mean size may reflect changes in number of different subtypes of synapses, correlated with the subclasses of retinal boutons suggested above. Alternatively, a single, but highly variable population of synapses may be present in the magnocellular region. These observations confirm previous quantitative estimates of cumulative contact area during the first eight postnatal weeks in the LGNd of monkeys (Pasik et al., 1978). Although these investigators do not specify the LGNd region examined, the pattern of changes conforms well to the present results obtained from the magnocellular layers.

In contrast, synapse elimination in the parvocellular laminae is apparent during the first eight postnatal weeks. The substantial reduction in number of contacts is paralleled by a severe monotonic retraction in cumulative area of contact, despite the increase in mean size of synapses observed over the first postnatal week. It is most likely that the synapses in the parvocellular LGNd, like the retinal boutons, comprise a homogeneous population. While the number of synapses drops steadily, the smaller elements disappear first, resulting in a temporarily inflated mean area value. As synapses continue to disappear, the larger elements are also affected, and the entire population tends toward fewer and smaller synapses in maturity. In general, therefore, synapse elimination occurs earlier in parvocellular than in magnocellular layers.

A similar quantitative analysis has been used in the cat (Cragg, 1975) to determine the average density of synapses in the developing visual system. While

synaptic density in the entirety of the LGNd increases sharply during the first four postnatal weeks, and attains the adult level by seven weeks, synapse elimination is apparent in the data during late prenatal and early postnatal material.

One of the possible explanations for the differences in synaptic development observed in the two laminar types could be the disparity in the proportion of R to P and R to I synapses in the magnocellular and parvocellular layers. The present results reveal a substantially higher percentage of R to I synapses present in the magnocellular region. These results are compatible with quantitative estimates obtained in mature monkeys, which indicate that approximately 16% of the neurons in magnocellular, and 4% of those in parvocellular laminae are interneurons (Hamori et al., in press). In addition, synapses involving presynaptic dendrites are more prevalent (Wilson and Hendrickson, 1981), and R to P synapses are proportionately less (Winfield, 1980) in the magnocellular region. It is possible, therefore, that these differential proportions represent the basis for the heterogeneous population of elements posited to exist in magnocellular layers. Perhaps the R to I synapse complement in L1 and L2 is of sufficient magnitude to be expressed as a difference in synapse type.

Immature synapses predominate in both laminar types throughout the 17-week period surveyed. In the magnocellular region, the total number of immature synapses decreases steadily, with no concomitant increase in mature elements. This may reflect the straightforward elimination of immature synapses or a dynamic interaction in which mature synapses retract while immature synapses become mature, thus explaining the fluctuations in number of mature synapses across development. However, the number of mature R to P synapses increases during maturation, counterpunctual to the decline in immature forms. It seems likely that the synaptic organization of this pathway is not fully developed by 17

weeks, that the R to P component begins to resemble a mature configuration after eight weeks, and that the R to I elements remain immature for a longer period of time.

In the parvocellular region, the number of immature synapses decreases only slightly over the 17 weeks, while substantial numbers of mature elements disappear. This pattern is also characteristic of the retinal to P synapse counts, suggesting that both the mature and immature populations undergo modification and elimination during development. The major portion of the immature synapse loss, and retinal to I stabilization, must occur after four months.

The morphological development of magnocellular and parvocellular projections must underlie the observed differences in maturation of the transient and sustained functional pathways. Although most X-cell characteristics mature before those of Y-cells (Norman et al., 177; Daniels et al., 1978; Ikeda and Tremain, 1978), the mature spatial resolution ability requires an equally protracted developmental period in both systems (Mangel et al., 1980; Wilson et al., 1982). Since the morphological organization of each of these projections is not fully mature by four months, it may be the case that spatial resolution, which matures only after six postnatal months in the cat, provides the most sensitive functional assay of morphologic development in the visual system.

The existence of a critical period in the development of the visual system is indicated by the results of behavioral studies in monkeys and humans. In the monkey, abnormalities in accommodation persist for one month postnatally (Howland et al., 1982), and acuity and contrast sensitivity require five to seven months to fully mature (Teller et al., 1978; Teller and Boothe, 1979; Boothe et al., 1980). In addition, learning set formation for visual discrimination tasks continues to improve during the second year of life (Zimmerman, 1958). On the basis of these observations, a behaviorally-defined critical period in the monkey appears to

begin at birth and continues for at least six to seven postnatal months.

In the human, abnormalities in accommodation (Braddick et al., 1979), stereopsis (Amigo et al., 1978; Fox et al., 1980; Petrig et al., 1981) and color vision (Staples, 1932; Dobson, 1976) persist for three to four months after birth, while astigmatism (Howland et al., 1978; Mohindra et al., 1978) and acuity (Gorman et al., 1957; Fantz, 1961; Harter and Suitt, 1970; Dobson and Teller, 1978; Atkinson et al., 1979) require several years to mature, and eye movements become adult-like after four to five years (Kowler and Martins, 1982). Apparently, the sensitive period for development of visual capacities in humans persists at least through the second year of life.

A critical period in visual development is also indicated by the results of deprivation studies. In monkeys, the duration of this period is unclear, although its existence is indicated by the permanence of visual dysfunction after monocular lid suture during the first two postnatal months (von Noorden and Dowling, 1970; von Noorden et al., 1970; von Noorden, 1973). Lid suture after nine months, however, causes only temporary visual deficits (Hendrickson et al., 1977), suggesting that the sensitive period lasts from birth until three to nine months of age.

In humans, recovery of visual function after cataract removal is observed in adults with protracted blindness, although cataracts in infants cause irreversible loss of sight (von Senden, 1960). Similar observations of individuals with congenital visual abnormalities (von Noorden and Maumanee, 1968; Hohmann and Creutzfeldt, 1975; Banks et al., 1975) indicate that the critical period for development of acuity and perception lasts at least two years, for stereopsis lasts perhaps six years and that early pattern deprivation is more deleterious to spatial than to temporal abilities (Hess et al., 1981).

Synapse Elimination During Postnatal Development

Synapse elimination during development has been demonstrated by other investigators in both the peripheral and central nervous systems. In the rat submandibular ganglion (Lichtman, 1977), polyneuronal innervation of ganglionic cells is observed at birth, but is absent five weeks postnatally, although a simultaneous increase in bouton number occurs. This indicates a substantial reorganization of connectivity in the first few postnatal weeks, during which more boutons appear, each establishing fewer synapses. A similar process of synaptic pruning is evident in the hamster superior cervical ganglion (Lichtman and Purves, 1980) and has been demonstrated physiologically at the neuromuscular junction of newborn rat soleus muscle (Brown, Jansen and Van Essen, 1976) in normal animals and those with neonatal nerve crush. Terminal bouton retraction in rat neuromuscular junction (Korneliussen and Jansen, 1976) is apparent between eight and 16 days postnatally as a decrease in bouton number, although no evidence of terminal degeneration is observed. Indeed, synapse elimination seems to be a common feature of development in the peripheral nervous system (for review, see Purves and Lichtman, 1980).

There are few reports of synapse elimination during development of the central nervous system. In the spinal cord of the cat, a reduction in the number of boutons on the initial segments of motor neuron axons is observed between birth and 11 days postnatally (Conradi and Ronnevi, 1977) as well as a radical decline in the number of synapses on motor neuron cell bodies and dendrites (Conradi and Ronnevi, 1975).

In the rhesus monkey, massive neuronal death and synaptic reorganization is reported in the sensory portion of the embryonic spinal cord (Knyihar, Csillik and Rakic, 1978). In addition, as noted earlier, synapse elimination is manifest during early postnatal development (Pasik et al., 1978) as a reduction in cumulative

contact area in the retinogeniculate pathway of monkeys. Recent light microscopic observations in prenatal and early postnatal monkeys suggest that synapse elimination may also occur in the cortico-striatal projection (Goldman-Rakic, 1981).

The present data support the findings of early postnatal synapse elimination in the monkey LGNd. As noted earlier, the reduction in number of retinal boutons during the first few postnatal weeks cannot solely be attributed to a decrease in optic nerve fiber number (Rakic and Riley, 1982). Taking the analysis a step further, the synapse loss could simply be attributable to bouton disappearance. However, if synapse elimination was purely a passive process, reflecting bouton death, the average number of synapses associated with each bouton would remain constant during development. The dynamic changes in the synapse/bouton ratio, expressed in magnocellular and parvocellular synaptic development, do not support this interpretation. Apparently, synapse elimination is related to, but not solely dependent upon, retinal bouton disappearance.

A possible mechanism to explain the phenomenon of synapse elimination has been offered by Changeux and Danchin (1976, 1977). According to these investigators, there is a secondary selection process in which some synapses capture a larger share of retrograde signals provided by the postsynaptic element, and consequently are selectively stabilized in the nervous system. Correspondingly, synapses lacking sufficient input from these signals regress and disappear. This process of selective stabilization of developing synapses has been successfully applied to explain the specification of neuronal networks (Changeux and Danchin, 1977).

Methodological Considerations

There are several methodological issues inherent in the present study which should be taken into account in the evaluation of the results. One of these

considerations is the number of experimental subjects. Although nine monkeys were examined qualitatively, only one animal per age was included in the quantitative analysis. Since the overall goal of this research was to provide normative developmental data of direct relevance to humans, and since monkeys are closely related to humans in phylogeny and in neuroanatomical organization, monkeys were the subjects of choice. However, the restricted availability and prohibitive expense, particularly of infant monkeys, limited the feasibility of larger groups of subjects. Nevertheless, the evaluation of the intra-subject variability analysis suggests that a sufficient and internally consistent sample was obtained within each age-lamina condition. The inter-subject variability for each condition could not be determined, for obvious reasons. However, the major finding of drastic synapse elimination is sufficiently robust to engender confidence.

A further point of methodology concerns the use of two alternative stereological procedures to analyze the data. This apparent redundancy was conducted in order to compare the approaches and evaluate the power of each, while gaining validation of the results through two independent analyses. Although the Palkovits (1976) method proved to be advantageous for simplicity in calculation, it was the less refined technique. With this method, particles were assumed to be cubes of uniform size. Therefore, any subpopulations or bimodality in the size distribution of boutons or contacts could not be reflected in the density values. In addition, the cuboidal particles, by assumption, were cut parallel to two faces; the numerous small profiles visible in the micrographs affected the calculation by substantially increasing N (raised to the third power) while only slightly increasing Σ a, resulting in an inflated density value. In fact, many of the small profiles represent tangential sections of larger particles (Coupland, 1968). However, partial compensation for the density overestimate was accomplished in

this method by the failure to account for profiles too small to be recognized in the micrographs. If performed, this adjustment would have further increased the density value. Finally, although the retinal boutons appear highly irregular in shape, so that any 3-dimensional solid might serve as a first approximation, the presence of smooth profile contours argues against the propriety of cubes.

In contrast, the Anker and Cragg approach (1974) requires an assumption of spherical boutons and flat circular synaptic disks. The retinal boutons appear highly variable in shape, and it is doubtful that any geometric solid accurately represents the population. While ellipsoids-of-rotation may ultimately prove to be a more appropriate model for the boutons, spheres are probably a good first approximation, and certainly more suitable than cubes. However, the possibility of irregularly-shaped contacts cannot be disregarded. For example, a crenulated axo-somatic junction, termed the "synapse en marron" (Chan-Palay and Palay, 1971a, b), has been observed between mossy fiber axon terminals and Golgi cell somata in cerebellar cortex. In single sections, in which only fragments of the contact region are visible, a variety of short synapses of nonuniform shape can be observed. Should such an arrangement be subjected to the present type of stereologic analysis, the result would be multiple short synaptic disks, although in fact they are derived from a single plaque. However, there is no evidence in the literature that such synaptic morphology exists in the LGNd.

Further, the results of the stereologic analysis are density values for L1 and L6. Density measurements are of limited interpretative value, however, since changes in the volume of the laminae during development are not taken into consideration. For example, equal bouton densities over time may result from equal but opposite changes in bouton number and laminar volume, or from no change in either. To more accurately characterize the developmental sequence, estimates of total numbers of boutons and synapses were obtained from laminar

volume data. However, the data was limited to a distinction between parvocellular and magnocellular regions. As a result, the numerical estimates presented above represent the products of L1 density and L1 + L2 volume to yield magnocellular data, and L6 density with L3-L6 volume for parvocellular data. Some error maybe introduced by this manipulation, since the density of boutons and synapses may not be equal in these different laminae.

Finally, the criterion used to judge synapses as mature or immature was somewhat strict, favoring immaturity. However, almost half of the synapses evaluated in the study were reviewed by a second investigator, using a more lenient, qualitative criterion, and similar results were obtained.

Future Research

The present results could be extended by future research directed toward further characterization of aspects of development in LGNd synaptology. For example, a comparable quantitative light microscopic study could yield data on the number of neurons present in L1 and L6 at each age. This data, applied to the present results, would provide estimates of the number of retinal boutons and the number of retinogeniculate synapses per LGNd neuron. These ratios serve as an index of the extent of convergence or divergence of retinal input to the LGNd during development. Data which is presently available on the proportion of P and I cells in magnocellular and parvocellular regions (Hámori et al., in press) can provide a further refinement of the convergence-divergence issue. In addition, afferents from striate cortex can be subjected to the identical stereological analysis. Quantification of the changes in number and size of cortical boutons and synapses during the same developmental period would allow a direct comparison of the time courses of retinal and visual cortical maturation. Further, the processes and synapses of LGNd interneurons can also be quantified stereologically. These neurons sport presynaptic dendrites, as well as axons, and constitute an integral

part of LGNd synaptology. Taken together, these studies would permit the complete characterization of the development of neuronal networks within the LGNd. As a further elaboration of this system, optic nerve axons can be counted at the light microscopic level using the same subjects examined in the present study. Although the data extrapolated from other investigators is of some value in clarifying the basis for synapse elimination, the precise relationship between changes in bouton number, synapse number and optic nerve fiber number during development can best be gleaned from their analysis within the same animals.

Future research might also focus on later postnatal development. It is clear from the present study, as well as the current literature on behavioral and physiological development, that the four-month-old monkey visual system is not fully mature. It would be extremely useful to extend the present results to older animals, and trace the changes in bouton number, and mature and immature synapse number, to the adult level.

Finally, the same stereological approach can be applied to other areas of the visual nervous system. Some insight into the significance of visual information processing in the superior colliculus, inferior pulvinar, and nucleus of the accessory optic tract, for example, may result from quantitative studies of ultrastructural development.

Appendix 1

Electron Microscope Calibration for Two Specimen Holders

Date	6000X Nominal Magnification for 18,000X Final			
	Specimen Holder #1		Specimen Holder #2	
	Actual Mag.	Photo Enlargement	Actual Mag.	Photo Enlargment
6/80	7,115	X2.53	7,347	X2.45
9/80	7,258	X2.48	7,317	X2.46
2/81	7,143	X2.52	7,059	X2.55
7/81	7,087	X2.54	7,563	X2.38
10/81	7,287	X2.47	--	--
1/82	6,977	X2.58	7,407	X2.43
1/82	7,004	X2.57	6,716	X2.68
2/82	6,792	X2.65	6,716	X2.68
2/82	6,767	X2.66	6,767	X2.66

Electron Microscope Calibration for Two Specimen Holders

Date	10,000X Nominal Magnification for 25,000X Final			
	Specimen Holder #1		Specimen Holder #2	
	Actual Mag.	Photo Enlargement	Actual Mag.	Photo Enlargement
3/80	10,730	X2.33	10,331	X2.42
6/80	10,684	X2.34	10,917	X2.29
9/80	10,730	X2.33	10,870	X2.30
2/81	10,638	X2.35	10,593	X2.36
7/81	9,843	X2.54	10,504	X2.38
10/81	10,730	X2.33	--	--
1/82	10,417	X2.40	10,917	X2.29
1/82	10,417	X2.40	10,000	X2.50
2/82	10,121	X2.47	10,000	X2.50
2/82	10,163	X2.46	10,040	X2.49

Appendix 2: Stereological Procedure

I. The stereological approach.

The purpose of the stereologic method is to reconstruct 3-dimensional spatial organization from 2-dimensional information. On the surface of a planar section cut through a solid body, the internal volumetric structures are visible as areas, the areas as lines, and the lines as points. For example, random sections through a tissue block containing a set of spherical particles will yield a set of circular profiles of varying sizes, since some spheres will be cut nearer the center and others nearer the poles, and the spheres may be of different sizes. The number of profiles visible in the sectional area will depend on the number of spheres present in the tissue volume, and also on the sizes of the spheres (the probability of any given sphere being cut by a random slice is directly proportional to the size of the sphere). The Delesse Theorem (Delesse, 1847) relates volume and area ratios of a class of particles randomly distributed within a 3-dimensional solid. It states that:

$a/A = v/V$ where

A = the area of sections through the volume

a = the total area of the cut surfaces of the particles within the sections

V = the total volume of the solid

v = the total volume of the particles.

In the present study, the component volume density was reconstructed from the profile areal density using two alternative stereologic procedures. For both, the bouton profile areas, synaptic profile lengths, and tissue sample areas were measured with a Numonics

graphics calculator which was serially interfaced for direct data entry to an Apple II Plus microcomputer. The data was stored on computer disks and analyzed using Pascal programs written by Mr. Alexander Pasik.

II. The method of Palkovits.

Palkovits (1976) has described a method for direct determination of component density from areal analysis of the profiles apparent in electron micrographs. The procedure assumes that the components of interest within a solid body are cubes of uniform size which have been cut parallel to two of the cube faces. If a = profile area, A = micrograph area, v = component volume, V = solid body volume, and N = number of profiles visible in the micrographs, then by the Delesse Principle, $\frac{\Sigma a}{A} = \frac{\Sigma v}{V}$. Since $\Sigma v = \bar{v} N$, $\frac{\Sigma a}{A} = \frac{\bar{v} N}{V}$.

Density (D) is defined as number per unit volume, so that $\frac{\Sigma a}{A} = \bar{v} D$.

Because the components are cubes, $\bar{v} = \left(\frac{\Sigma a}{N}\right)^{\frac{3}{2}} = \sqrt{\left(\frac{\Sigma a}{N}\right)^3}$ and

$\frac{\Sigma a}{A} = \left[\sqrt{\left(\frac{\Sigma a}{N}\right)^3}\right]\left[D\right]$. Therefore, $D = \frac{\frac{\Sigma a}{A}}{\sqrt{\left(\frac{\Sigma a}{N}\right)^3}} = \sqrt{\frac{N^3}{A^2 \Sigma a}}$.

The Palkovits procedure was used to directly determine retinal bouton and synapse densities. For example, in L1 of the 17-week-old monkey (#873), 52 retinal bouton profiles, occupying a total area of 106.51 μm^2, were observed in 2303.483 μm^2 of gross neuropil. The

density of retinal boutons is

$$D = \sqrt{\frac{n^3}{A^2 \Sigma s}} = \sqrt{\frac{52^3}{(2303.48^2)(106.5)}} = 1.577 \times 10^7/mm^3 .$$

III. The method of Anker and Cragg.

A more elaborate stereological approach, which involves reconstruction of the particle size-frequency distribution from that of the profiles (Coupland, 1968) and density calculations based on that distribution (Abercrombie, 1946) has been applied to the CNS by Anker and Cragg (1974). This procedure assumes spherical particles, but does not assume that the spheres are of uniform size. It was used in the present study to determine the distribution and density of retinal boutons in L1 and L6 of each animal, and the distribution and density of mature and immature retinal to principal cell and retinal to interneuron synapses, as well as retinal to principal cell nonsynaptic contacts. The following explanatory example is taken from the L1 retinal bouton data of the 17-week-old monkey and, for clarity, uses 5 diameter classes.

A. Determination of the bouton size-frequency distribution.

Once the area of each profile is measured, the equivalent circle diameters are computed and a table is constructed listing the number of profiles which fall into each of 5 diameter classes, the class interval being 20% of the maximum observed value.

In μm:	0.0-0.7	0.7-1.4	1.4-2.1	2.1-2.8	2.8-3.5
# Profiles:	3	19	21	8	1

The profiles in the highest interval (2.8-3.5 μm) represent a pure, but incomplete population derived from the largest boutons. The actual

number of these boutons ($N_{3.5}$) is greater than the number of profiles initially placed in that class ($n_{2.8-3.5}$) since boutons sectioned off-center yield smaller profiles than boutons of equal size cut through their equators. Those smaller profiles will be assigned to the smaller diameter classes. The actual number of 3.5 µm diameter boutons is given by

$$N_{3.5} = \frac{n_{2.8-3.5}}{y_{2.8-3.5}}$$

where n = number of profiles counted in that class (in the present example, $n_{2.8-3.5} = 1$) and y = probability that a bouton of 3.5 µm diameter will be sectioned such that a 2.8-3.5 µm diameter profile results. That is, y% of all sections of a 3.5 µm diameter bouton will yield profiles with diameters between 2.8 and 3.5 µm.

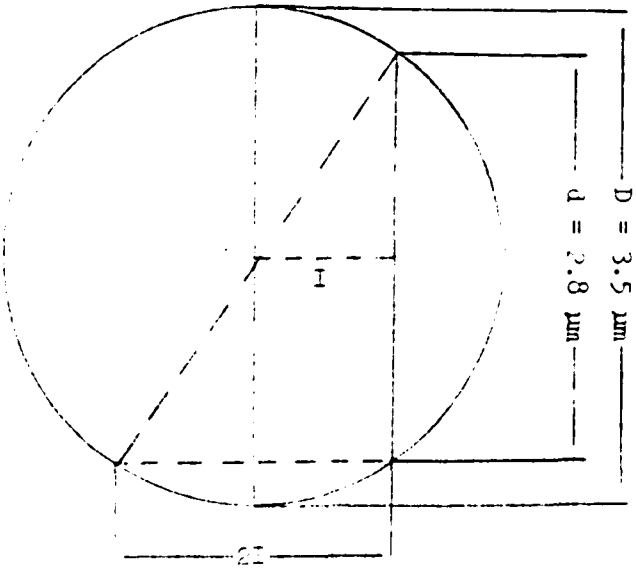

Referring to the figure,

$$y = \frac{2I}{D} \quad \text{and} \quad 2I = \sqrt{D^2 - d^2}$$

$$y = \frac{\sqrt{D^2 - d^2}}{D} = \sqrt{1 - \frac{d^2}{D^2}}$$

In the present example,

$$y = \sqrt{1 - \frac{2.8^2}{3.5^2}} = 0.6$$

$$N_{3.5} = \frac{1}{0.6} = 1.6$$

In each of the smaller diameter classes, the profiles can have originated from boutons with diameters within that interval or from larger boutons sectioned far off-center. To adjust the distribution, the

profiles in each class are subjected to a series of subtractions to reclassify the smaller profiles derived from larger boutons. To begin, the total number of boutons of maximum diameter expected in the second class interval ($N_{2.8}$) is determined from the number of profiles counted in that interval and the number of profiles of the same diameter which belong to boutons of the larger class:

1. The probability that profiles of 2.1-2.8 µm diameter are derived from 3.5 µm diameter boutons is:

$$y_{2.1\text{-}2.8,\ 3.5} = \sqrt{1 - \frac{2.1^2}{3.5^2}} - \sqrt{1 - \frac{2.8^2}{3.5^2}} = 0.2$$

2. The number of profiles of 2.1-2.8 µm diameter cut from boutons of 3.5 µm diameter is:

$$n_{2.1\text{-}2.8,\ 3.5} = (N_{3.5})\ (y_{2.1\text{-}2.8,3.5})$$

$$= (1.67) \quad (0.2) \qquad = 0.3333$$

3. The number of profiles of 2.1-2.8 µm diameter cut from boutons of 2.8 µm diameter is:

$$n_{2.1\text{-}2.8,2.8} = n_{2.1\text{-}2.8} - n_{2.1\text{-}2.8,3.5}$$

$$= \quad 8 \quad - \quad 0.334 \qquad = 7.667$$

4. The probability that profiles of 2.1-2.8 µm diameter belong to boutons of 2.8 µm diameter is:

$$y_{2.1\text{-}2.8,2.8} = \sqrt{1 - \frac{2.1^2}{2.8^2}} = 0.6614$$

5. The number of boutons of 2.8 μm diameter is:

$$N_{2.8} = \frac{n_{2.1\text{-}2.8,2.8}}{y_{2.1\text{-}2.8,2.8}} = \frac{7.4667}{0.6614} = 11.29$$

The same method is followed for each successive class, applying iterative subtractions from all preceding intervals. Negative remainders often appear in the smallest diameter class(es), indicating small, unrecognized profiles. In the final reconstructed distribution, these negative values are set to zero. To continue the example through the third class:

1. The probability that profiles of 1.4-2.1 μm diameter are derived from boutons of 3.5 μm diameter is:

$$y_{1.4\text{-}2.1,3.5} = \sqrt{1 - \frac{1.4^2}{3.5^2}} - \sqrt{1 - \frac{2.1^2}{3.5^2}}$$

$$= 0.9165 - 0.8 = 0.1165$$

2. The number of profiles of 1.4-2.1 μm diameter cut from 3.5 μm diameter boutons is:

$$n_{1.4\text{-}2.1,3.5} = (N_{3.5})\ (y_{1.4\text{-}2.1,3.5})$$

$$= (1.67)\quad (0.1165) = 0.195$$

3. The probability that profiles of 1.4-2.1 μm diameter have been cut from 2.8 μm diameter boutons is:

$$y_{1.4\text{-}2.1,2.8} = \sqrt{1 - \frac{1.4^2}{2.8^2}} - \sqrt{1 - \frac{2.1^2}{2.8^2}}$$

$$= 0.866 \quad - \quad 0.6614 \quad = 0.2046$$

4. The number of profiles of 1.4-2.1 μm diameter which belong to boutons of 2.8 μm diameter is:

$$n_{1.4\text{-}2.1,2.8} = (N_{2.8}) \quad (y_{1.4\text{-}2.1,2.8})$$

$$= (11.59) \ (0.2046) \quad = 2.3713$$

5. The number of profiles of 1.4-2.1 μm diameter derived from boutons of 2.1 μm diameter is:

$$n_{1.4\text{-}2.1,2.1} = n_{1.4\text{-}2.1} - n_{1.4\text{-}2.1,3.5} - n_{1.4\text{-}2.1,2.8}$$

$$= \quad 21 \quad - \quad 0.195 \quad - \quad 2.3713 \quad = 18.4337$$

6. The probability that profiles of 1.4-2.1 μm diameter have been cut from boutons of 2.1 μm diameter is:

$$y_{1.4\text{-}2.1,2.1} = \sqrt{1 - \frac{1.4^2}{2.1^2}} \quad = 0.7454$$

7. Finally, the number of boutons of 2.1 μm diameter is:

$$N_{2.1} = \frac{n_{1.4\text{-}2.1,2.1}}{y_{1.4\text{-}2.1,2.1}} = \frac{18.4337}{0.7454} \quad = 24.73$$

When this procedure is repeated for the remaining class intervals of the profile distribution, the following reconstructed bouton size-frequency distribution results:

In μm:	0.0-0.7	0.7-1.4	1.4-2.1	2.1-2.8	2.8-3.5
# Profiles:	3	19	21	8	1
# Boutons:	-0.8	14.81	24.73	11.59	1.67

B. Density determination.

The density is calculated separately for each class interval, in order to adjust the sample volume for different bouton sizes. For N = number of boutons and V = tissue volume in which the bouton centers are distributed, density (D) = N/V, where V is given by the product of sample area and the sum of section thickness and bouton diameter (Abercrombie, 1946). For the present example, the sample area was 2303.5 μm^2 of gross neuropil and the sections were 0.07 μm thick.

The density of 3.5 μm diameter boutons is:

$$D_{3.5} = \frac{1.67}{(2303.5)\ (3.5 + 0.07)} = 0.000203/\mu m^3$$

$$= 0.20 \times 10^6/mm^3$$

The density of 2.8 μm diameter boutons is:

$$D_{2.8} = \frac{11.59}{(2303.5)\ (2.8 + 0.07)} = 0.001753/\mu m^3$$

$$= 1.75 \times 10^6/mm^3$$

The density of 2.1 μm diameter boutons is:

$$D_{2.1} = \frac{11.73}{(2303.5)\ (2.1 + 0.07)} = 0.004947/\mu m^3$$

$$= 4.95 \times 10^6/mm^3$$

The density of 1.4 μm diameter boutons is:

$$D_{1.4} = \frac{14.81}{(2303.5)\ (1.4 + 0.07)} = 0.004374/\mu m^3$$

$$= 4.37 \times 10^6/mm^3$$

Since the number of boutons of 0.0-0.7 μm diameter was corrected to zero,

$D_{0.7} = 0.$

The total retinal bouton density in L1 of the 17-week-old monkey is:
$(0.20 \times 10^6) + (1.75 \times 10^6) + (4.95 \times 10^6) + (4.34 \times 10^6) + 0 = 11.28 \times 10^6/mm^3$.

Appendix 3

Contact Density Values ($x10^7$ per mm^3 of tissue)

	All Synapses		Mature Synapses		Immature Synapses	
Postnatal Weeks	L1	L6	L1	L6	L1	L6
0	8.29	11.74	3.57	6.83	4.72	4.91
1	4.61	8.06	1.19	3.67	3.42	4.39
2	8.83	6.02	3.76	1.05	5.07	4.97
4	6.86	5.88	2.45	2.55	4.41	3.33
8	6.59	3.44	3.19	1.11	3.40	2.33
17	3.98	5.29	1.55	2.21	2.43	3.08

	R to Pd Synapses		Mature R to Pd Synapses		Immature R to Pd Synapses	
	L1	L6	L1	L6	L1	L6
0	6.75	11.09	2.88	6.44	3.87	4.65
1	3.68	7.54	1.09	3.58	2.59	3.96
2	6.92	6.02	3.04	1.05	3.88	4.97
4	5.51	5.04	2.38	1.68	3.13	3.36
8	4.60	2.97	2.76	1.11	1.84	1.86
17	2.94	4.62	1.55	2.02	1.39	2.60

	R to Id Synapses		Nonsynaptic Contacts	
	L1	L6	L1	L6
0	1.54	0.65	1.82	2.46
1	0.93	0.52	0.64	2.58
2	1.91	--	1.68	1.40
4	1.35	0.84	0.55	2.19
8	1.99	0.47	0.81	3.07
17	1.04	0.67	1.18	3.46

REFERENCES

Abercrombie, M. Estimation of nuclear population from microtome sections. Anat. Rec., 1946, 94, 239-247.

Amigo, G., Fiorentini, A., Pirchio, M. and Spinelli, D. Binocular vision tested with visual evoked potentials in children and infants. Invest. Ophthal., 1978, 17(9), 910-915.

Anker, R. The prenatal development of some of the visual pathways in the cat. J. comp. Neurol., 1977, 173, 185-204.

Anker, R. and Cragg, B. Estimation of the number of synapses in a volume of nervous tissue from counts in thin sections by electron microscopy. J. Neurocytol., 1974, 3, 525-535.

Atkinson, J., Braddick, O. and Braddick, F. Acuity and contrast sensitivity of infant vision. Nature, 1974, 247, 403-404.

Atkinson, J., Braddick, O. and French, J. Contrast sensitivity of the human neonate measured by the visual evoked potentials. Invest. Ophthal. Visual Sci., 1979, 18(2), 210-213.

Ball', T., Portugalov, V. and Shkol'nik-Yarros, E. On the structural and histochemical characteristics of the lateral geniculate body in monkeys. Zh. vyssh. nerv. Deyat., 1965, 4, 707-713 (in Russian).

Banks, M., Aslin, R. and Letson, R. Sensitive period for the development of human binocular vision. Science, 1975, 190, 675-677.

Banks, M. and Salapatek, P. Contrast sensitivity function of the infant visual system. Vision Res., 1976, 16, 867-869.

Banks, M. and Salapatek, P. Acuity and contrast sensitivity in 1-, 2-, and 3-month old human infants. Invest. Ophthal., 1978, 17(4), 361-365.

Bishop, P., Kozak, W., Levick, W. and Vakkur, G. The determination of the projection of the visual field onto lateral geniculate nucleus in the cat. J. Physiol., 1962, 163, 503-539.

Blakemore, C. and Vital-Durand, F. Development of the neural basis of visual acuity in monkeys. Speculation on the origin of deprivation amblyopia. Trans. Ophthalmol. Soc. UK, 1979, 99, 363-368.

Boothe, R., Williams. R., Kiorpes, L. and Teller, D. Development of contrast sensitivity in infant Macaca nemestrina monkeys. Science, 1980, 208, 1290-1291.

Bower, T. Discrimination of depth in premotor infants. Psychonomic Sci., 1964, 1, 368.

Bower, T. Heterogeneous summation in human infants. Animal Behav., 1966, 14, 395-398.

Braddick, O., Atkinson, J., French, J. and Howland, H. A photorefractive study of infant accommodation. Vision Res., 1979, 19, 1319-1330.

Brouwer, B. and Zeeman, W. The projection of the retina in the primary optic neuron in monkeys. Brain, 1926, 49, 1-35.

Brown, M., Jansen, J. and Van Essen, D. Polyneuronal innervation of skeletal muscle in newborn rats and its elimination during maturation. J. Physiol., 1976, 261, 387-422.

Campos-Ortega, J. and Glees, P. The termination of ipsilateral and contralateral optic fibers in the lateral geniculate body of Galago crassicaudatus. J. comp. Neurol., 1967a, 129, 279-284.

Campos-Ortega, J. and Glees, P. The subcortical distribution of optic fibers in the Saimiri sciureus (squirrel monkey). J. comp. Neurol., 1967b, 131, 131-142.

Campos-Ortega, J., Glees, P. and Neuhoff, V. Ultrastructural analysis of individual layers in the lateral geniculate body of the monkey. Z. Zellforsch., 1968, 87, 82-100.

Changeux, J. and Danchin, A. The selective stabilization of developing synapses: a plausible mechanism for the specification of neuronal networks. Nature, 1976, 264, 705-712.

Changeux, J. and Danchin, A. Biochemical models for the selective stabilization of developing synapses. In: Cotrell and Usherwood (Eds.), Synapses, Academic Press, 1977,

pp. 239-248.

Cleland, B., Dubin, M. and Levick, W. Sustained and transient neurons in the cat's retina and lateral geniculate nucleus. J. Physiol. (Lond.), 1971, 217, 473-496.

Colonnier, M. and Guillery, R. Synaptic organization in the lateral geniculate nucleus of the monkey. Z. Zellforsch, 1964, 62, 333-355.

Conradi, S. and Ronnevi, L.-O. Spontaneous elimination of synapses on cat spinal motoneurons after birth: do half of the synapses on the cell bodies disappear? Brain Res., 1975, 92, 505-510.

Conradi, S. and Ronnevi, L.-O. Ultrastructure and synaptology of the initial axon segment of cat spinal motoneurons during early postnatal development. J. Neurocytol., 1977, 6, 195-210.

Coupland, R. Determining sizes and distribution of sizes of spherical bodies such as chromaffin granules in tissue sections. Nature, 1968, 217, 384-388.

Cragg, B. The development of synapses in the visual system of the cat. J. comp. Neurol., 1975, 160, 147-166.

Daniels, J., Pettigrew, J. and Norman, J. Development of single-neuron responses in kitten's lateral geniculate nucleus. J. Neurophysiol., 1978, 41, 1373-1393.

DeCourten, C. and Garey, L. Morphology of the neurons in the human lateral geniculate nucleus and their normal development. A Golgi study. Exp. Brain Res., 1982, 47, 159-171.

Delesse, A. Procédé mécanique pour déterminer la composition des roches (Extrait). C.r. hebd. séanc. Acad. Sci., Paris, 1847, 25, 544.

Dember, W. and Warm, J. Psychology of Perception. Holt, Rinehart and Winston, New York, 1979.

DeMonasterio, F.M. Properties of concentrically organized X and Y ganglion cells of macaque retina. J. Neurophysiol., 1978, 41, 1394-1417.

Des Rosiers, M., Sakurada, O., Jehle, J., Shinohara, M., Kennedy, C. and Sokoloff, L. Functional plasticity in the immature striate cortex of the monkey shown by the (^{14}C) deoxyglucose method. Science, 1978, 200, 447-449.

DeValois, R., Morgan, H. and Snodderly, D. Psychophysical studies of monkey vision. III. Spatial luminance contrast sensitivity tests of macaque and human observers. Vision Res., 1974, 14, 75-81.

Dobson, V. Spectral sensitivity of the 2-month old infant as measured by the visually evoked potential. Vision Res., 1976, 16, 367-374.

Dobson, V. and Teller, D. Visual acuity in human infants: A review and comparison of behavioral and electrophysiological studies. Vision Res., 1978, 18, 1469-1483.

Doty, R., Glickstein, M. and Calvan, W. Lamination of the lateral geniculate nucleus in the squirrel monkey. Saimiri sciureus. J. comp. Neurol., 1966, 127, 335-340.

Dreher, B., Fukuda, Y. and Rodieck, R. Identification, classification and anatomical segregation of cells with X-like and Y-like properties in the lateral geniculate nucleus of old-world primates. J. Physiol. (Lond.), 1976, 258, 433-452.

Duke-Elder, S. System of Ophthalmology, Vol. 3. Normal and Abnormal Development. St. Louis. Mosby, 19[illegible].

Elegeti, H., Eleg[illegible], R. and Fleischhauer, K. Postnatal growth of the dorsal lateral geniculate nucleus of the cat. Anat. Embryol., 1976, 149, 1-13.

Enroth-Cugell, C. and Robson, J. The contrast-sensitivity of retinal ganglion cells of the cat. J. Physiol. (Lond.), 1966, 187, 517-552.

Famiglietti, E. Dendrodendritic synapses in the lateral geniculate nucleus of the cat. Brain Res., 1970, 20, 181-191.

Famiglietti, E. and Peters, A. The synaptic glomerulus and the intrinsic neurons in the dorsal lateral geniculate nucleus of the cat. J. comp. Neurol., 1972, 144, 285-334.

Fantz, R. The origin of form perception. Sci. Am., 1961, 204(5), 66-72.

Fantz, R., Ordy, J. and Udelf, M. Maturation of pattern vision in infants during the first six months. J. comp. Physiol. Psychol., 1962, 55, 907-917.

Ferster, D. and LeVay, S. The axonal arborization of lateral geniculate neurons in the striate cortex of the cat. J. comp. Neurol., 1978, 182, 923-944.

Fox, R., Aslin, R., Shea, S. and Dumais, S. Stereopsis in human infants. Science, 1980, 207, 323-324.

Friedlander, M., Lin, C.-S. and Sherman, S. Structure of physiologically identified X and Y cells in the cat's lateral geniculate nucleus. Science, 1979, 204, 1114-1117.

Garey, L.,Fisken, R. and Powell, T. Observations of the growth of cells in the lateral geniculate nucleus of the cat. Brain Res., 1973, 52, 359-362.

Garey, L. and Powell, T. The projection of the lateral geniculate nucleus on the cortex in the cat. Proc. Roy. Soc. B., 1967, 169, 107-126.

Garey, L. and Saini, K. Golgi studies of the normal development of neurons in the lateral geniculate nucleus of the monkey. Exp. Brain Res., 1981, 44, 117-128.

Gibson, E. and Walk, R. The "visual cliff". Sci. Am., 1960, 202, 64-71.

Glees, P. The termination of optic fibers in the lateral geniculate body of the cat. J. Anat. (Lond.), 1941, 75, 434-440.

Glees, P. and Clark, L. The termination of optic fibers in the lateral geniculate body of the monkey. J. Anat. (Lond.), 1941, 75, 295-304.

Gorman, J., Cogan, D. and Gellis, S. An apparatus for grading the visual acuity on the basis of optokinetic nystagmus. Pedriatrics, 1957, 19, 1088-1092.

Gottlieb, M., Pasik, P. and Pasik, T. The volume of the lateral geniculate nucleus and striate cortex as a function of postnatal age in monkeys. Soc. Neurosci. Abstr., 1981, 7, 672.

Gottlieb, M., Pasik, T. and Pasik, P. Developmental features of dorsal lateral geniculate nucleus in monkeys. Soc. Neurosci. Abstr., 1980, 6, 662.

Guillery, R. A study of Golgi preparations from the dorsal lateral geniculate nucleus of

the adult cat. J. comp. Neurol., 1966, 128, 21-50.

Guillery, R. Patterns of fiber degeneration in the dorsal lateral geniculate nucleus of the cat following lesions in the visual cortex. J. comp. Neurol., 1967, 130, 197-222.

Guillery, R. A quantitative study of synaptic interconnections in the dorsal lateral geniculate nucleus of the cat. Z. Zellforsch., 1969, 96, 39-48.

Guillery, R. Patterns of synaptic interconnections in the dorsal lateral geniculate nucleus of cat and monkey: A brief review. In: Shipley, T. and Dowling, J. (Eds.), Visual Processes in Vertebrates. Vision Res. Suppl. No. 3, Pergamon Press, Oxford, 1971, pp. 211-227.

Guillery, R. and Colonnier, M. Synaptic patterns in the dorsal lateral geniculate nucleus of the monkey. Z. Zellforsch., 1970, 103, 90-108.

Hámori, J., Pasik, P. and Pasik, T. Postnatal differentiation of "presynaptic dendrites" in the lateral geniculate nucleus of the rhesus monkey. In: G. Kreutzberg (Ed.), Physiology and Pathology of Dendrites, Adv. in Neurol., Vol. 12, Raven Press, New York, 1975, pp. 149-161.

Hámori, J., Pasik, P. and Pasik, T. Differential frequency of P-cells and I-cells in magnocellular and parvocellular laminae of monkey lateral geniculate nucleus. An ultrastructural study. In press.

Hámori, J., Pasik, T. and Pasik, P. Electron microscope identification of axonal initial segments belonging to interneurons in the dorsal lateral geniculate nucleus of monkey. Neuroscience, 1978, 3, 403-412.

Hámori, J., Pasik, T., Pasik, P. and Szentagothai, J. Triadic synaptic arrangements and their possible significance in the lateral geniculate nucleus of the monkey. Brain Res., 1974, 80, 379-393.

Harding, T. and Yates, J. Monkey contrast threshold for aperiodic patterns. J. Opt. Soc. Am., 1976, 66, 131-138.

Harter, M. and Suitt, C. Visually-evoked cortical responses and pattern vision in the

infant: a longitudinal study. Psychonomic Sci., 1970, 18, 235-237.

Harwerth, R., Crawford, M., Smith, E. and Boltz, R. Behavioral studies of stimulus deprivation amblyopia in monkeys. Vision Res., 1981, 21, 779-789.

Headon, M. and Powell, T. Cellular changes in the lateral geniculate nucleus of infant monkeys after suture of the eyelids. J. Anat., 1973, 116, 135-145.

Headon, M., Sloper, J., Hiorns, R. and Powell, T. Cell sizes in the lateral geniculate nucleus of normal infant and adult rhesus monkeys. Brain Res., 1981a, 229, 183-186.

Headon, M., Sloper, J., Hiorns, R. and Powell,T. Shrinkage of cells in undeprived laminae of the monkey lateral geniculate nucleus following late closure of one eye. Brain Res., 1981b, 229, 187-192.

Hendrickson, A., Boles, J. and McLean, E. Visual acuity and behavior of monocularly deprived monkeys after retinal lesions. Invest. Ophthal. Visual Sci., 1977,16, 469-473.

Hendrickson, A., Lund, J. and Kalina, R. The interaction of retinal lesions and eyelid closure in the monkey dorsal lateral geniculate. Soc. Neurosci. Meeting, 1975, Abst. #101.3

Hendrickson, A. and Rakic, P. Histogenesis and synaptogenesis in the dorsal lateral geniculate nucleus (LGd) of the fetal monkey brain. Anat. Rec., 1977, 187, 602.

Hendrickson, A., Wilson, M. and Toyne, M. The distribution of optic nerve fibers in Macaca mulatta. Brain Res., 1970, 23, 425-427.

Hess, R., France, T. and Tulunay-Keesey, U. Residual vision in humans who have been monocularly deprived of pattern stimulation in early life. Exp. Brain Res., 1981, 44, 295-311.

Hickey, T. Postnatal development of the human lateral geniculate nucleus: relationship to a critical period for the visual system. Science, 1977a, 198, 836-838.

Hickey, T. Human lateral geniculate nucleus: laminar patterns and postnatal development. ARVO Abstracts, 1977b, p. 87.

Hickey, T. Development of the LGNd in normal and visually deprived cats. J. comp.

Neurol., 1980, 189, 467-481.

Hickey, T. and Guillery, R. A study of Golgi preparations from the human lateral geniculate nucleus. J.comp. Neurol., 1981, 200, 545-577.

Hohmann, A. and Creutzfeldt, O. Squint and the development of binocularity in humans. Nature, 1975, 254, 613-614.

Howland, H., Atkinson, J., Braddick, O. and French, J. Infant astigmatism measured by photorefraction. Science, 1978, 202, 331-333.

Howland, H., Boothe, R. and Kiorpes, L. Accommodative defocus does not limit development of acuity in infant Macaca nemestrina monkeys. Science, 1982, 215, 1409-1411.

Hubel, D. and Wiesel, T. Integrative action in the cat's lateral geniculate body. J. Physiol., 1961, 155, 385-398.

Hubel, D., Wiesel, T. and LeVay, S. Plasticity of ocular dominance columns in monkey striate cortex. Phil. Trans. R. Soc. Lond. B., 1977, 278, 377-409.

Ikeda, H. and Tremain, K. The development of spatial resolving power of lateral geniculate neurons in kittens. Exp. Brain Res., 1978, 31, 193-206.

Jones, E. and Powell, T. Electron microscopy of synaptic glomeruli in the thalamic nuclei of the cat. Proc. Roy. Soc. B., 1969, 172, 153-171.

Kaas, J., Harting, J. and Huerta, M. A new interpretration of the laminar organization of the dorsal lateral geniculate nucleus of primates. ARVO Abstracts, 1977, p. 87.

Kaas, J., Huerta, M., Weber, J. and Harting, J. Patterns of retinal terminations and laminar organization of the lateral geniculate nucleus of primates. J. comp. Neurol., 1978, 182, 517-554.

Kaas, J., Lin, C. and Casagrande, V. The relay of ipsilateral and contralateral retinal input from the lateral geniculate nucleus to striate cortex in the owl monkey: transneuronal transport study. Brain Res., 1976, 106, 371-378.

Kalil, R. Development of the dorsal lateral geniculate nucleus in the cat. J. comp.

Neurol., 1978, 182, 265-292.

Knyihar, E., Csillik, B. and Rakic, P. Transient synapses in the embryonic primate spinal cord. Science, 1978, 202, 1206-1209.

Korneliussen, H. and Jansen, J. Morphological aspects of the elimination of polyneuronal innervation of skeletal muscle fibres in newborn rats. J. Neurotytol., 1976, 5, 591-604.

Kowler,E. and Martins, A. Eye movements of preschool children. Science, 1982, 215, 997-999.

Laemle, L. and Noback, C. The visual pathways of the lorisid lemurs (Nycticebus coucang and Galago crassicaudatus). J. comp. Neurol., 1970, 138, 49-62.

LeVay, S. On the neurons and synapses of the lateral geniculate nucleus of the monkey and the effects of eye enucleation. Z. Zellforsch., 1971, 113, 396-419.

LeVay, S. and Ferster, D. Relay cell classes in the lateral geniculate nucleus of the cat and the effects of visual deprivation. J. comp. Neurol., 1977, 172, 563-584.

Lichtman, J. The reorgnization of synaptic connexions in the rat submandibular ganglion during post-natal development. J. Physiol., 1977, 273, 155-177.

Lichtman, J. On the predominantly single innervation of submandibular ganglion cells in the rat. J. Physiol., 1980, 302, 121-130.

Lichtman, J. and Purves, D. The elimination of redundant preganglionic innervation to hamster sympathetic ganglion cells in early post-natal life. J. Physiol., 1980, 301, 213-228.

Lund, J., Remington, F. and Lund, R. Differential central distribution of optic nerve components in the rat. Brain Res., 1976, 116, 83-100.

Mangel, S., Wilson, J. and Sherman, S. Development of neuronal response properties in the cat lateral geniculate nucleus during monocular lid suture. Soc. Neurosci. Abstr., 1980, 6, 584.

Marrocco, R. Sustained and transient cells in monkey lateral geniculate nucleus: conduction velocities and response properties. J. Neurophysiol., 1976, 39, 340-353.

Mason, C. and Robson, J. Morphology of retino-geniculate axons and their terminals in the dorsal lateral geniculate nucleus (LGN) of the cat. Soc. Neurosci. Abstr., 1977, 3, 569.

Matthews, M., Cowan, W. and Powell, T. Transneuronal cell degeneration in the lateral geniculate nucleus of the macaque monkey. J. Anat. (Lond.), 1960, 94, 145-169.

Mayhew, T. Basic stereological relationships for quantitative microscopical anatomy — a simple systematic approach. J. Anat., 1979, 1, 95-105.

Mayer, D. and Dobson, V. Assessment of vision in young children: a new operant approach yields estimates of acuity. Invest. Ophthal. Visual Sci., 1980, 19, 566-570.

Miller, M., Pasik, P. and Pasik, T. Extrageniculostriate vision in the monkey. VII. Contrast sensitivity functions. J. Neurophysiol., 1980, 43(6), 1510-1526.

Minkowski, M. Experimentelle Untersuchungen über die Beziehungen der Grobhirnrinde und Netzhaut zu den primaren optischen Zentren, besonders zum Corpus genicolatum externum. Arb. Hirnanat. Inst. Zürich, 1913, 7, 259-362.

Minkowski, M. Über den Verlauf, die Endigung und die zentral Repräsentation von gekreuzten Schnervenfasern bei einigen Säugetieren und biem Menshen. Schweiz. Arch. Neurol. Psychiat., 1920, 6, 201-252.

Mohindra, I., Held, R., Gwiazda, J. and Brill, S. Astigmatism in infants. Science, 1978, 202, 329-330.

Norman, J., Pettigrew, J. and Daniels, J. Early development of X-cells in kitten lateral geniculate nucleus. Science, 1977, 198, 202-204.

O'Leary, J. A structural analysis of the lateral geniculate nucleus of the cat. J. comp. Neurol., 1940, 73, 405-430.

Palkovits, M. Determination of axon terminal density in the central nervous system. Brain Res., 1976, 108, 413-417.

Pasik, T., Pasik, P. and Hámori, J. Quantitative aspects of synaptogenesis in monkey dorsal lateral geniculate nucleus (LGNd). Exp. Brain Res., 1975, 23 (Suppl.), 156.

Pasik, P., Pasik, T. and Hámori, J. Neuronal circuits with "presynaptic dendrites" in dorsal lateral geniculate nucleus (LGNd) of monkeys. Soc. Neurosci. Abstr., 1977, 3, 572.

Pasik, P., Pasik, T. and Hámori, J. Synapse elimination in the LGNd of monkeys during early postnatal development. Invest. Ophthal., 1978, 17 (Suppl.), 291.

Pasik, P., Pasik, T., Hámori, J. and Szentágothai, J. Golgi type II interneurons in the neuronal circuit of the monkey lateral geniculate nucleus. Exp. Brain Res., 1973, 17, 18-34.

Peters, A. and Palay, S. The morphology of lamina A and A1 of the dorsal nucleus of the lateral geniculate body of the cat. J. Anat. (Lond.), 1966, 100, 451-486.

Petrig, B., Julesz, B., Kropfl, W., Baumgartner, G. and Anliker, M. Development of stereopsis and cortical binocularity in human infants: electrophysiological evidence. Science, 1981, 312, 1402-1405.

Polyak, S. The Vertebrate Visual System. Chicago University Press, Chicago, 1957.

Pratt, K. The neonate. Manual of Child Psychology. New York: Wiley, 1954, pp. 215-291.

Purves, D. and Lichtman, J. Elimination of synapses in the developing nervous system. Science, 1980, 280, 153-157.

Rakic, P. Time of origin, mode of organization and patterns of distribution of neurons in the dorsal lateral geniculate body of the rhesus monkey: H^3-thymidine autoradiographic analysis. Anat. Rec., 1976a, 184, 507-508.

Rakic, P. Prenatal genesis of connections subserving ocular dominance in the rhesus monkey. Nature, 1976b, 261, 467-471.

Rakic, P. Genesis of the dorsal lateral geniculate nucleus in the rhesus monkey: site and time of origin, kinetics of distribution of neurons. J. comp. Neurol., 1977a, 176, 23-52.

Rakic, P. Prenatal development of the visual system in rhesus monkey. Phil. Trans. R Soc. B., 1977b, 278, 245-260.

Rakic, P. Development of visual centers in the primate brain depends on binocular

competition before birth. Science, 1981, 214, 928-931.

Rakic, P. and Riley, K. Number of axons in the optic nerve of the developing rhesus monkey: overproduction and elimination before birth. Soc. Neurosc. Abstr., Vol. 8, p. 814, 1982.

Ralston, H. and Herman, M. The fine structure of neurons and synapses in the ventrobasal thalamus of the cat. Brain Res., 1969, 14, 77-97.

Ramón y Cajal, S. Histologie du Système Nerveux de l'Homme et des Vertébrés, Vol. 2, Paris: Maloine, 1911.

Reinis, S. and Goldman, J. The Development of the Brain. Charles Thomas, Springfield, Ill., 1980.

Richards, W. and Kalil, R. Dissociation of retinal fibers by degeneration rate. Brain Res., 1974, 72, 288-293.

Robson, J. and Mason, C. The synaptic organization of terminals traced from individual labeled retinogeniculate axons in the cat. Soc. Neurosci. Abstr., 1977, 3, 574.

Robson, J., Mason, C. and Guillery, R. Terminal arbors of axons that have formed abnormal connections. Science, 1978, 201, 635-637.

Rosenblum, L. and Cross, H. Performance of neonatal monkeys in the visual cliff situation. Am. J. Psychol., 1963, 76, 318-320.

Saini, K.D. and Garey, L.J. Morphology of neurons in the lateral geniculate nucleus of the monkey. A Golgi study. Exp. Brain Res., 1981, 42, 235-248.

Sherman, S., Wilson, J., Kaas, J. and Webb, S. X- and Y-cells in the dorsal lateral geniculate nucleus of the owl monkey (Aotus trivirgatus). Science, 1976, 192, 475-477.

Shkol'nik-Yarros, E. The structure of visual analyzer and colour vision. Arh. Anat. Gisztol. Embriol., 1962, 42, 12-30 (Russian, English summary).

Sivak, J. and Bobier, C. Accommodation and chromatic aberration in young children. Invest. Ophthal., 1978, 17, 705-709.

Staples, R. The responses of infants to color. J. Exp. Psychol., 1932, 15, 119-141.

Stone, J., Dreher, B. and Leventhal, A. Hierarchical and parallel mechanisms in the organization of visual cortex. Brain Res. Reviews, 1979, 1, 345-394.

Stone, S. and Fukuda, Y. Properties of cat retinal ganglion cells: a comparison of W-cells with X- and Y-cells. J. Neurophysiol., 1974, 37, 722-748.

Szentágothai, J. The structure of the synapse in the lateral geniculate body. Acta. Anat., 1963, 55, 166-185.

Szentágothai, J. Neuronal and synaptic architecture of the lateral geniculate body. In: R. Jung (Ed.), Handbook of Sensory Physiology, Springer, Berlin, 1973, Vol. 7/B, pp. 141-176.

Szentágothai, J., Hámori, J. and Tömböl, T. Degeneration and electron microscope analysis of the synaptic glomeruli in the lateral geniculate body. Exp. Brain Res., 1966, 2, 283-301.

Toboada, R. Note sur la structure du corps genouillé externe. Trav. du lab. de rech. biol. Madrid, 1927-28, 25, 319-329.

Talbot, S. and Marshall, W. Physiological studies on neural mechanisms of visual localizations and discriminations. Am. J. Ophthal., 1941, 24, 1255-1263.

Teller, D. and Boothe, R. Development of vision in infant primates. Trans. ophthal. Soc. U.K., 1979, 99, 333-337.

Teller, D., Regal, D., Videen, T. and Pulos, E. Development of visual acuity in infant monkeys (Macaca nemestrina) during the early postnatal weeks. Vision Res., 1978, 18, 561-566.

Tello, F. Disposición macroscopica y estructura del cuerpo geniculado externo. Trabajos del Laboratorio de Investigaciones Biologicas de la Universidad de Madrid, 1904, 3, 39-62.

Tigges, J. and O'Steen, W. Terminations of retinofugal fibers in squirrel monkey: a reinvestigation using autoradiographic methods. Brain Res., 1974, 79, 489-495.

Tigges, M. and Tigges, J. The retinofugal fibers and their terminal nuclei in Galago crassicaudatus (primates). J. comp. Neurol., 1970, 138, 87-102.

Tuttle, L. and Satterly, J. Theory of Measurements, Logmans, London, 1925.

von Noorden, G. Histological studies of the visual system in monkeys with experimental amblyopia. Invest. Ophthal., 1973, 12, 727-738.

von Noorden, G. and Crawford, M. Lid closure and refractive error in macaque monkeys. Nature, 1978a, 272, 53-54.

von Noorden, G. and Crawford, M. Morphological and physiological changes in the monkey visual system after short-term lid suture. Invest. Ophthal. Visual Sci., 1978b, 17, 762-768.

von Noorden, G., Crawford, M. and Middleditch, P. The effects of monocular visual deprivation: disuse or binocular interaction? Brain Res., 1976, 111, 277.

von Noorden, G. and Dowling, J. Experimental amblyopia in monkeys. II. Behavioral studies in strabismic amblyopia. Arch. Ophthalmol., 1970, 84, 215-220.

von Noorden, G., Dowling, J. and Ferguson, O. Experimental amblyopia in monkeys. Arch. Ophthalmol., 1970, 84, 206-214.

von Noorden, G. and Maumanee, A. Clinical observations on stimulus-deprivation amblyopia (amblyopia ex anopsia). Am. J. Ophthal., 1968, 65, 220-224.

von Noorden, G. and Middleditch, P. Histology of the monkey lateral geniculate nucleus after unilateral lid closure and experimental strabismus. Further observations. Invest. Ophthalmol., 1975, 14, 674.

Von Senden, M. Space and Sight. Translated by P. Heath. Methuen: London and Free Press: Glencoe, Ill., 1960.

Walls, G. The lateral geniculate nucleus and visual histophysiology. Univ. Calif. Publ. Physiol., 1953, 9, 1-100.

Weiskrantz, L. and Cowey, A. Striate cortex lesions and visual acuity of the rhesus monkey. J. comp. Physiol. Psychol., 1963, 56, 225-231.

Wiesel, T. and Raviola, E. Myopia and eye enlargement after neonatal lid fusion in monkeys. Nature, 1977, 266, 66-68.

Wilson, J. and Hendrickson, A. Neuronal and synaptic structure of the dorsal lateral geniculate nucleus in normal and monocularly deprived Macaca monkeys. J. comp. Neurol., 1981, 197, 517-539.

Wilson, J., Tessin, D. and Sherman, S. Development of the electrophysiological properties of Y-cells in the kitten's medial interlaminar nucleus. Neurosci., 1982, 2, 562-571.

Wilson, P., Rowe, M. and Stone, J. Properties of relay cells in the cat's lateral geniculate nucleus. A comparison of W-cells with X- and Y-cells. J. Neurophysiol., 1976, 39, 1193-1209.

Winfield, D. The synaptic organization of glomeruli in the magnocellular and parvocellular laminae of the lateral geniculate nucleus in the monkey. Brain Res., 1980, 198, 55-62.

Winfield, D., Headon, M. and Powell, T. Postnatal development of the synaptic organization of the lateral geniculate nucleus in the kitten with unilateral eyelid closure. Nature, 1976, 263, 591-594.

Wong-Riley, M. Neuronal and synaptic organization of the normal dorsal lateral geniculate nucleus of the squirrel monkey, Saimiri sciureus. J. comp. Neurol., 1972, 144, 25-60.

Zimmerman, R. Analysis of discrimination learning in infant rhesus monkeys. Unpublished doctoral dissertation. University of Wisconsin, 1958.